Ministère de l'Enseignement Supérieur et de la Recherche Scientifique
Université Hassiba Benbouali de Chlef
Faculté de Génie Civil et d'Architecture
Département de Génie Civil

THÈSE

Présentée pour l'obtention du diplôme de

DOCTORAT

Filière : Génie Civil

Spécialité : Matériaux et Structures

Par

Abdelkadir FELLOUH

Thème :

ANALYSE DU COMPORTEMENT AU FEU DES POTEAUX MIXTES SOLLICITES A LA FLEXION COMPOSEE

Soutenue le 04/02/2021, devant le jury composé de :

Hassen AIT ATMANE	Professeur	UHB Chlef	Président
Amar KASSOUL	Professeur	UHB Chlef	Examinateur
Tahar HASSAINE DAOUADJI	Professeur	UIK Tiaret	Examinateur
Abdallah BENAROUS	Professeur	USD Blida 1	Examinateur
Abdelkader BOUGARA	Professeur	UHB Chlef	Rapporteur
Noureddine BENLAKEHAL	MCB	UHB Chlef	Co-Rapporteur

Ministry of Higher Education and Scientific Research
The University Hassiba Benbouali of Chlef
Faculty of Civil Engineering and Architecture
Civil Engineering Department

DOCTORAL THESIS

In Civil Engineering, Specialty Materials and Structures

Presented By
Abdelkadir FELLOUH

Theme

ANALYSIS OF THE FIRE BEHAVIOR OF COMPOSITE COLUMNS SUBJECTED TO COMBINED COMPRESSION AND BENDING

The thesis is defended before an assessment committee and graded on 04/02/2021, including:

Hassen AIT ATMANE	Professor	University of Chlef	President
Amar KASSOUL	Professor	University of Chlef	Examiner
Tahar HASSAINE DAOUADJI	Professor	University of Tiaret	Examiner
Abdallah BENAROUS	Professor	University of Blida 1	Examiner
Abdelkader BOUGARA	Professor	University of Chlef	Supervisor
Noureddine BENLAKEHAL	A. Professor	University of Chlef	Co-Supervisor

ACKNOWLEDGEMENTS

First of all, I would like to express a special thanks to my supervisors, Professor Abdelkader Bougara; coordinator Professor from the Faculty of Civil Engineering and Architecture of University Hassiba Benbouali of Chlef, Professor Paulo Piloto co-supervisor from the Department of Applied Mechanics, School of Technology and Management, Polytechnic Institute of Bragança, and Dr. Nourredine Benlakehal; co-supervisor from the Faculty of Civil Engineering and Architecture of University Hassiba Benbouali of Chlef, for their guidance, encouragement, time and efforts in helping me to complete this thesis.

I would like to thank all members of the committee dissertation for agreeing to read the manuscript and to participate in the defense of this thesis, namely Pr Hassen AIT ATMANE, Pr Amar KASSOUL, Pr Tahar HASSAINE DAOUADJI and Pr Abdallah BENAROUS.

I would like also to thank my family and friends for their endless support. I want to thank my wife who always stays by my side and gives me countless suggestions.

Abstract

Composite structures made from the combination of steel profile and concrete have a significant loadbearing capacity which depends on the behaviour of the two material components and their interaction, particularly in fire conditions. This work includes two parts, notably the thermal and mechanical behaviour of the composite column under compression and combined compression and bending. The aim of the first part is to develop an efficient non-linear 3D finite element model to investigate the behaviour of pin-ended axially loaded composite column made from high strength concrete and normal strength concrete at different fire rating classes. The fire behaviour of the columns was tested according to ISO-834 standard fire. The results show that the use of HSC reduces the level of the fire protection with the regard to NSC. NSC in composite structures accommodates higher deflections than HSC, which is safer in case of fire accident. In the second part of this work, the Fire performance of partially encased composite columns (PEC) subjected to eccentric loading is studied. Numerical and analytical methods are used to evaluate the load bearing capacity of PEC composite columns under combined compression and bending moment. The parametric study includes the buckling length, the load eccentricity, the fire exposure time and the fire scenario. It is found that the analytical results agree well with those of the numerical method, particularly for higher fire rating classes (R60-R90-R120). The results show also that the PEC composite column loaded by an axial compression resists better to fire than the composite column subjected to an eccentric loading.

Keywords: Composite column; Fire ; Numerical Method ; Analytical method ; Buckling; Combined Compression and bending.

ملخص

تتمتع الهياكل المركبة المصنوعة من مزيج من مقاطع الفلاذ والخرسانة بقدرة تحمل كبيرة تعتمد على سلوك المكونين وتفاعلهما ، خاصة في ظروف نشوب الحريق. تحتوي هذه الدراسة على جزأين ،لاسيما السلوك الحراري والميكانيكي للعمود المركب الخاضع لقوة ضغط والخاضع لضغط مع وجود عزم انحناء. الهدف من الجزء الأول هو تصميم نموذج فعال غير خطي ثلاثي الأبعاد للعناصر المحدودة للتحقق من سلوك العمود المركب المحمل محوريًا ذي النهايات المفصلية المصنوعة من الخرسانة عالية المقومة والخرسانة ذات المقاومة العادية.العمود يخضع لمختلف فئات معدل تصنيف الحريق. تم التطرق الى سلوك النار في الأعمدة وفقًا لمعيار الجودة للحريقISO-834 . أظهرت النتائج أن استخدام الخرسانة عالية المقاومة يقلل من مستوى الحماية من الحرائق مقارنتا بالخرسانة ذات المقاومة العادية. الخرسانة ذات المقاومة العادية تسمح في الهياكل المركبة بتشوهات اكبر من الخرسانة عالية المقاومة ، وهي أكثر أمانًا في حالة وقوع حريق. في الجزء الثاني من هذه المذكرة ، تمت دراسة السلوك الناري للأعمدة المركبة المغلفة جزئيًا بالخرسانة المعرضة للتحميل غير مركزي. يتم استخدام الطرق الرقمية والتحليلية لتقييم قدرة تحمل لأعمدة المركبة المغلفة جزئيًا تحت ضغط محوري و ضغط غير محوري. تتضمن الدراسة عدة متغيرات مثل طول الالتواء ، الانحراف اللامركزي للحمولة ، مدة التعرض للحريق وسيناريوالحريق. وجد أن النتائج التحليلية تتفق بشكل جيد مع تلك الخاصة بالطريقة الرقمية ، خاصة بالنسبة لفئات معدل تصنيف الحريق العالية (R60-R90-R120). تظهر النتائج أيضًا أن العمود المركب المغلف جزئيًا و المحمل بضغط محوري يقاوم بشكل أفضل الحريق من العمود المركب و المعرض لتحميل غير محوري.

كلمات البحث: عمود مركب ؛ حريق ؛ طريقة رقمية ؛ طريقة تحليلية ؛ الضغط المحوري. الضغط الامحوري.

Résumé

Les structures mixtes constituées de la combinaison de profilés en acier et de béton ont une capacité de charge importante qui dépend du comportement des deux constituants du matériau composite et de leur interaction, en particulier en situations d'incendie. Cette étude comprend deux parties, à savoir le comportement thermique et mécanique du poteau mixte sous deux sollicitations ; la compression simple et la flexion composée. Le but de la première partie est de développer un modèle d'éléments finis 3D non linéaire permettant d'analyser le comportement d'un poteau mixte chargé axialement et articulé aux extrémités. Le poteau est fabriqué avec deux types de béton, un béton de résistance normale et un béton à haute résistance. Ce poteau est sujet à différentes classes d'exposition au feu. Le comportement au feu des poteaux a été testé selon la norme au feu ISO-834. Les résultats montrent que l'utilisation de béton à haute résistance réduit le niveau de protection contre le feu par rapport à l'utilisation du béton de résistance normal. Dans les structures mixtes, le béton de résistance normal tolère des déformations plus élevées que le béton à haute résistance, ce qui offre plus de sécurité en cas d'incendie. Dans la deuxième partie de ce travail, la performance au feu des poteaux mixtes partiellement enrobés, soumis à des sollicitations excentriques est analysée. La capacité de charge des poteaux mixtes sous un effort de compression combiné avec un moment de flexion est évaluée par des méthodes numériques et analytiques. Les paramètres de variation de cette étude comprennent la longueur de flambement, l'excentricité de la charge, le temps d'exposition au feu et le scénario d'incendie. On constate que les résultats analytiques concordent bien avec ceux de la méthode numérique, en particulier pour les classes de résistance au feu supérieures (R60-R90-R120). Les résultats montrent également que le poteau mixte partialement enrobé chargée axialement résiste au feu mieux que le poteau soumis à un chargement excentrique.

Mots clés : Poteau mixte; Feu ; Méthode numérique ; méthode analytique ; flambement ; flexion composée.

TABLE OF CONTENTS

LIST OF FIGURES

LIST OF TABLES

Latin upper case letters

A_c	Cross-sectional area of the concrete.
A_s	Cross-sectional area of the reinforcement
A_m/V	Section factor
CFT	Concrete field tubular steel column
E	Modulus of elasticity.
E_a	Modulus of elasticity of the structural steel at room temperature.
$E_{a,\theta}$	Modulus of elasticity of the structural steel at elevated temperature.
E_c	Effective modulus of elasticity of the concrete at room temperature.
E_{cm}	Secant modulus of elasticity of the concrete at room temperature.
$E_{c,\sec,\theta}$	Characteristic value for the secant modulus of concrete in the fire situation.
$(EI)_{fi,c,z}$	Effective flexural stiffness of the concrete around the z-axis exposed to fire
$(EI)_{fi,eff,z}$	Effective flexural stiffness of a composite section around the z-axis exposed to fire.
$(EI)_{fi,f,z}$	Effective flexural stiffness of the flange around the z-axis exposed to fire.
$(EI)_{fi,w,z}$	Effective flexural stiffness of the web around the z-axis exposed to fire.
$(EI)_{fi,s,z}$	Effective flexural stiffness of the reinforcement around the z-axis exposed to fire.
E_s	Modulus of elasticity of the steel reinforcement at room temperature.
$E_{s,\theta}$	Characteristic value for the slope of the linear elastic range of the stress-strain relationship of reinforcing steel at elevated temperatures.
H_t	Factor.
ISO	International organization for standardization
I_y	Moment of inertia relative to the axis y-y.

I_z	Moment of inertia relative to the axis z-z.
Q_c	Is the convective part of the rate of heat release.
$[K]$	The element stiffness matrix.
$[S]$	Geometric stiffness matrix of the element.
L	Length of the column.
L_{cr}	Buckling length.
$N_{fi,cr,z}$	Elastic critical load (≡ Euler buckling load) around the axis Z in the fire situation.
N_{ed}	Applied eccentric load
$N_{fi,pl,Rd}$	Normal plastic stress resistant exposed to fire.
$N_{b,pl,Rd}$	Buckling resistant exposed to fire.
$N_{pm,Rd}$	design value of the concrete resistance to compression
M-N	Interaction polygon and corresponding stress distributions
M_{adm}	Resistance moment
$M_{pl,Rd}$	Plastic resistance moment
$M_{n,Rd}$	Bending moment according to the neutral axis
$M_{\max,Rd}$	Maximum bending moment capacity
M_{sd}	Design moment
PEC	Partially encased column
T,θ	Temperature.
TEC	Totally encased column
W_{pl}	Plastic section modulus.

Latin lower case letters

b	Width of the cross section.

b_w	Width of the web element.
$b_{c,\,fi}$	Neglected external layer of concrete.
$b_{c,\,fi,horizontal}$	Neglected external layer of concrete in horizontal directions.
$b_{c,\,fi,vertical}$	Neglected external layer of concrete in vertical directions.
$c_a(\theta)$	Specific heat of steel.
$c_p(\theta)$	Specific heat of concrete.
f_{cd}	Design value of the yield strength of the steel at room temperature.
f_{cm}	The average design value of the yield strength of the steel at room temperature.
f_{sk}	Characteristic value of the yield strength of the steel reinforcement at room temperature
f_{ck}	Characteristic value of the compressive strength of the concrete at room temperature.
$f_{u,\theta}$	The ultimate strength at elevated temperature, allowing for strain-hardening.
h	Total height of a cross section.
h_n	Position of the plastic neutral axis
h_1	Height between web.
$\dot{h}_{net}$	Net heat flow per unit area.
$\dot{h}_{net,c}$	Net convective heat flux per unit surface area.
$\dot{h}_{net,d}$	Design value of the density of heat flow per unit area.
$\dot{h}_{net,r}$	Net radioactive heat flux per unit surface area.
$h_{w,\,fi}$	Height reduction of the web.
$k_{E,\theta}$	Reduction factor for the slope of linear elastic range at the steel temperature θ_a reached at time t.
k_n	Reduction factor for the greatest first-order bending moment
$k_{c\theta}$	Reduction factor for the tensile strength of concrete.

$k_{p,\theta}$	Reduction factor of the yield point of structural steel giving the proportional limit at temperature θ_a reached at time t.
$k_{y,\theta}$	Reduction factor for effective yield strength at the steel temperature θ_a reached at time t.
t	Time.
t_f	Flange thickness.
t_w	Web thickness.
u	Geometric mean of the distances u_1 u_2 .
u_1 u_2	Shortest distance between the reinforcing steel centre and inner face of the flange or the nearest end of concrete.
z	Height along the flame axis.

Greek upper case letters

$\nabla\theta$	$\nabla\theta = \langle d_\theta/d_x \quad d_\theta/d_y \quad d_\theta/d_z \rangle^t$
ϕ	Configuration factor.
ϕ_{LT}	Value to determine the reduction factor χ_{LT} .
$\phi_{LT,\theta,com}$	Value to determine the reduction factor χ_{LT} at elevated temperature θ .
Ψ_i	Displacement vector.

Greek lower case letters

α	Imperfection factor, thermal elongation coefficient.
α_c	Coefficient of heat transfer by convection.
β	Parameters to take into account the effect of biaxial bending.
ε	Emissivity of material.
$\varepsilon_{c,\theta}$	Thermal strain of concrete.
$\varepsilon_{p,\theta}$	Thermal strain of prestressing steel.

$\varepsilon_{s,\theta}$	Thermal strain of steel.
$\varepsilon_{cu,\theta}$	Thermal strain of reinforcing concrete
ε_f	Emissivity of the fire.
ε_m	Surface emissivity of the member.
$\eta_{fi,t}$	Amplitude charging for fire resistance calculation.
θ_a	Temperature of steel profile [°C].
θ_c	Temperature of concrete [°C].
θ_s	Temperature of reinforcement [°C].
θ_g	Gas temperature in the vicinity of the element or in the fire compartment.
θ_r	Effective radiation temperature of the fire environment.
$\theta_{c,t}$	Average temperature in the concrete at time t.
$\theta_{f,c}$	Average temperature in the flange at time t.
$\theta_{w,c}$	Average temperature in the web at time t.
$\theta_{s,c}$	Average temperature in the reinforcement at time t.
μ_d	Factor related to design for compression and bending
λ_a	Thermal conductivity of steel.
λ_c	Thermal conductivity of concrete.
$\lambda_{(\theta)}$	Thermal conductivity.
$\overline{\lambda}_{LT}$	Relative slenderness for lateral torsional bending.
ρ	Density.
ν	Poisson coefficient in elastic regime.
σ	Stefan Boltzmann constant.
σ_x	Principal stress in the x direction.
χ	Reduction factor for buckling
χ_d	Parameter representing the axial load

χ_{LT}	Reduction factor for lateral torsional buckling.
$\chi_{LT,fi}$	Reduction factor for buckling torsional lateral sections exposed to fire.

Chapter 1

INTRODUCTION

1.1 Background

Combining different materials in a single structural member to take advantage of the good qualities that they both have separately, has always been a recognized strategy in building industry. One of the most used technology in construction is composite structure, this type of construction had been used for the first time to improve the safety of the structures under fire and reduce the loss caused by the fire. Initially the increases of the performance of the composite structure due to the composite action, was not taken into consideration. This performance was not recognized until the middle of the 20th century when it began to use in High-rise, super high-rise and complex high-rise buildings related to the good mechanical performance and economic performance. Many studies have demonstrated the increase of the rigidity and the strength of the structural composite elements. In composite structure, the columns constitute only a small part of the building. However, they are the main elements which ensure the stability of the construction. Since the 1960s, composite columns have been used for the construction of multi-storey buildings related to their structural performances. Examples of composite column commonly used are partially or totally concrete encased column (PEC, TEC). Partially Encased Columns are usually made of hot rolled steel profiles, reinforced with concrete between the flanges. The composite section is responsible for increasing the torsional and bending stiffness when compared to the same section of the steel profile. In addition to these advantages, the reinforced concrete is responsible for increasing the fire resistance. PEC sections resist around 120 min before collapsing in fire conditions (Piquer and Hernández-Figueirido, 2016). Totally Encased Columns have many advantages including higher strength, full usage of materials, higher stiffness and ductility, toughness against seismic loads, significant savings in construction time and particularly higher fire resistance (Ellobody and Young, 2010). The concrete cover have a big influence on the fire critical time of the composite column, increasing the concrete cover around the steel profile and rebars increases the critical times and fire resistance (Rodrigues et al., 2015). Fire accident is considered as one of the most sever environmental hazard to building construction, which makes people's life and property safety in danger. Nowadays for building structures, the performance under fire conditions is much requested for safety and stability conditions. The construction industry gives a significant importance to the use of

composite steel concrete structure over steel structure or reinforced concrete structure at elevated temperatures. Many investigations have carried out on the composite column at elevated temperature and they proved to have the best structural behaviour under fire (Huang et al., 2008; Liu et al., 2017; Bihina et al., 2013).

1.2 Fire Safety objectives

Fire has always been a very destructive natural and accidental phenomenal. The fire risk will always exist because of fire accidents and also it is impossible to use only incombustible products in building. To reduce the risks of fire, a series of measures must be taking into account, each of these measures is in itself insufficient, but their conjunction helps to achieve the good safety.

The Fire engineering is a design philosophy based on the application of scientific and engineering principles rules. The process of fire engineering takes into account the risk of fire and the fire scenarios. The most important objectives of the fire engineering is to limit the probability of death, minimise the property losing and the environmental damage in an unwanted fire. To reach a sufficient level of fire protection, a preventive measures must be followed. These measures are divided into passive and active protection measures:

- The active protection are carried out during the construction of the building and are operational at all times. The best forms of an active fire protection are:

  - Automatic sprinkler system which spray water over a local area under the activated splinker head.
  - Alert people to provide suitable escape paths and ensure that they are not affected by fire or smoke while escaping through those paths to a safe place by an active control of smoke.
  - Giving much time to intervention fire-fighters services before the collapse of building by increasing the fire rating class of the structure.

- The passive protection can be made during or after the construction, this protection is controlled by systems that are built into the building. The passive protection does not required operation by people or automatic controls.

- Uses in the building a principle of compartmentalization (insulating part of the building) and the compartments are formed by material that is resistant to fire.
- Protect the steel structural by concrete (composite structure) or by using an intumescent coating which foams and swells when heated, producing an insulating char layer.

1.3 Problem Statement

Concrete has a great fire resistance related to its low thermal conductivity and the high specific heat compared to steel, The use of high strength concrete (HSC) in multi-story buildings has become increasingly popular because of its high loadbearing resistance at room temperature. However, it is reported that HSC performs worse than normal strength concrete (NSC) in fire because of its constituent materials (Gernay, 2016). The microstructure of the type of the concrete may play a great role in modifying the thermal properties of concrete (Luccioni et al., 2003). Moreover, the relative loss of compressive strength with temperature and the higher probability occurrence of explosive spalling are two important factors in HSC which leads to the redaction of the fire performance of this material (Kodur, 2014). Up to date, there is a still lack of information about composite columns made with HSC at elevated temperatures, particularly under combined compression and bending solicitations. Therefore, it is important to explore the effect of the type of concrete on the thermal and mechanical behaviour of composite column under different solicitations. In this study, we used a finite element method to investigate the behaviour of HSC due to the limitation of the simplified method to Normal Strength Concrete (NSC) (EN 1994-1-2, 2005).

In most composite structures with portal frame, compression load in columns are applied with bending moments (eccentric loading), which may create instability problems, particularly in fire accident. These two parameters must be taken into account during the design and the dimensioning of the structures. Some experimental (Su et al., 2016; Jiang et al., 2017; Ren et al., 2017) and numerical (Mago and Hicks, 2016; Feng et al., 2004) studies are conducted to analyse the behaviour of composite columns under combined compression and bending at elevated temperature. It was observed that the steel ratio, slenderness and the load eccentricity have a noticeable influence on the fire resistance of composite columns. Moreover, spalling of the concrete was found to decrease the fire resistance of composite

columns. The fire resistance of partially encased composite columns under loading eccentricity can be evaluated using the simplified method given in Eurocode 4 Annex G (EN 1994-1-2, 2005). However, when the eccentricity of loading is considered, the method of EN-1994-1-2 is somewhat relatively complex for an everyday practice and it needs necessarily the computer programming. For that reason, an advanced calculation method is developed based on finite elements approximation using ANSYS 18.2 (ANSYS 18.2, 2017) to determine the thermal behaviour of PEC column under eccentric loading. The comparison between the results of the different methods demonstrates the unsafety of the current calculation method used in Eurocode 4 (EN 1994-1-2, 2005).

1.4 Objectives of the study

Based on these above mentioned issues, the main objectives of this research are:

-To develop an efficient Non-linear 3-D finite element model to investigate the behaviour of axially loaded composite columns made from high strength concrete and normal strength concrete at elevated temperatures. The model was developed using the software ANSYS (ANSYS 18.2, 2017). This numerical analysis enables to assess the effect of the materials on the thermal and mechanical behaviour of composite columns under fire.

-To investigate the fire performance of eccentrically loaded concrete partially encased column (PEC), using the advanced calculation method (ANSYS 18.2, 2017) and the simple calculation method in Annex G of Eurocode 4 (EN 1994-1-2, 2005). This work examines the influence of a range of parameters on fire behaviour of the composite column including: eccentricity loading, slenderness, reinforcement, fire rating and fire scenario. In this study, ISO-834 (ISO834-1, 1999) was used as fire source.

1.5 Organisation of the thesis

The thesis is organised in seven chapters. In the following paragraphs, a brief description of the content of each chapter is presented.

The thesis starts by an introduction to the research work, where the objectives and motivations are mentioned. The fire safety is also included.

Chapter 2 presents the thermal behaviour of columns and materials according to European standards. The thermal and mechanical properties of steel and concrete are mentioned. The definition of the thermal actions and the nominal and natural fire curves are also described. Finally, a definition and state of the art about steel, reinforced concrete and composite column are presented.

In Chapter 3, we present a literature review about the many numerical and experimental investigations on the compression and combined compression and bending behaviour of composite columns at elevated temperature.

The analysis methods of composite columns are presented in Chapter 4. The first method deals with the simple calculation method according to Eurocode 4 (EN 1994-1-2, 2005). This method is based on the summation of four components to determine the uniaxial buckling resistance of PEC. The second part presents the advanced calculation method for the analysis of the uniaxial buckling load of the PEC composite column. The numerical simulations use the finite element ANSYS software with an uncoupled thermal and mechanical analysis under standard fire ISO-834.

The results of the behaviour of Pin-ended axially loaded composite column made from High Strength Concrete (HSC) and Normal Strength Concrete (NSC) at different fire rating classes are presented Chapter 5. Two types of column section were selected, namely HEB 160 profile totally encased with concrete (TEC) and HEB220 partially encased with concrete (PEC). The fire behaviour of the columns was tested according to ISO-834 standard fire.

Chapter 6 includes the numerical results of the fire resistance of eccentrically loaded around the minor axis of partially encased composite columns (PEC). These results are compared with those of the simplified method of EN-1994-1-2.

Finally, the main conclusions and proposals for the future work are summarized in the last chapter

Chapter 2

THERMAL BEHAVIOUR OF THE COLUMNS

2.1 Introduction

This chapter is divided into four parts, the first part introduces the structural technology and the fire resistance characteristics of steel; reinforced concrete and composite columns. The benefits of using these composite columns as well as some of their applications are described. The second part describes the thermal and mechanical material properties as a function of temperature as used by the numerical and the mechanical method to study the non-linear behaviour of composite columns under fire temperature. The different material component of the composite column are steel; concrete and reinforcement. Finally, we try to define the fire models and the heat transfer processes adopted in Eurocodes (EN 1991-1-2, 2009; EN 1992-1-2, 2004; EN 1993-1-2, 2005).

2.2 Columns under fire

2.2.1 Steel columns

At the beginning of the 20th century, steel quickly became the main material used in the construction of high-rise building. Compared to the reinforced concrete columns, the steel columns have great advantages because of its high rigidity and ductility, good strength in tension and compression, simple assemblies and procedures for rapid implementation and cost efficiency (Benlakehal et al., 2017). But this type of columns has many problems of instability (buckling-local buckling) due to the small thickness of the profiles. The problem of the local buckling is almost always encountered caused by the thin-walled steel constructions. Therefore, design calculations must always check the local buckling (Wang, 2002). The buckling problem is the dominant failure mode in steel column. However, for slender columns, the interaction between the buckling and the local buckling decreases clearly the bearing capacity of the thin steel columns (Yang and Hancock, 2004).

In 1990, a major fire accident occurred in a 14-storey building under construction in Broadgate, London. The fire temperature reached 1000°C during a substantial period of burning. As a result, very high temperatures were attained in the steel work. The building contractor's accommodation was completely destroyed, but the steel frame survived the fire without a collapse. During the fire, the heavier columns survived undamaged and the lighter columns deformed in the heat and contracted by as much as 100 mm, see Figure 2.1. This

behaviour of the steel frame could be attributed to the continuity of the structure; as soon as plastic deformation occurred in the failed columns (local failure), their loads were redistributed to other cooler members and the structure as a whole survived without a collapse. The structure was repaired in 30 days at a cost less than 4% of the total repair cost and no lives were lost (Wang, 2002). When designing steel structures, it is worthwhile to favour the local buckling in construction in order to avoid the entire collapse of the structure.

Figure 2. 1- Damaged steelwork after the Broadgate fire accident (Wang, 2002).

In 2001, Feng et al. (2001) reported some results of fire tests carried out on unloaded small panels (300 mm by 300 mm) constructed using gypsum boards, mineral wool insulation and channel studs. They observed some elevated temperatures load on short channel sections. These tests were performed under steady state in an electrically heated kiln. Recorded temperatures indicate near uniform temperature distribution in the column. The target temperatures were 250°C, 400°C, 550°C and 700°C. Figure 2.2 shows a set of samples after fire test. It is obvious that thin-walled columns undergo a variety of buckling modes as the increase of the temperature kiln, including local buckling, distortional buckling, global flexural buckling and torsional buckling.

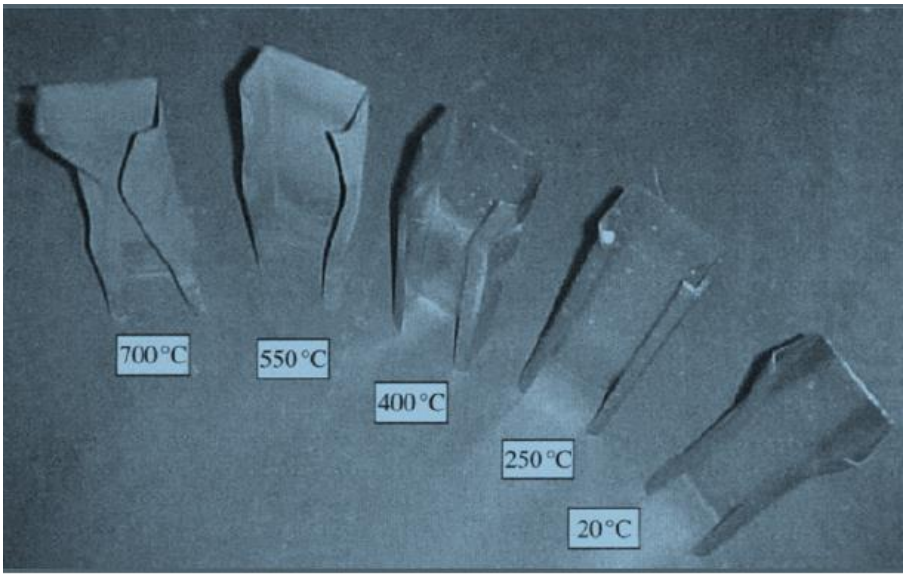

Figure 2. 2 - Deformed shape of thin-walled stub columns at different temperatures (Feng et al., 2001).

Wang et al (2014) tests indicate that the buckling resistance of the H-shaped steel columns decreases with the increase of the temperature, a degradation on the column strengths about 50% and 80 % at 450 °C and 650 °C respectively are reported. They concluded that the occurrence of a fire can lead to stability problems and therefore unsafety situations, see Figure 2.3. Steel columns need regular maintenance of protective coatings or concrete protection against corrosion and fire. The latter is the major disadvantage of the steel profile.

Figure 2. 3 - Buckling problem at high temperature (Wang et al., 2014).

2.2.2 Reinforced concrete columns

During the second half of the 20th century, reinforced concrete columns became the important structural elements for the building structures. The main function of this column is supporting the horizontal and the vertical loads, transmitting these loads to the foundations. Reinforced concrete columns are economically attractive alternatives to steel columns because of the low cost of concrete, the problem with these columns is their great weight and dimensions, low ductility, time consuming performance and bad resistance to shear and bending failure mode (MacGregor and Bartlett, 2000). The presence of a steel profile with concrete provides beneficial residual strength after concrete crushing which leads to improved ductility and higher bearing capacity (El-Tawil and Deierlein, 1999). The mechanical properties of concrete are significantly reduced during fire exposure. This may result in undesirable structural failures in the reinforced concrete column. Arioz (2007) reported that the damage of the concrete after being subjected to high temperatures can be roughly detected by observing the concrete surface, see Figure 2.4.

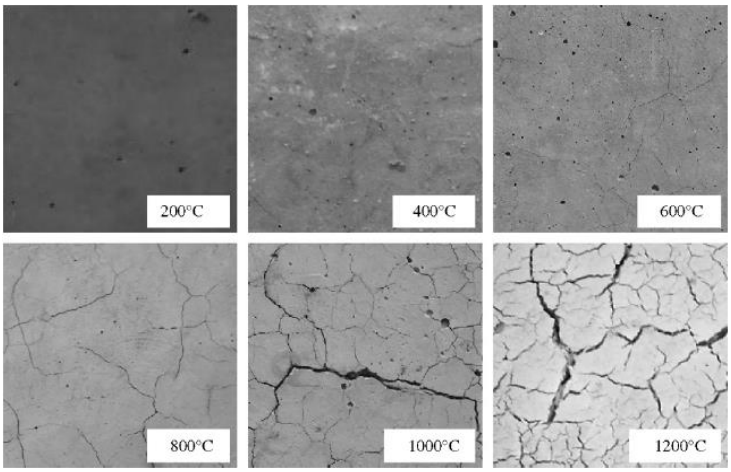

Figure 2. 4 - Surface texture of the concrete samples exposed to elevated temperatures (Arioz, 2007).

There was no visible effect on the surface of the specimens heated up to 400 °C. The concrete started to crack when the temperature increased to 600 °C but the effect was not significant at that temperature level. The cracks became very pronounced at 800 °C and extensively increased at 1000 °C. The specimens completely decomposed and lost their binding properties after exposure to 1200 °C, where the spalling of the samples due to excessive

cracking was observed. The high fire resistance of the concrete may be the greatest advantage regarding the steel.

In 2017, Shah and Sharma (2017) present results from fire resistance experiments on eight different types of reinforced columns (RC). The effect of concrete strength, confining reinforcement and the configuration of confining reinforcement on the fire resistance of RC columns were investigated. They found that the confinement parameters have an important role to play on the fire rating of the reinforced concrete columns. The disadvantage of high strength concrete (being prone to spalling) can be mitigated by the enhanced confinement of the RC columns, see Figure 2.5. The effect of confinement is more pronounced in normal strength concrete (NSC) columns than in high strength concrete (HSC). Increasing the confinement by 50% increases the fire resistance by 12% and 3.5% for NSC and HSC columns respectively. The temperatures in NSC column are generally lower than the corresponding temperatures in HSC column during the fire exposure. This variation can be attributed partly to the variation of the thermal properties of the two concretes and to the higher compactness (lower porosity) of HSC.

Figure 2. 5 - Reinforced concrete column after fire exposure (Shah and Sharma, 2017).

In 2017, Klabník and Králik (2017) made a comparison between reinforced concrete column and totally encased composite column. They concluded that the composite steel-concrete column has the highest level of fire resistance. The use of high strength concrete (HSC) over normal concrete (NSC) for design of multi-storey buildings, increases the axial capacity of the columns and reduce the size of the column. However, high-performance concrete

generally exhibits more cracking and spalling problem than normal concrete (Saric-Coric and Aïtcin, 2003) see Figure 2.6. Moreover, Gernay (2016) concluded that the relative loss of load bearing capacity during the fire is found to be more pronounced for HSC columns than for NSC columns. This is related to the higher susceptibility to spalling of HSC under fire.

Figure 2. 6 - Relative spalling of high strengths concrete at elevated temperature (Kodur, 2014).

2.2.3 Composite columns

Since the 1960s, composite steel-concrete columns have been used for multi-story building construction. This type of columns are used to support the vertical load-bearing elements. Composite columns are usually made with steel profile and reinforced or unreinforced concrete. The composite section is responsible for increasing the torsional and bending stiffness when compared to the same section of the steel profile. In addition to these advantages, the reinforced concrete is responsible for increasing the fire resistance (Lacki et al., 2018; Li et al., 2021). Composite columns are classified into two principal categories: partially or fully concrete encased steel profile and concrete filled tubular steel column, see Figure 2.7.

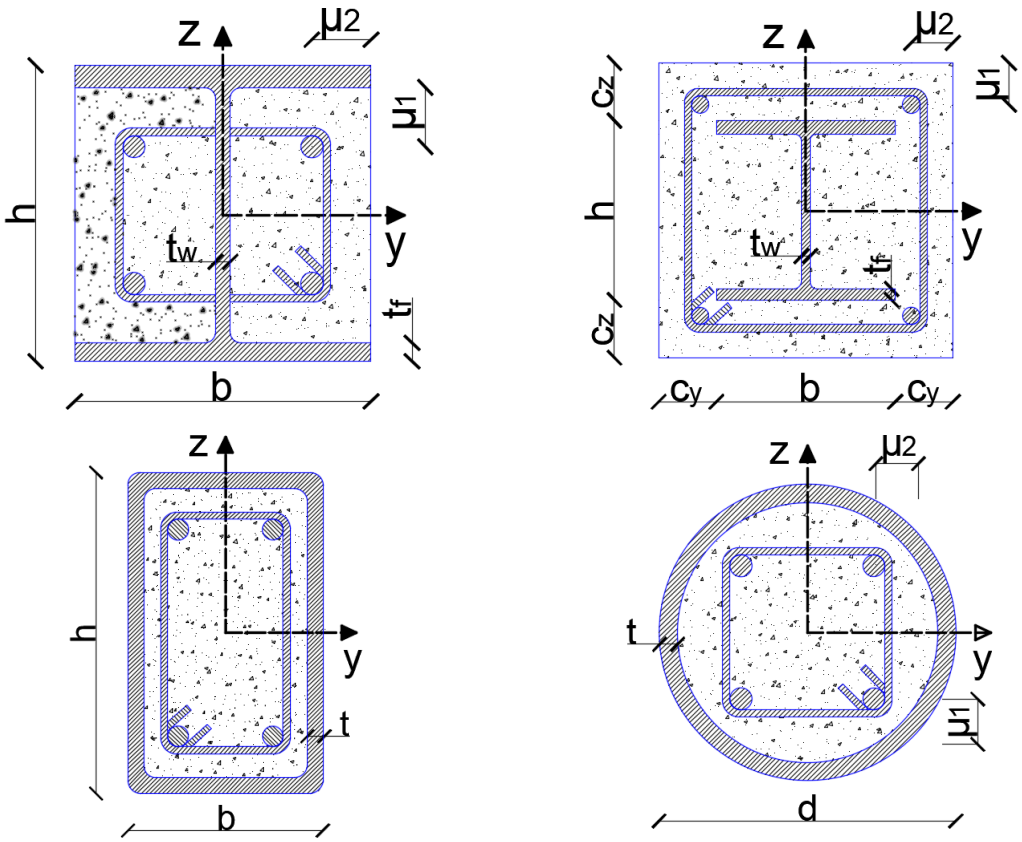

Figure 2. 7 - The most used different types of composite column.

Moreover, composite columns have many advantages compared with steel profile and reinforced concrete column; small cost and performance ratio; great fire resistance; improved load bearing and stiffness (Piloto et al., 2013); fast construction (because the steel section can support the construction loads), late serve as formwork for concrete and small required sections to support the same axial load of reinforced concrete.

2.2.3.1 Behaviour of composite columns at ambient temperature

In 1998, Scheich et al. (1998) present a load bearing capacity comparison of different columns (see Figure 2.8) with a buckling length of 4 m at ambient temperature, Partially encased column (PEC) with HEB240 profile, steel column (SC) with HEB280 profile and reinforced concrete column (RCC) with a section of 500*500 mm² reached the same applied axial load of 3.2 KN. It can be said that with the use of composite column section, an amount of material is saved and more space is available in the construction.

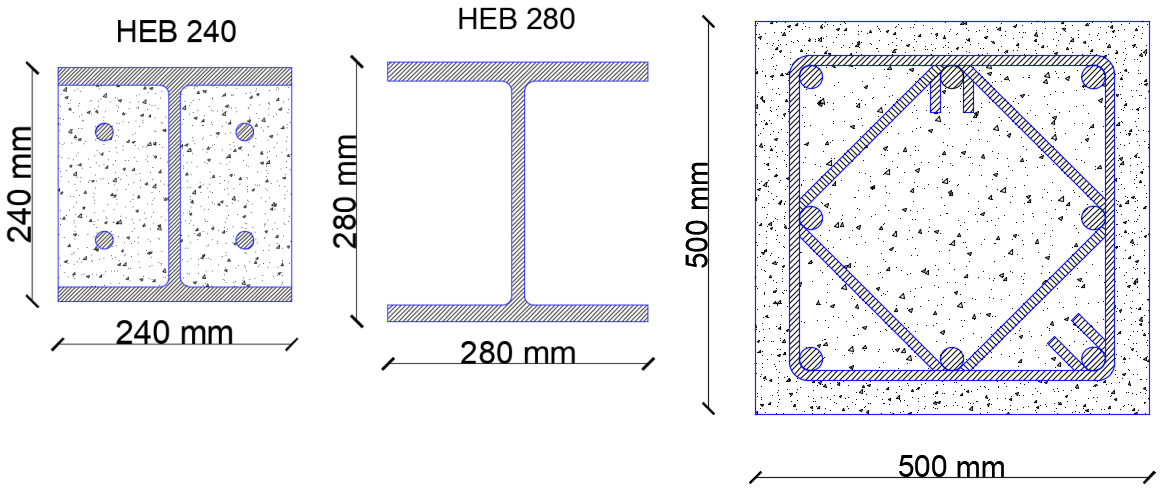

Composite Column Steel Column Reinforced Concrete Column

Figure 2. 8 - Load bearing capacity of different types of columns.

In 2014, Han et al. (2014) conducted a comparison study between a steel tubular column, a reinforced concrete (RC) stub column and a concrete filled steel tubular stub column without reinforcing bars under axial compression at ambient temperature. As illustrated in Figure 2.9, the summation of the steel tube and the RC columns ultimate strength (represented by the discontinuous line) gives a load bearing capacity less than that achieved by the CFST composite column acting alone. It is thought that the interaction of different materials of the composite section is responsible for the improvement of the load bearing capacity of the section.

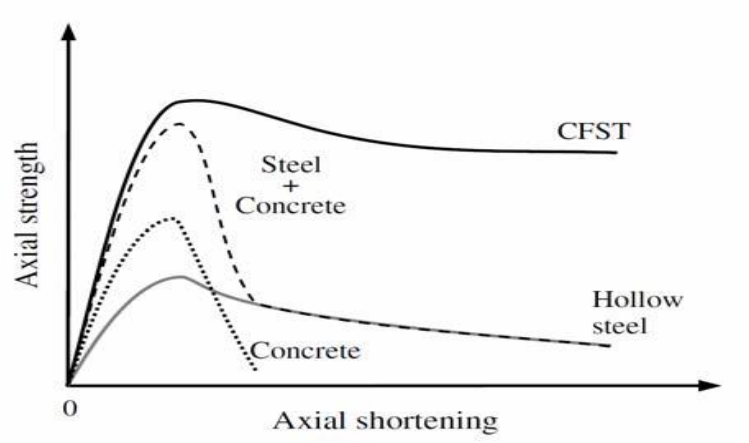

Figure 2. 9 - Axial compressive behaviour of stub columns (Han et al., 2014).

2.2.3.2 Behaviour of composite columns at elevated temperature

In 1964, Malhotra et al. (1964) presented the results of fourteen fire resistance tests on totally encased steel stanchions with free thermal elongation, The results showed that the concrete cover has a significant effect on the fire resistance, and the lightweight concrete has higher fire resistance compared to normal gravel concrete which has more spalling. Also they found that the load intensity played a very important role to minimise the fire resistance of the columns.

In 2003, Han et al. (2003) carried out an investigation on concrete filled hollow SHS and RHS columns subjected to the ISO 834 fire curve (ISO834-1, 1999), see Figure 2.10. The tests were performed on columns with and without fire protection. The main purpose of this study is to report a set of fire resistance tests on composite columns with square and rectangular sections and to develop formulas for the calculation of the fire resistance and fire protection thickness of this type of columns.

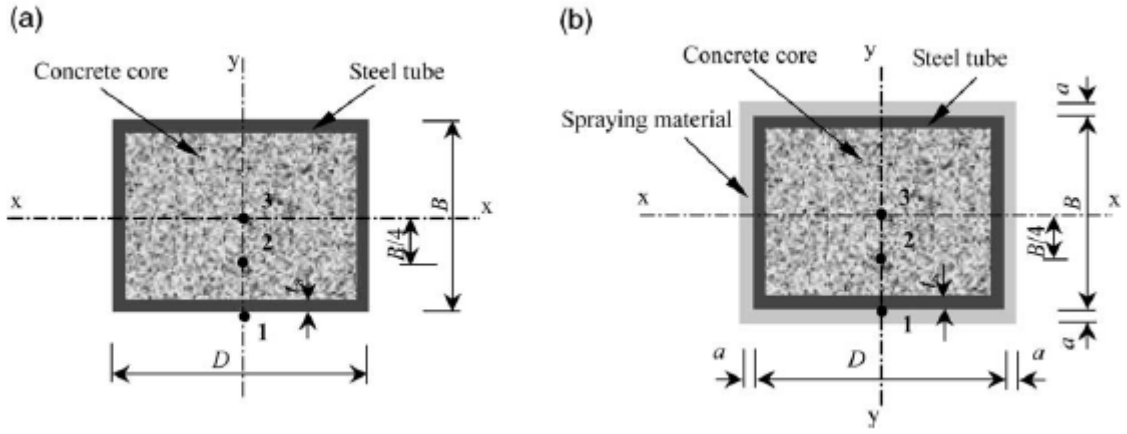

Figure 2. 10 - Typical cross-section of the specimens, (a) without fire protection; (b) with fire protection (Han et al., 2003).

They concluded that despite the presence of the concrete, the tested concrete-filled steel SHS and RHS columns still show a ductile behaviour. Also, the fire protection thickness for these composite columns can be reduced about 25% to 70% of that for bare steel tube columns. The authors found a relationship expressing the fire protection thickness for the composite columns as follows:

$$a = (2.5R + 22).C^{-(0.42+0.0017\lambda - 2.10^{-5}\lambda^2)} \qquad (2.\ 1)$$

Where R in [min]; C in [mm] is the perimeter of the column section.

It is noticed that all the tested columns failed by compression or overall buckling as shown in Figure 2.11. It seems that mode failure of the tested columns is independent of the section shape.

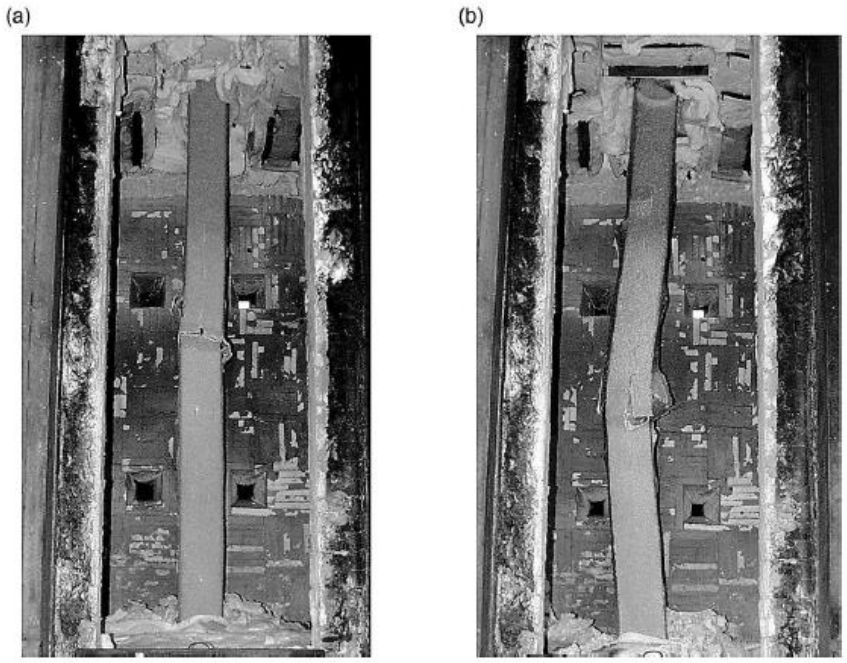

Figure 2. 11 - Typical failure mode of the tested columns. (a) RP-1; (b) RP-2 (Han et al., 2003).

Not long ago, Y. Dong and Prasad (2009) presented an experimental study on the behaviour of two full-scale composite steel frames under furnace loading. In one frame, the beam-to-column connections were protected while in the second frame the columns as well as the beam-to-column connections were protected, see Figure 2.12. The test results indicate that the fire resistance of the composite beam is significantly better than that of the steel column. Finally, experimental data on fire resistance of composite frames with conventional floor slab construction was compared with data from slim floor slab construction. Furthermore, experiment results show that the behaviour of the frames built with slim floor slab with a regard to the fire resistance rating is similar to that of the frames with conventional floor slab. It is suggested that in a typical composite structures, composite beams need less or no

insulation in comparison to composite column because of their position in the building when considering the different fire scenarios.

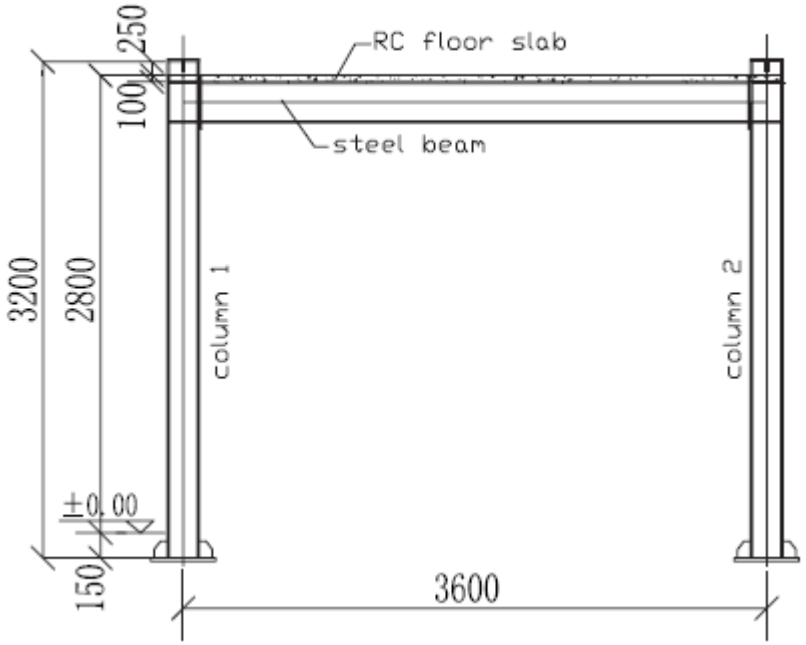

Figure 2. 12 - Construction of a single-story, one-bay, two-dimensional, sway portal frame with fixed bases for furnace testing. All dimensions are in millimetres (Dong and Prasad, 2009).

The research conducted by Mao and Kodur (2011) on the fire resistance of totally encased steel composite column (TEC) has shown that the temperatures in these columns increase more slowly under 3-side heating than that of 4-side heating indicating that the later scenario maybe the most unsafe case. The authors explain that the higher load and eccentricity produce cracking in the concrete under tension, which in turn accelerates temperature rise to the inner layers of the column. It results in an additional moment which enhances the reduction of fire resistance. The temperatures at the inner layers of concrete rise slowly as compared to the outer layers, and these measured temperatures decrease with increasing depth from the surface (see Figure 2.13).

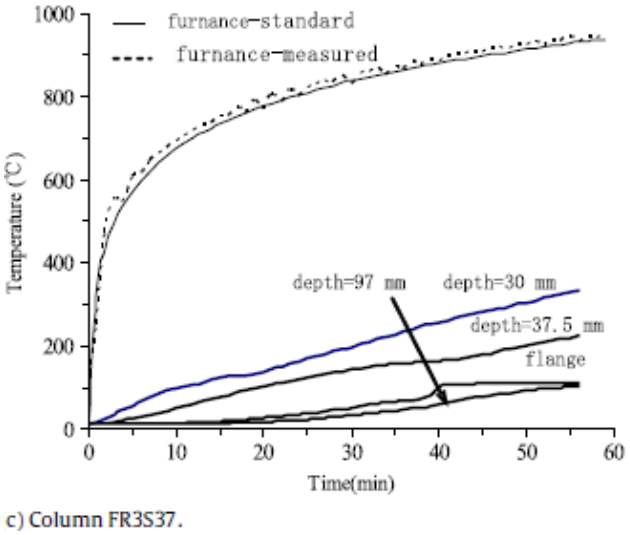

Figure 2. 13 - Measured temperatures as a function of time at various depths in CES columns (Mao and Kodur, 2011).

This is due to low thermal conductivity and high thermal capacity of the concrete, which slows down the heat penetration to the inner layers of concrete. Other studies conclude that the fire induces spalling in concrete, spalling leads to the reduction of the cross section of the column, accelerates the temperature rise in the internal steel profile and induces additional second order effects in TEC columns (Phan et al., 1996), see Figure 2.14.

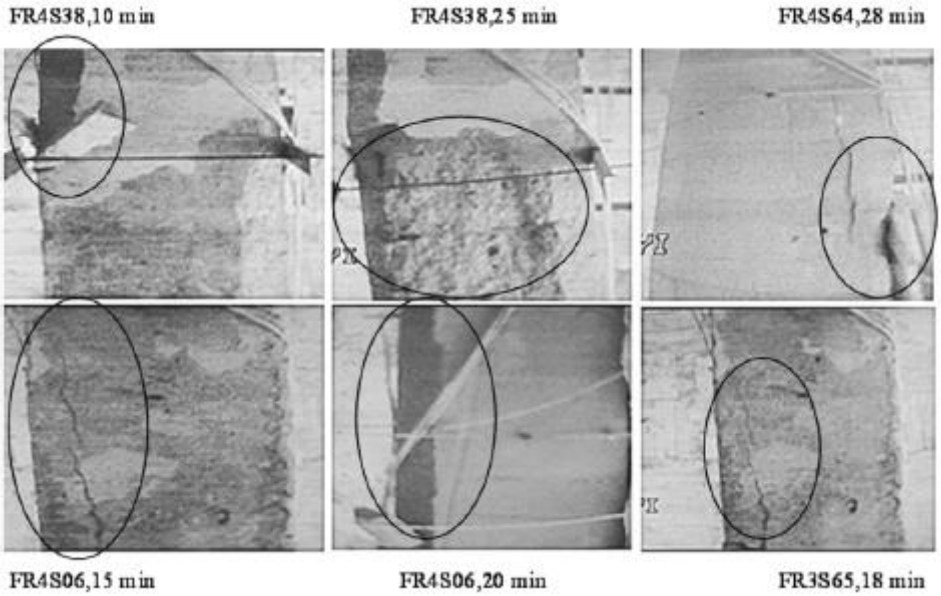

Figure 2. 14 - Illustration of spaling in TEC columns (Phan et al., 1996).

Romero et al (2011) presented a study in which sixteen fire tests were conducted on slender circular hollow section columns filled with normal and high strength concrete, subjected to concentric axial loads, see Figure 2.15.

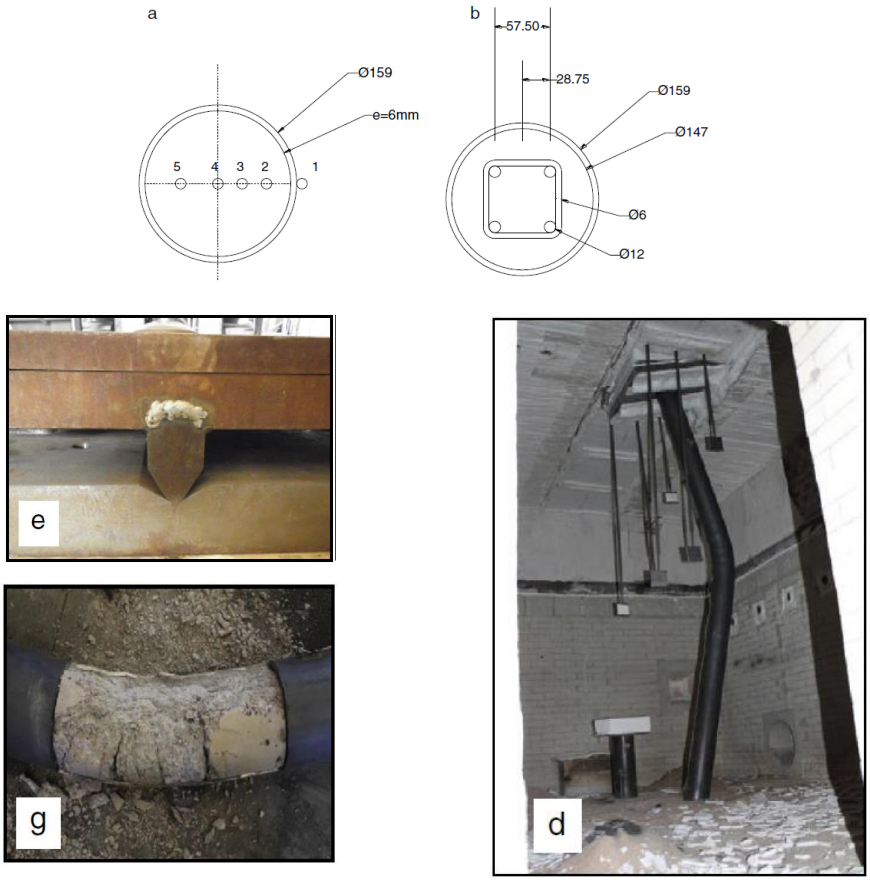

Figure 2. 15 - General view of: a) thermocouples layout. b) reinforcement arrangement. c) furnace d) column after failure e) pinned support f) burners g) concrete cracking at mid-section (Romero et al., 2011).

The test parameters were the nominal strength of concrete (30 and 80 MPa), the infilling type (plain concrete, reinforced concrete and steel fibre reinforced concrete) and the axial load level (20% and 40%). The columns were tested under fixed-pinned boundary conditions and the relative slenderness at room temperature was higher than 0.5 in all cases. In order to extend the results and understand the failure mode of such columns, a numerical model was validated against the tests. Furthermore, the aim of this paper is to study the influence, in a fire situation, of the use of high strength concrete, comparing to normal strength concrete. The results have shown that for slender columns subjected to high temperatures, the

behaviour of high strength concrete was different than for stub columns, spalling has not been observed in the experiments. Furthermore, the addition of steel fibres was not found very advantageous in slender columns, since no increment in terms of fire resistance was obtained for the columns which used this type of reinforcement. However, the addition of reinforcing bars seems to be the solution in some cases, where the use of external fire protection wants to be avoided in the design of HSS structures, since the reinforcing bars allow the tube to resist a higher axial load. From the results of this study, it can be concluded that in slender HSS columns filled with HSC, the spalling does not appear, probably due to the reduced length of the fire tests and the reduced size of the section, which does not generate high enough pore pressures inside the concrete as to produce such phenomenon. The utilization of reinforcing bars was found more useful for HSC than for NSC, because maintaining the same FRR the axial load applied can be increased.

Correia and Rodrigues (2011) developed a new experimental set-up, specially conceived for fire resistance tests on building columns, was used to study the fire resistance of partially encased steel columns with restrained thermal elongation, see Figure 2.16. The experimental set-up was conceived so that the axial and rotational restraint of the columns would be similar to the conditions in a real building. The parameters studied were the load level, the axial and rotational restraint ratios and the slenderness of the PEC. The main conclusion of this work is that for low load levels the stiffness of the surrounding structure has a major influence on the behaviour of the column subjected to fire. Increasing the stiffness of the surrounding structure led to reductions in the critical times. The same behaviour was not observed for the higher load levels.

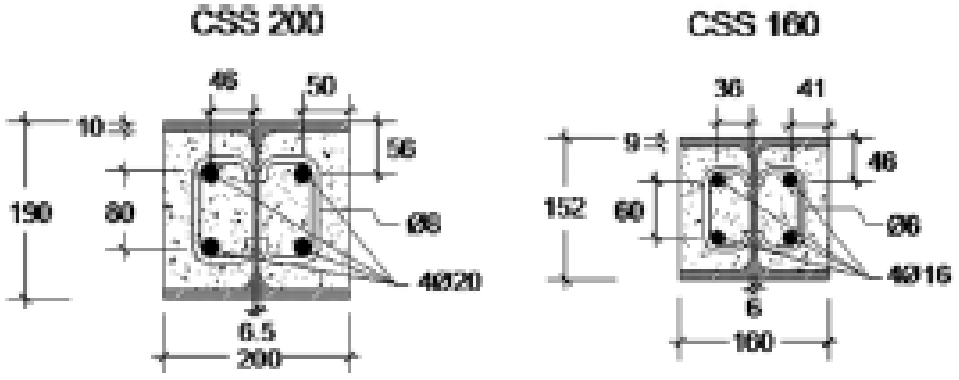

Figure 2. 16 - Cross sections of the test columns (Correia and Rodrigues, 2011).

In 2012, Dai and Lam (2012) studied the shape effect on the behaviour of axially loaded concrete filled steel tubular stub columns at elevated temperature, see Figure 2.17. It has been recognized that concrete filled tubular columns provide excellent structural properties such as high load bearing capacity, ductility, large energy-absorption capacity and good structural fire behaviour.

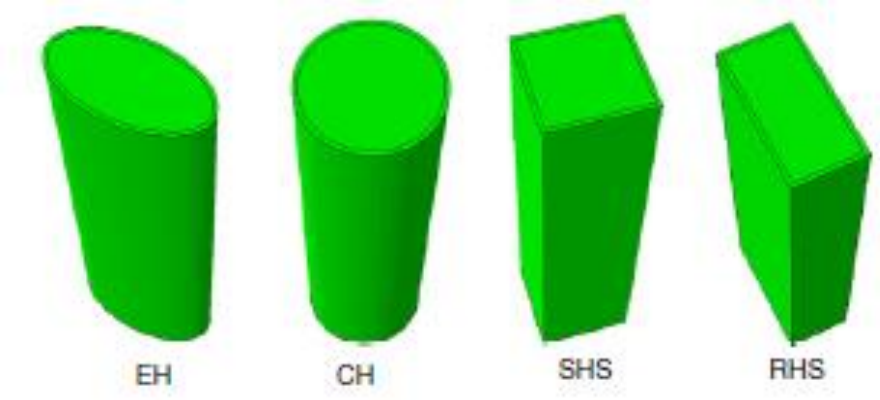

Figure 2. 17 - Typical shapes of selected concrete filled steel tubular stub columns (Dai and Lam, 2012).

The selected concrete filled steel tube stub columns are divided into three groups by equal section strength at ambient temperature, equal steel cross sectional areas and equal concrete core cross sectional areas. For columns with equal section strength at ambient temperature and columns with equal steel sectional areas, the columns with circular sectional shape have the longest fire exposing time before failure, followed by the columns with elliptical sectional shape. Columns with rectangular sectional shape are the worst in fire resistant duration. This shows the advantage of circular and elliptical sectional shapes.

2.3 Thermal properties of materials

The physical and mechanical behaviour of any material depends mainly of its properties. To understand the response of structures in a fire situation, it is necessary to know the changes that originate in the properties of the materials with which it is constructed. The increase in temperatures and the appearance of thermal gradients inside the elements cause thermal stresses and deformations, as well as the degradation of the material. This section analyses the thermal and mechanical properties of the constituent materials of composite column.

These properties are evaluated by taking into consideration the elevated temperatures considering the Standard Europeans proposals for both carbon steel (EN 1993-1-2, 2005) and concrete (EN 1992-1-2, 2004).

2.3.1 Steel profile and reinforcing

Thermal conductivity λ_a is the coefficient which define the rate at which heat arriving at the steel surface is conducted through the metal as defined in EN 1993-1-2 (EN 1993-1-2, 2005). The variation of thermal conductivity with temperature is represented in Figure 2.18. According to this figure, it is noticed that below 800 °C, the thermal conductivity decreases linearly with the increase of the temperature. However over 800 °C, it is not affected with the change of the temperature. The thermal conductivity of steel remains high even at very elevated temperatures. The thermal conductivity of steel λ_a should be determined from the following equations:

$$\lambda_a = 54 - 3{,}33.10^{-2}\theta_a \ [\text{w/mk}] \quad \text{for} \quad 20[°C] \le \theta < 800[°C]: \tag{2. 2}$$

$$\lambda_a = 27{,}3 \ [\text{w/mk}] \quad \text{for} \quad 800[°C] \le \theta \le 1200[°C]: \tag{2. 3}$$

Where: θ_a is the temperature of the steel.

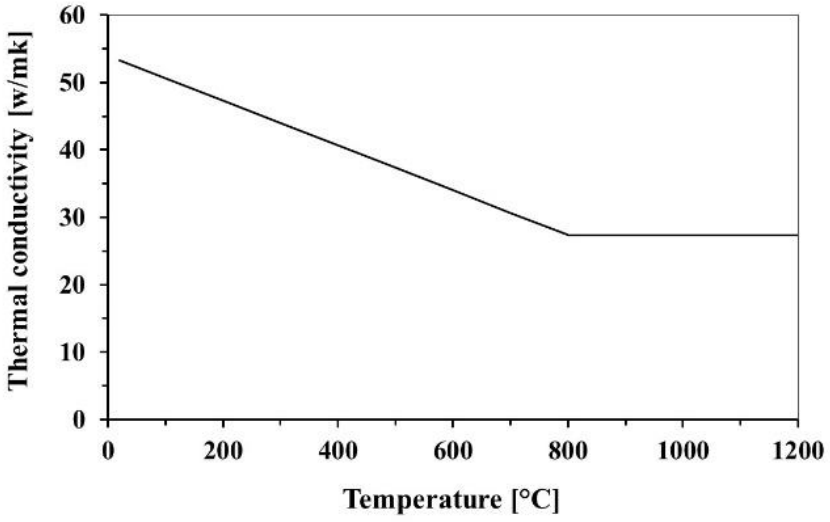

Figure 2. 18 - Thermal conductivity of steel.

The Specific heat C_a of steel represents the amount of energy that is necessary to raise the unit mass of steel temperature by 1 °C, it is also the measure of the materials ability to absorb heat (see Figure 2.19). It can be said that the steel material loses its characteristics when the temperature is around 735 °C, corresponding to a pic observed on the specific heat variation. The specific heat of steel C_a defined according to EN 1993-1-2 (EN 1993-1-2, 2005) by the following equations:

$$C_a = 425 + 7{,}73.10^{-1}\theta_a - 1{,}69.10^{-3}.\theta_a^2 + 2{,}22.10^{-5}.\theta_a^3 \left[J/Kg.K\right] \qquad 20\left[°C\right] \le \theta \le 600\left[°C\right] \qquad (2.\ 4)$$

$$C_a = 666 + 13002/\left(738 - \theta_a\right)\left[J/Kg.K\right] \qquad 600\left[°C\right] < \theta \le 735\left[°C\right] \qquad (2.\ 5)$$

$$C_a = 545 + 17820/\left(\theta_a - 731\right)\left[J/Kg.K\right] \qquad 735\left[°C\right] < \theta \le 900\left[°C\right] \qquad (2.\ 6)$$

$$C_a = 650\left[J/Kg.K\right] \qquad 900\left[°C\right] < \theta \le 1200\left[°C\right] \qquad (2.\ 7)$$

Where: θ_a is the temperature of the steel.

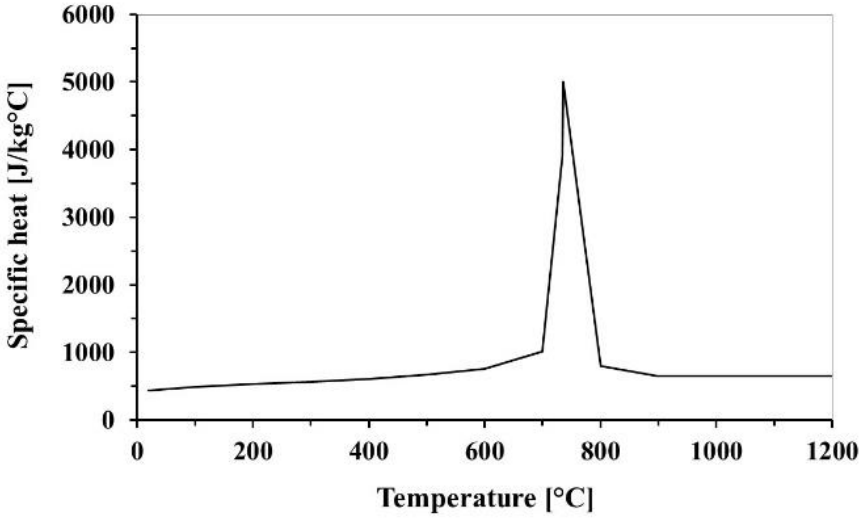

Figure 2. 19 - Specific heat of steel.

The density of steel is kept constant ρ = 7850 kg/m3, even when the temperature is modified as specified EN 1993-1-2 (EN 1993-1-2, 2005).

2.3.2 Concrete features

The physical properties of concrete are significantly influenced by the aggregate type, moisture content, and composition of concrete mix. During the recent years, Kodur and Khaliq (2011) have investigated the effect of fire on high strength concrete (HSC) experimentally and found some relationships witch involve the thermal concrete properties at elevated temperatures. These relationships are used to model HSC behaviour within a numerical study. However for normal strength concrete (NSC), the thermal properties can be found in Eurocede 2 (EN 1992-1-2, 2004).

The thermal conductivity λ_c depends generally on the material components of the concrete. Both concretes are made with siliceous aggregates. In Figure 2.20, the variation of the thermal conductivity for both concretes as a function of the temperature is plotted. The reduction of the thermal conductivity with the increase of the temperature is more pronounced for HSC than NSC as illustrated in Figure 2.20. This variation is attributed to the low water cement (*W/C*) ratio of HSC taken in the mix design of the concrete (Kodur, 2014). The thermal conductivity of concrete λ_c defined according to Eurocode 2 (EN 1992-1-2, 2004) for NSC and to Kodur and Khaliq (2011) for HSC by the following equations:

HSC:

$$\lambda_c = 2 - 0{,}0011.\theta\,[w/mk] \qquad (2.8)$$

NSC:

$$\lambda_c = 2 - 2451(\theta/100) + 0{,}0107.(\theta/100)^2\,[w/mk] \qquad (2.9)$$

Where: θ is the temperature of the concrete.

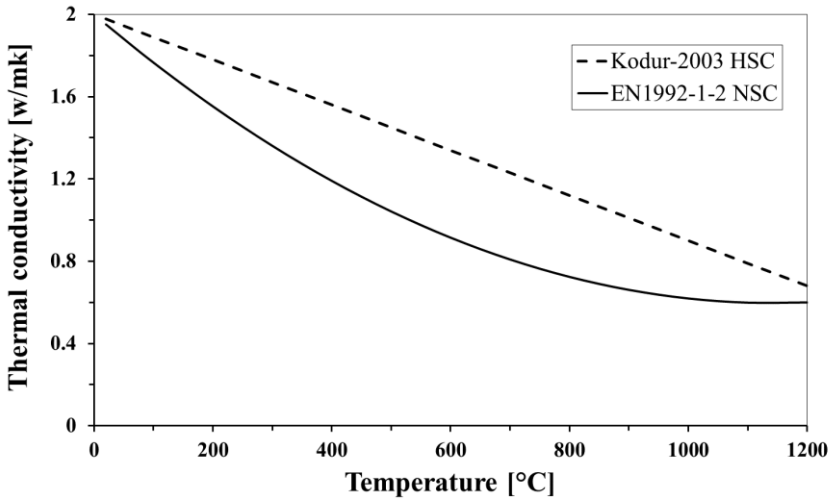

Figure 2. 20 - Thermal conductivity of high and normal strength concrete.

Specific heat C_p variation with the temperature for both concrete is illustrated in Figure 2.21. NSC displays a high peak at around 100 °C, however HSC presents a relative small peak at around 500 °C. Probably, these differences associated with the two curves are due to the concrete composition. At elevated temperatures (more than 600 °C), the specific heat values of both concretes become similar and the temperature will have no effect (Kodur and Khaliq, 2011). The specific heat variation for both concrete are defined by the following equations:

Normal strength concrete (NSC): $C_p = \left[2{,}20.10^6\right] / \rho$

$$C_p = 900 \quad \text{for} \quad 20[°C] \le \theta \le 100[°C] \qquad (2.\ 10)$$

$$C_p = 2020 \quad \text{for} \quad 100[°C] < \theta \le 115[°C] \qquad (2.\ 11)$$

$$C_p = 2020 - (\theta - 115)/12 \quad \text{for} \quad 115[°C] < \theta \le 200[°C] \qquad (2.\ 12)$$

$$C_p = 1000 - (\theta - 200)/2 \quad \text{for} \quad 200[°C] < \theta \le 400[°C] \qquad (2.\ 13)$$

$$C_p = 1100 \quad \text{for} \quad 400[°C] < \theta \le 1200[°C] \qquad (2.\ 14)$$

High strength concrete (HSC):

$$C_p = \left[(0{,}006.\theta + 1{,}6).10^6\right] / \rho \quad \text{for} \quad 20[°C] \le \theta \le 200[°C] \qquad (2.\ 15)$$

$$C_p = \left[2{,}20.10^6\right] / \rho \quad \text{for} \quad 200[°C] < \theta \le 400[°C] \qquad (2.\ 16)$$

$$C_p = \left[(0{,}011.\theta - 2{,}20).10^6\right]/\rho \quad \text{for} \quad 400[°C] < \theta \le 500[°C] \qquad (2.\ 17)$$

$$C_p = \left[(0{,}011.\theta + 8{,}80).10^6\right]/\rho \quad \text{for} \quad 500[°C] < \theta \le 600[°C] \qquad (2.\ 18)$$

$$C_p = \left[2{,}20.10^6\right]/\rho \quad \text{for} \quad 600[°C] < \theta \le 1200[°C] \qquad (2.\ 19)$$

Where: θ is the temperature of concrete. ρ is the density of concrete at ambient temperature.

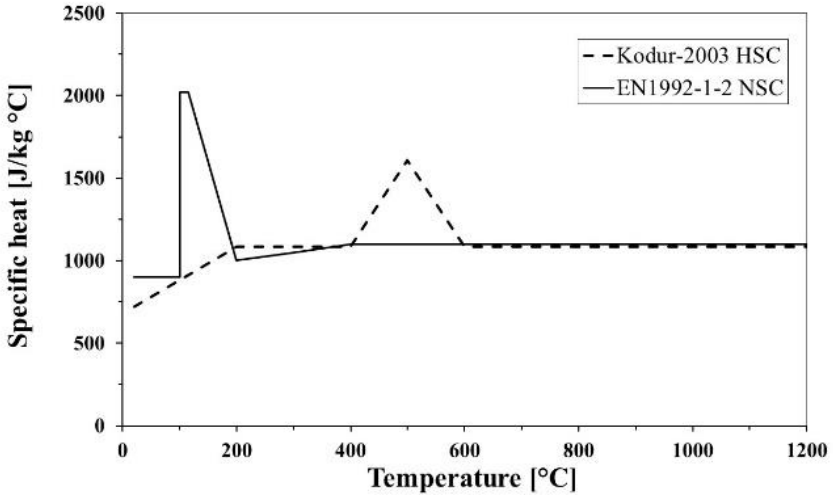

Figure 2. 21 - Specific Heat of high and normal strength concrete.

The specific density ρ of both types of concrete depends on the temperature variation as shown in Figure 2.22. NSC present a higher mass loss with regard to HSC, because of the evolution of concrete properties with time and the amount of water content in concrete composition. The Eurocode 2 (EN 1992-1-2, 2004) and Kodur and Khaliq (2011) recommends the following relationship for calculation of concrete density for both concrete.

Normal strength concrete: $\rho(\theta) = \rho(1 - 0{,}00005.\theta)$

$$\rho(\theta) = \rho \quad \text{for} \quad 20[°C] \le \theta \le 115[°C] \qquad (2.\ 20)$$

$$\rho(\theta) = \rho(1 - 0{,}02(\theta - 115)/85) \quad \text{for} \quad 115[°C] < \theta \le 200[°C] \qquad (2.\ 21)$$

$$\rho(\theta) = \rho(0{,}98 - 0{,}03(\theta - 200)/200) \quad \text{for} \quad 200[°C] < \theta \le 400[°C] \qquad (2.\ 22)$$

$$\rho(\theta) = \rho(0{,}95 - 0{,}07(\theta - 400)/800) \quad \text{for} \quad 400[°C] < \theta \le 1200[°C] \qquad (2.\ 23)$$

High strength concrete:

$$\rho(\theta) = \rho(1 - 0{,}00005\theta) \quad \text{for} \quad 20[°C] \le \theta \le 1200[°C] \qquad (2.\ 24)$$

Where: θ is the temperature of concrete. ρ is the density of concrete at ambient temperature.

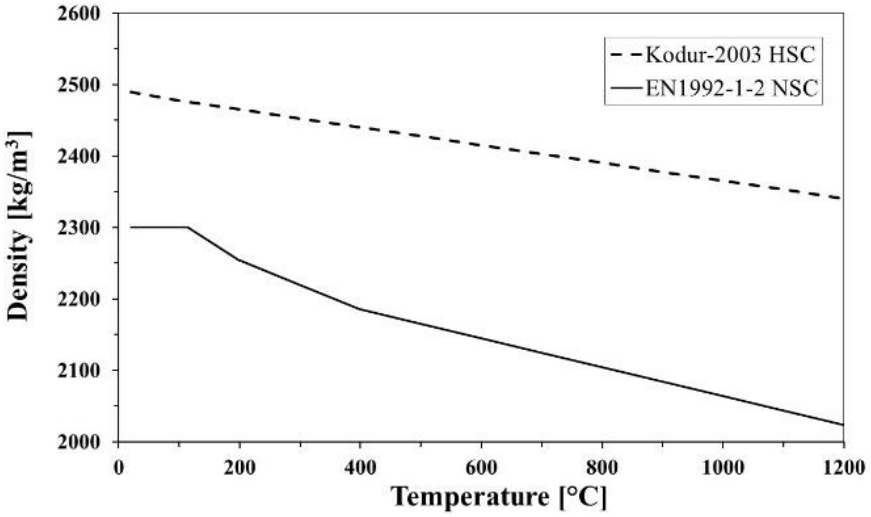

Figure 2. 22 - Density of high and normal strength concrete.

2.4 Mechanical properties

2.4.1 Steel Profile

The stress-strain relationship are used to determine the strength of structural elements in compression, tensile, shear and bending efforts. EN-1993-1-1 (EN 1993 -1-1, 2005) defines the mechanical properties at ambient temperature, the mechanical properties of the steel used in this study are shown in Table 2.1.

Table 2. 1- Mechanical characteristics of steel S275.

$E_a[GPa]$	$f_y[MPa]$	$f_u[MPa]$	$G_a[GPa]$	ν
210	275	430	81	0,3

Reduction coefficients are suggested to take into account the effect of high temperatures on the mechanical properties of the steel as elaborated by EN 1993-1-2 (EN 1993-1-2, 2005), see Figure 2.23. Reduction coefficients represent the degradation effect on the steel related to the temperature evolution in fire situation.

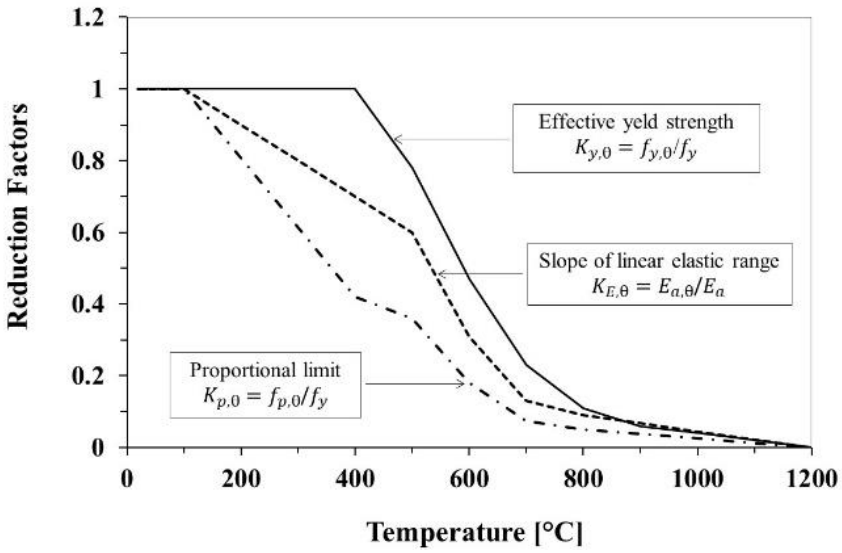

Figure 2. 23 - Reduction factors for steel s275 at elevated temperature.

The steel profile is known to suffer from a loss of resistance and rigidity when exposed to fire. To take into account the effect of high temperatures on the mechanical properties of the steel, EN-1993-1-2 (EN 1993-1-2, 2005) propose some relationships for evaluating the stress-strain curves as defined in Table 2.2.

The non-linear variation of the stress-strain curves are plotted in Figure 2.24, according to this figure, the properties of steel become weak when the temperature increases.

Table 2. 2 - Stress-strain relationship for steel at elevated temperatures.

Strain range	Stress σ	Tangent modulus
$\varepsilon \le \varepsilon_{p,\theta}$	$\varepsilon E_{a,\theta}$	$E_{a,\theta}$
$\varepsilon_{p,\theta} < \varepsilon < \varepsilon_{y,\theta}$	$f_{p,\theta} - c + (b/a)\left[a^2 - (\varepsilon_{y,\theta} - \varepsilon)^2\right]^{0.5}$	$\frac{b(\varepsilon_{y,\theta} - \varepsilon)}{a\left[a^2 - (\varepsilon_{y,\theta} - \varepsilon)^2\right]^{0.5}}$
$\varepsilon_{y,\theta} \le \varepsilon \le \varepsilon_{t,\theta}$	$f_{y,\theta}$	0
$\varepsilon_{t,\theta} < \varepsilon < \varepsilon_{u,\theta}$	$f_{y,\theta}\left[1 - (\varepsilon - \varepsilon_{t,\theta})/(\varepsilon_{u,\theta} - \varepsilon_{t,\theta})\right]$	-
$\varepsilon = \varepsilon_{u,\theta}$	0,00	-
Parameters	$\varepsilon_{p,\theta} = f_{p,\theta}/E_{a,\theta}$ $\varepsilon_{y,\theta} = 0{,}02$ $\varepsilon_{t,\theta} = 0{,}15$ $\varepsilon_{u,\theta} = 0{,}20$	
Functions	$a^2 = (\varepsilon_{y,\theta} - \varepsilon_{p,\theta})(\varepsilon_{y,\theta} - \varepsilon_{p,\theta} + c/E_{a,\theta})$ $b^2 = c(\varepsilon_{y,\theta} - \varepsilon_{p,\theta})E_{a,\theta} + c^2$ $c = \frac{(f_{y,\theta} - f_{p,\theta})^2}{(\varepsilon_{y,\theta} - \varepsilon_{p,\theta})E_{a,\theta} - 2(f_{y,\theta} - f_{p,\theta})}$	

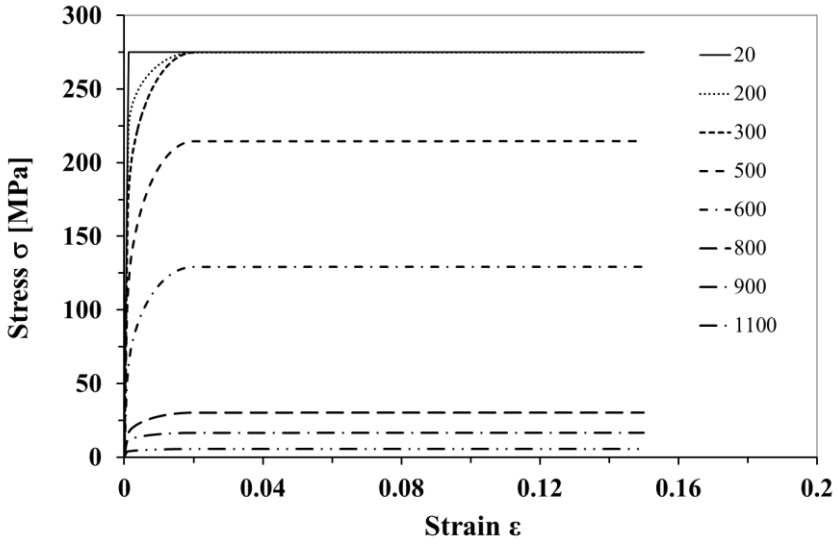

Figure 2. 24 - Stress-strain curve for steel S275 for different temperatures.

2.4.2 Steel reinforcement

The characteristics of the steel reinforcement at ambient temperature are described in Eurocode 2 (EN 1992-1-1, 2004). Steel S500 class B with the properties described in Table 2.3 is used in this study.

Table 2. 3 - Mechanical characteristics of steel reinforcement S500.

$E_a[GPa]$	$f_y[MPa]$	$f_u[MPa]$	$G_a[GPa]$	ν
210	500	540	81	0,3

When the steel reinforcement is subjected to high temperatures, the stress-strain relationship is reduced. Eurocode 2 (EN 1992-1-2, 2004) defines some reduction factors which are applied to the mechanical properties. See Figure 2.25. These factors are introduced in this analysis to consider the effect of fire on the effective yield strength f_y, the proportional limit f_p and the modulus of elasticity E_s.

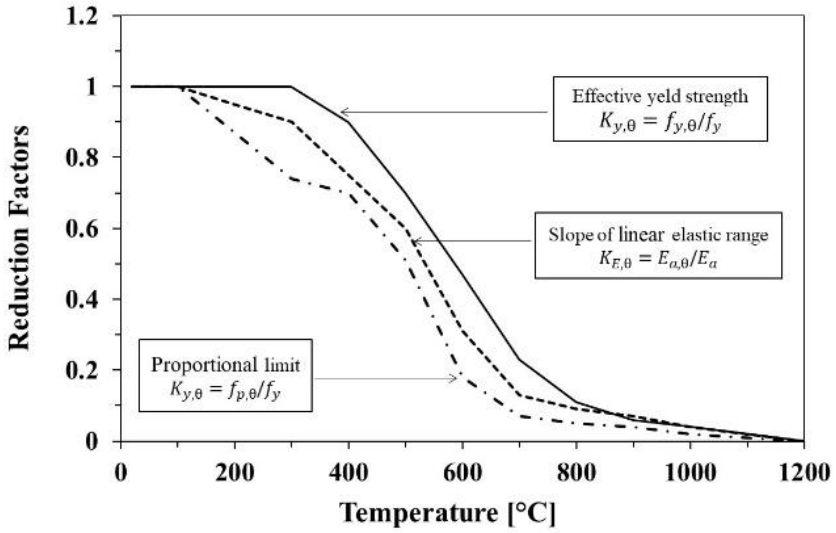

Figure 2. 25 - Reduction factors for steel reinforcement S500 at elevated temperature.

Eurocode 2 (EN 1992-1-2, 2004) establish the following equations to determine the stress-strain relationships, see Table 2.4. Figure 2.26 shows the variation of stress-strain curves plotted according to the following equations.

Table 2. 4 - Stress-strain relationship for reinforcement at elevated temperatures.

Strain range	Stress σ	Tangent modulus
$\varepsilon_{sp,\theta}$	$\varepsilon E_{s,\theta}$	$E_{s,\theta}$
$\varepsilon_{sp,\theta} < \varepsilon < \varepsilon_{sy,\theta}$	$f_{sp,\theta} - c + (b/a)\left[a^2 - (\varepsilon_{sy,\theta} - \varepsilon)^2\right]^{0.5}$	$\frac{b(\varepsilon_{sy,\theta} - \varepsilon)}{a\left[a^2 - (\varepsilon - \varepsilon_{sy,\theta})^2\right]^{0.5}}$
$\varepsilon_{sy,\theta} \le \varepsilon \le \varepsilon_{st,\theta}$	$f_{sy,\theta}$	0
$\varepsilon_{st,\theta} < \varepsilon < \varepsilon_{su,\theta}$	$f_{sy,\theta}\left[1 - (\varepsilon - \varepsilon_{st,\theta})/(\varepsilon_{su,\theta} - \varepsilon_{st,\theta})\right]$	-
$\varepsilon = \varepsilon_{su,\theta}$	0,00	-
Parameters	$\varepsilon_{sp,\theta} = f_{sp,\theta}/E_{s,\theta}$ $\varepsilon_{sy,\theta} = 0{,}02$ $\varepsilon_{st,\theta} = 0{,}15$ $\varepsilon_{su,\theta} = 0{,}20$	
Functions	$a^2 = (\varepsilon_{sy,\theta} - \varepsilon_{sp,\theta})(\varepsilon_{sy,\theta} - \varepsilon_{sp,\theta} + c/E_{s,\theta})$	
	$b^2 = c(\varepsilon_{sy,\theta} - \varepsilon_{sp,\theta})E_{s,\theta} + c^2$	
	$c = \frac{(f_{sy,\theta} - f_{sp,\theta})^2}{(\varepsilon_{sy,\theta} - \varepsilon_{sp,\theta})E_{s,\theta} - 2(f_{sy,\theta} - f_{sp,\theta})}$	

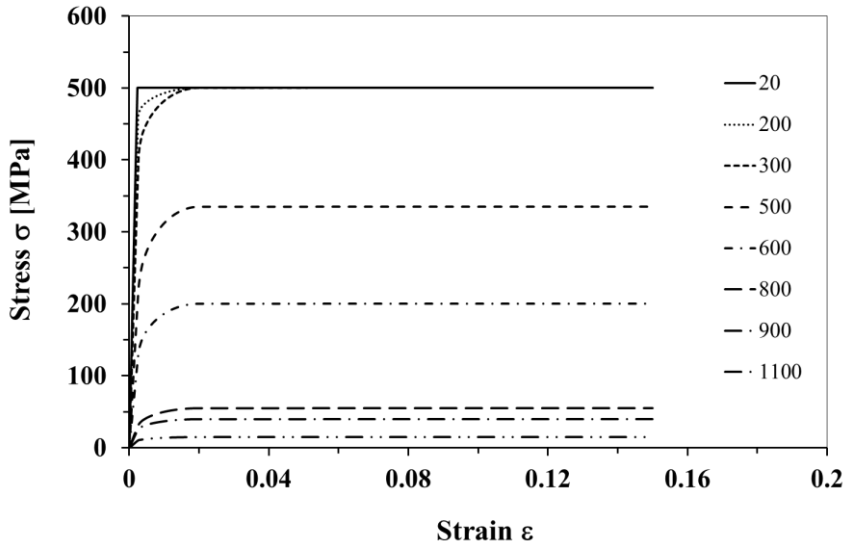

Figure 2. 26 - Stress-strain curve for steel reinforcement S500 for different temperatures.

2.4.3 Normal strength concrete

The compressive strength of concrete is the most basic and important mechanical behavior. It acts as a fundamental parameter to identify the strength grade and quality index of the concrete, and to determine the values of other types of mechanical behaviour. Stress-strain curve of concrete at elevated temperatures has crucial influence on the fire response of structural systems. The Normal Strengths Concrete [NSC] properties at room temperature are defined in Eurocode 2 (EN 1992-1-1, 2004). The mechanical characteristics of concrete C30/37 used in this study are defined in Table 2.5.

Table 2. 5 - Mechanical characteristics of concrete C30/37.

$f_{ck}[MPa]$	$f_{ck,cube}[MPa]$	$f_{cm}[MPa]$	$f_{ctm}[MPa]$	$E_{cm}[GPa]$	ε_{c1} [‰]	ε_{cu1} [‰]
30	37	38	2,9	33	2,0	3,5

Eurocode 2 (EN 1992-1-2, 2004) is the reference document for normal strength concrete materials under fire conditions. A reduction factor $K_{c,\theta}$, define as the reduction of the characteristic compressive strength of concrete with the increase of the temperature, is introduced and can be represented in Figure 2.27.

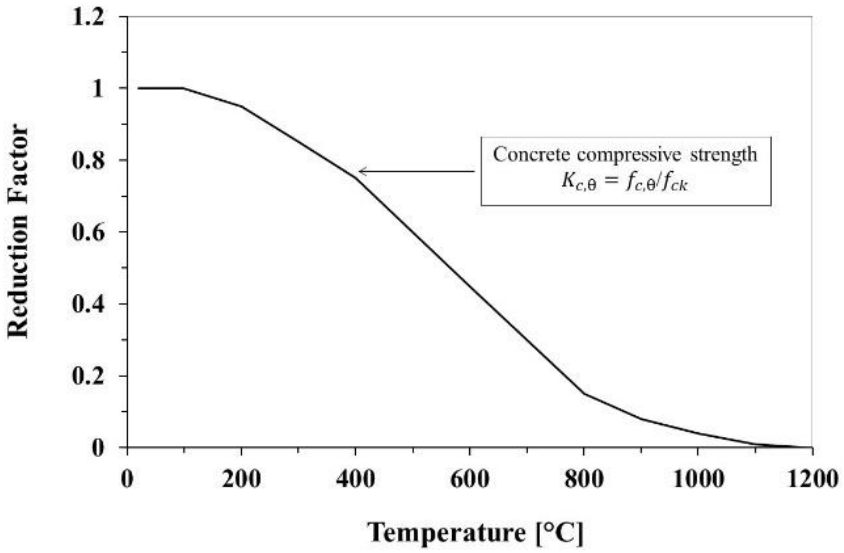

Figure 2. 27 - Reduction factors for concrete C30/37 at elevated temperature.

The stress-strain relationship for concrete at elevated temperatures is illustrated in Table 2.6 according to Eurocode 2 (EN 1992-1-2, 2004). The expected nonlinear variation of stress-strain for concrete C30/37 at elevated temperatures is illustrated in Figure 2.28. According to Figure 2.28, the normal strengths concrete present a relatively higher ductility at high temperatures with the decrease of the pic value of the compressive strength.

Table 2. 6- Stress-strain relationship for normal strength concrete at elevated temperatures.

Range	Stress σ(θ)
$\varepsilon \le \varepsilon_{c1,\theta}$	$\dfrac{3.\varepsilon.f_{c\theta}}{\varepsilon_{c1,\theta}\left(2+\left(\dfrac{\varepsilon}{\varepsilon_{c1,\theta}}\right)^3\right)}$
$\varepsilon_{c1,\theta} < \varepsilon \le \varepsilon_{cu1,\theta}$	For numerical purposes a descending branch should be adopted. Linear or non-linear models are permitted.

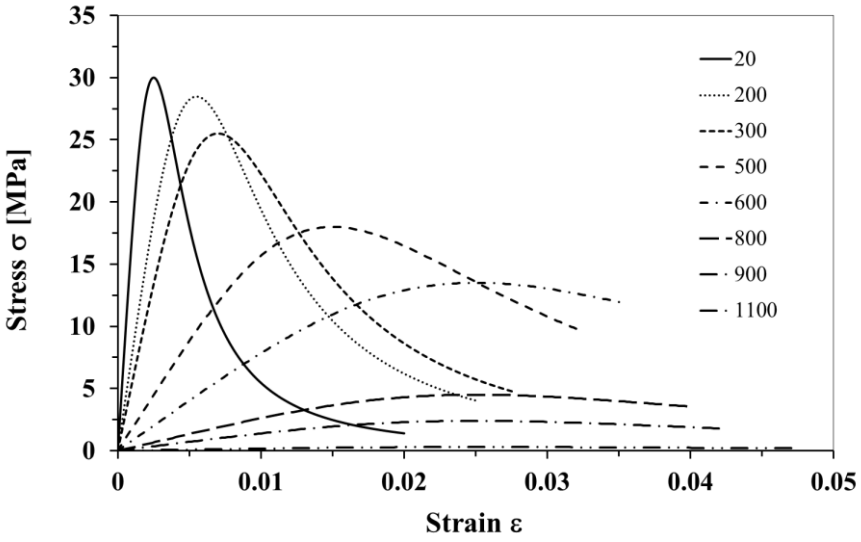

Figure 2. 28 - Stress-strain curve for concrete C30/37 for different temperatures.

2.4.4 High strength concrete

In this work, it is studied the influence of concrete strengths on thermal and mechanical behaviour of composite columns. HSC type C80/95 is used in this work (see Table 2.7).

Table 2. 7 - Mechanical characteristics of concrete C80/95

$f_{ck}[MPa]$	$f_{ck\,cube}[MPa]$	$f_{cm}[MPa]$	$f_{ctm}[MPa]$	$E_{cm}[GPa]$	ε_{c1} [‰]	ε_{cu1} [‰]
80	95	88	4,8	42	2.4	5

The effect of the temperature on the compressive strength of HSC is expressed by the coefficient $k_{c,\theta}$ according to the values given in Eurocode 2 (EN 1992-1-2, 2004). It can be noted that EN-1992-1-2 define only the reduction factors without giving equations for stress-stain curves for HSC. Class 2 is used for HSC C80/95 as recommended by EN-1992-1-2. According to Figure 2.29, it is observed that the down curve for the stress-strain of HSC at different temperatures is not the same as for that of NSC. Moreover, the reduction on the compressive strength due to the influence of the temperature is more pronounced for HSC than NSC.

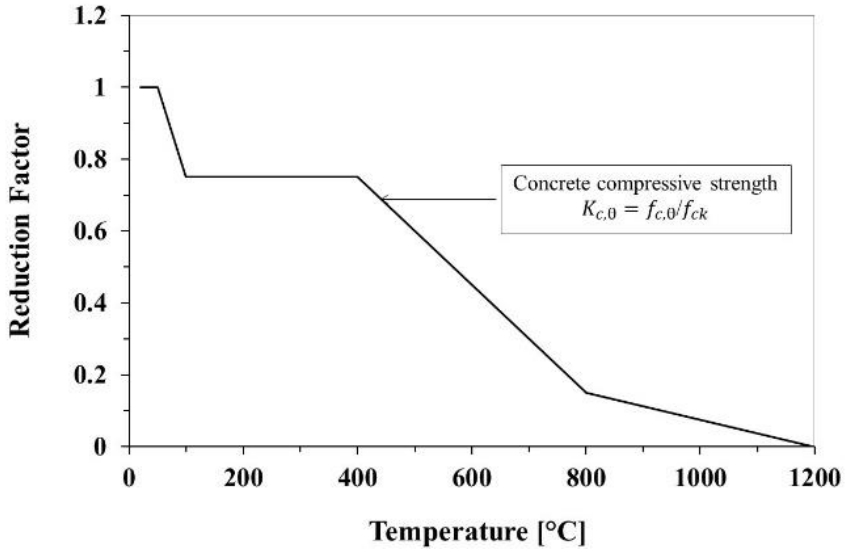

Figure 2. 29 - Reduction factors for concrete C80/95 at elevated temperature.

High Strengths Concrete [HSC] have a higher stiffness and higher initial slope when compared to NSC (Kodur et al., 2004). However, NSC presents relatively higher ductility than HSC at low and high temperature. The expected nonlinear variation of the stress-strain for HSC are plotted at different temperatures, see Figure 2.30 according to kodur and Wang relationship (Kodur et al., 2004), see Table 2.8.

Table 2. 8 - Stress-strain relationship for high strength concrete at elevated temperatures.

Range	Stress σ(θ)
$\varepsilon_c \le \varepsilon_{\max}$	$\sigma = f_c^{'}\left[1-\left(\frac{\varepsilon_{\max}-\varepsilon_c}{\varepsilon_{\max}}\right)^H\right]$
$\varepsilon_c > \varepsilon_{\max}$	$\sigma = f_c^{'}\left[1-\left(\frac{30(\varepsilon_c-\varepsilon_{\max})}{(130-f_{co}^{'})\varepsilon_{\max}}\right)^2\right]$

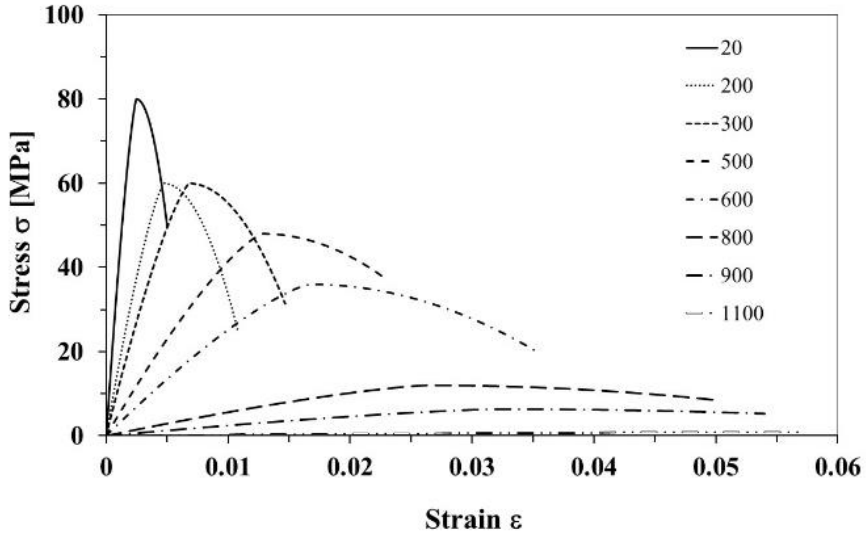

Figure 2. 30 - Stress-strain curve for concrete C80/95 for different temperatures.

2.5 Fire actions

2.5.1 Heat transfer $h_{net}^{\cdot}\left[W/m^2\right]$

The heat transfer is defined in Eurocode (EN 1991-1-2, 2009) as the net heat flux to unit surface area $\overset{*}{h}_{net}\left[W/m^2\right]$ of the element. All surfaces exposed to fire must assume the transfer of heat by convection and radiation according to the following equation:

$$\overset{*}{h}_{net} = \overset{*}{h}_{net,c} + \overset{*}{h}_{net,r}\left[W/m^2\right] \qquad (2.\ 25)$$

The convection heat transfer is presented as the energy transferred between a solid and a moving fluid or gas, each being at different temperatures. The rate at which this exchange of energy occurs is given by Newton's law of cooling as shown in the following equation.

$$\dot{h}^{*}_{net,c} = \alpha_c \left(\theta_g - \theta_m\right) \left[W/m^2\right] \qquad (2.\ 26)$$

Where, α_c is the heat transfer coefficient by convection [w/m2k], θ_g is the gas temperature in the vicinity of the fire exposed member [°C] and θ_m is the surface temperature of the member [°C].

The heat transfer by radiation represents the energy transfer between two bodies through electromagnetic waves. This form of energy transfer is exhibit by all bodies, and requires no medium for the heat to be transferred. It can even occur in a vacuum the amount of energy that can be radiated by a surface as expressed by Stefen-Boltzmann law equation.

$$\dot{h}_{net,r} = \phi \times \varepsilon_f \times \varepsilon_m \times \sigma \left[\left(\theta_r + 273\right)^4 - \left(\theta_m + 273\right)^4\right] \quad \left[W/m^2\right] \qquad (2.\ 27)$$

Where ϕ represents the view factor; ε_f represents the emissivity of the fire; ε_m is the emissivity of the surface of the element; σ is the Stephan Boltzmann constant 5,67x10-8 [w/m2k4]; θ_r represents is the effective radiation temperature of the fire environment [°C]; θ_m represents the surface temperature of the member [°C].

The emissivity of the material for steel and concrete is equal to ε_m = 0,7. The emissivity of the fire (flames) is assumed ε_f = 1,0 and the view factor can be assumed equal to 1,0 when not specified. The convection coefficient value depends on the velocity of the fluid or gas and should be considered equal to 25 for case of exposed surface with ISO834 curve (ISO834-1, 1999).

2.5.2 Nominal fire curves

A real fire in building grows and decreases according to the mass and energy balance within the compartment where it is originated. The amount of energy released depends on the quantity and type of combustible materials and the existing ventilation conductions in the compartment (Espinos Capila, 2012). The development of an enclosure fire may be divided

into four stages; Incipient, growth, fully developed and decaying or cooling stage, see Figure 2.31. The fastest temperature rises after a point of sudden generalized ignition which called flashover. At this stage, the most of the combustible materials is spontaneously burnt. After flashover, the temperature increases rapidly and the fire enter fully developed stage. The burning rate depends on the amount of the fresh air and the fire become ventilation controlled. After the fully developed stage most combustible material will be consumed and the burning rate of the fire start to decrease. This is known as decaying stage (Usach, 2016).

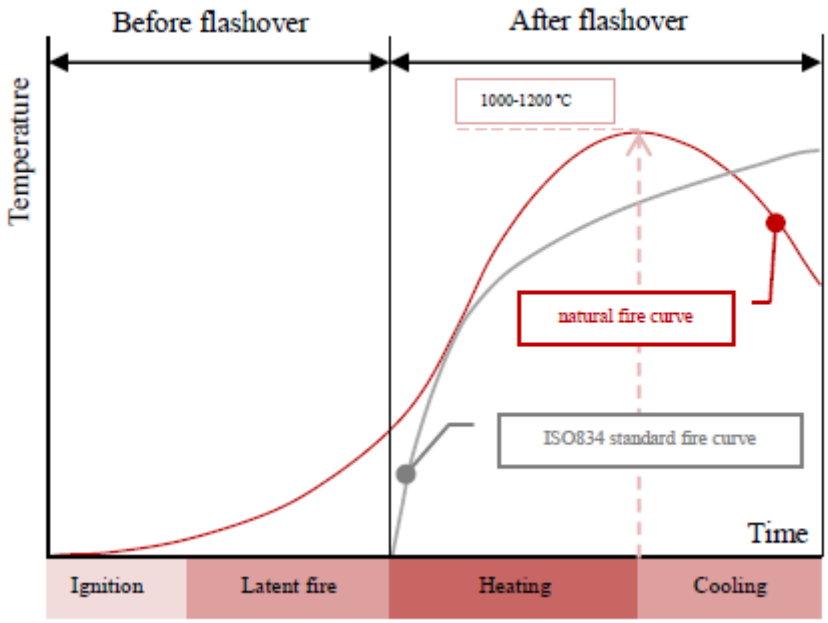

Figure 2. 31 - Different stages in the evolution of a real fire (Usach, 2016).

The action of fires on structures of buildings is characterized by scenarios of actions which are not always easy to determine. Eurocode (EN 1991-1-2, 2009) presents a different fire curves to model this fire actions.

The Standard temperature-time curve ISO834 (ISO834-1, 1999), also known as the Cellulosic curve and/or the standard nominal fire curve, is used as test method for determining the fire resistance of various elements of construction when subjected to standard fire exposure conditions. The test data thus obtained will permit subsequent classification on the basis of the duration for which the performance of the tested elements under these conditions satisfies specified criteria.

The standard temperature-time curve does not decrease in time. This curve realised with continuous alimentation by the fuel. The standard temperature-time curve is given according to the following expression.

$$\theta_g = 20 + 345.\log_{10}(8.t + 1)[°C] \qquad (2.\ 28)$$

The external fire curve is intended for the outside of separating external walls which are exposed to the external plume of a fire coming either from the inside of the respective fire compartment, from a compartment situated below or adjacent to the respective external wall. This curve is not to be used for the design of external steel structures for which a specific model exists. The external fire curve is given by:

$$\theta_g = 20 + 660(1 - 0{,}687.e^{-0{,}32t} - 0{,}67.e^{-0{,}38t})[°C] \qquad (2.\ 29)$$

The hydrocarbon is a nominal temperature-time curve used in case where storage of hydrocarbon materials makes fires extremely severe. This curve is developed by oil company Mobil in the 1970s. From Figure 2.32 we can see that the hydrocarbon curve presents a heist increase in the temperature witch rich 900 °C in the first 5 min. The hydrocarbon temperature-time curve is given by:

$$\theta_g = 20 + 1080.(1 - 0{,}325.e^{-0{,}167.t} - 0{,}675.e^{-2{,}5.t})\ [°C] \qquad (2.\ 30)$$

Where θ_g is the gas temperature in the fire compartment [°C], t is the time [min], assuming the coefficient of heat transfer by convection equal to α_c = 25 [w/m2k] for the ISO 834 and the external fire curve. However, α_c = 50 [w/m2k] for the hydrocarbon fire curve.

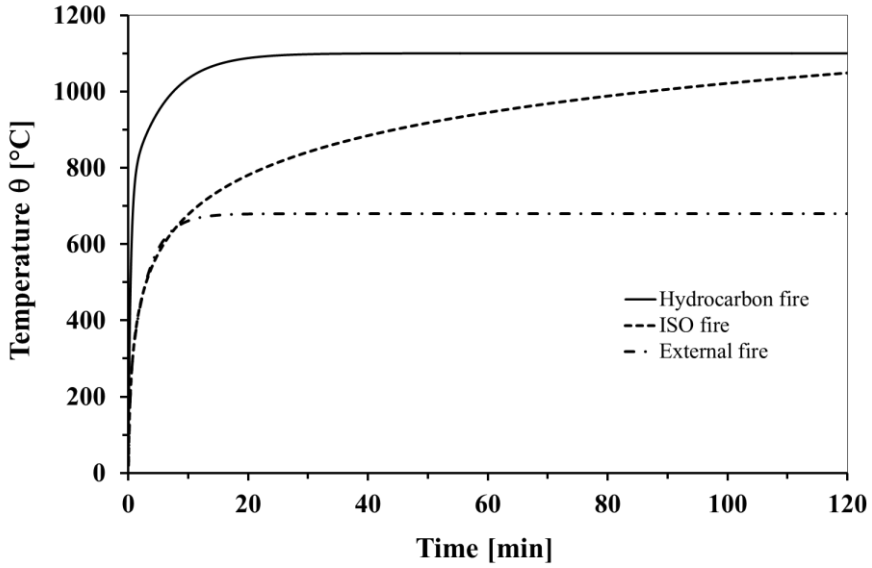

Figure 2. 32 - Nominal fire curves.

2.5.3 Natural fire curves

2.5.3.1 Simplified Fire Models

The simple fire models are based on specific physical parameters that, despite of obtaining satisfactory results, have some limitations in its application. The temperature is determined from a compartment fire model (parametric fire model as proposed by Eurocode 1 (EN 1991-1-2, 2009) or models of localized fire, which depend among other parameters, the fire load and characteristics of the compartment on fire. Assuming a uniform distribution of temperature in the compartment, a model of fire compartment should be used. If we assume a non-uniform distribution of temperatures, a localized fire model should be used. When using the simplified fire methods, the coefficient of heat transfer by convection should be taken the value $\alpha_c = 35$ w/m^{2}k.

In a localized fire, there is an accumulation of smoke and hot gas in a layer below the ceiling (upper layer), with a horizontal interface between this layer and the cold lower layer when the gas temperature remains much lower. The thermal action of a localized fire can be assessed using the method Heskestad (Heskestad and Hamada, 1993). Localized fire temperature-time curve may be calculated according to:

$$\theta_z = 20 + 0{,}25.Q_c^{2/3}\left(Z - Z_0\right)^{-5/3}\left[°C\right] \qquad (2.\ 31)$$

Where θ_z is the temperature of the plume along the vertical flame axis [°C], Q_c is the convective part of the heat release rate [w] , Z is the height along the flame axis and Z_0 is the virtual origin of the fire, see Figure 2.33, this figure presents an example of localised fire curve.

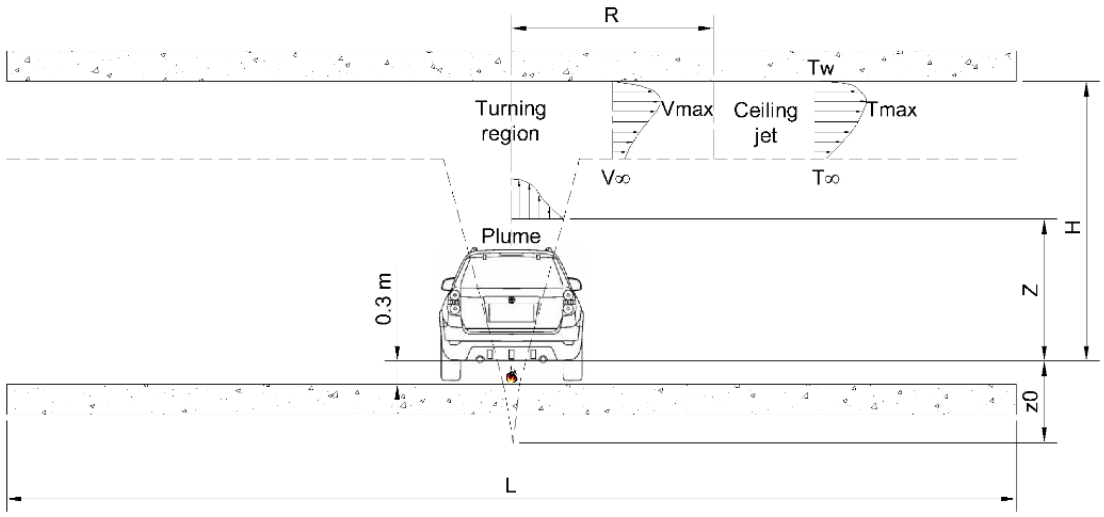

Figure 2. 33 - Parameters of localized fire.

The gas temperature representing the fire can also be given by the parametric temperature–time curve model given from annex A of Eurocode 1 (EN 1991-1-2, 2009). This annex presents all equations required to calculate the temperature–time curve based on the value of the parameters that describe the particular situation. The model is valid for fire compartments up to 500 m^2 of floor area and a maximum height of 4 meters without openings in the roof.

Parametric fires provide a simple means to take significant account physical phenomena that can influence the development of a fire in a particular building. As nominal fires, they provide a temperature-time curves, but these curves include some parameters intended to represent some real aspects in fire compartment. These curves have a heating and a cooling phases, see Figure 2.34. The heating and cooling phase can be defined by the next equations.

$$\theta_g = 20 + 1325.\left(1 - 0{,}324.e^{-0{,}2.t^*} - 0{,}204.e^{-1{,}7.t^*} - 0{,}472.e^{-19.t^*}\right) [°C] \quad (2.\ 32)$$

$$\theta_g = \theta_{\max} - 250.\left(t^* - t^*_{\max}\right) [°C] \quad (2.\ 33)$$

Where θ_g is the gas temperature in the fire compartment [°C], t is the time [min]; t^* is the time parameter that depends on the time factor, which itself depends on the opening factor and the thermal absorptivity.

$t^* = t * \Gamma\ [h],\ \Gamma = [o/b]^2 / (0{,}04/1160)^2, b = \sqrt{\rho.c.\lambda}$ with 100<b<2200 [J/m^{2}s$^{1/2}$K]

ρ is the density of boundary of enclosure [kg/m^3]

C is the specific heat of boundary of enclosure [J/kg.K]

O is the opening factor: $O = A_v h_{eq} / A_t$ with 0,02<O<0,20 [m$^{1/2}$]

A_v is the total area of vertical openings on all walls [m2]

H_{eq} is the weighted average of window heights on all walls [m];

A_t is the total area of enclosure (walls, ceiling and floor, including openings) [m^2]

Figure 2.34 represents the variation of temperature versus time for natural fire curves.

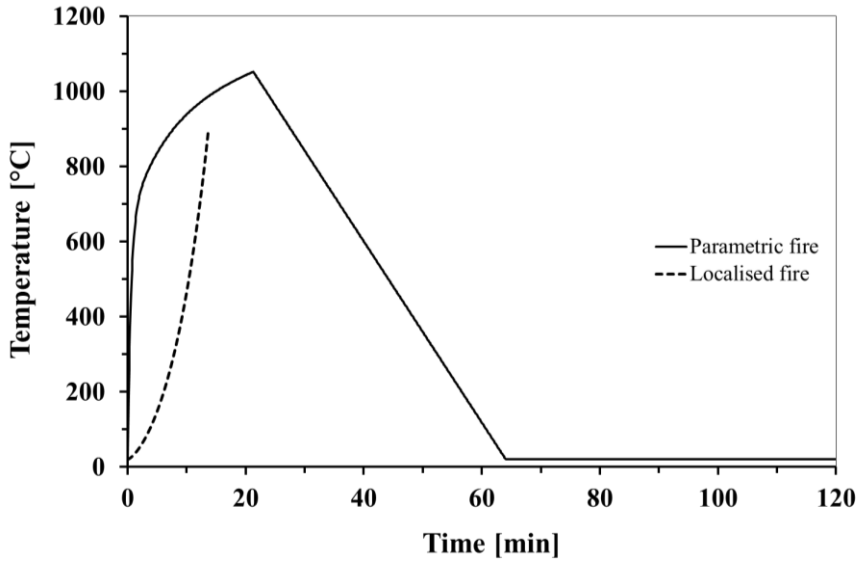

Figure 2. 34 - Example of parametric and localised fire.

2.5.3.2 The CFD (Computational Fluid Dynamics) fire model

The CFD fire model is given in Eurocoede 1 (EN 1991-1-2, 2009). The field models are based on equations that describe the phenomena of combustion and heat transfer, in which the initial conditions are needed in advance. In these models, the compartment is divided into a finite number of elements, to each one the energy balance is made, obtaining as a result, in particular, the values of temperature, velocity and pressure (Correia, 2011). These equations represent the mathematical statements of the conservation laws of physics:

- The mass of a fluid is conserved;
- The rate of change of momentum equals the sum of the forces on a fluid particle (Newton´s second Law);
- The rate of change of energy is equal to the sum of the rate of heat increase and the rate of work done on a fluid particle (first law of thermodynamics).

For any of the presented models, the coefficient of heat transfer by convection should be αc = 35 [W/m2], if no more precise information is available.

2.6 Conclusion

From the literature presented in this chapter, it's became clear that the composite column present a high thermal and mechanical performance compared to the steel or the reinforced concrete column. This chapter presented the thermal and mechanical properties data used in this study for the different material component of the composite column (steel; concrete and reinforcement) at elevated temperatures, moreover, the thermal action and heat transfer according to EN-1991-1-2 exposed in this chapter, will be used in the parametric study in chapter 5 and chapter 6.

Chapter 3

STATE OF THE ART OF COMPOSITE COLUMNS UNDER FIRE

3.1 Introduction

This chapter provides a review of previous research works, which are related to this research study. The literature review includes two parts. In the first part we present both numerical and experimental research on thermal and mechanical behaviour of different types of composite columns under compression loading. In the second part, review is performed on previous research of composite columns at ambient and elevated temperatures under combined compression and bending loading condition.

3.2 Compression

3.2.1 Experimental research

In 2007, Huang et al (2007) published a study regarding the effects of the axial restraint on the behaviour of composite columns subjected to fire. During the analysis the author tested four unprotected real-sized axially-restrained encased I-section composite columns. All columns height were 3.54m and were subjected to a compression load ratio of 0.7, see Figure 3.1.

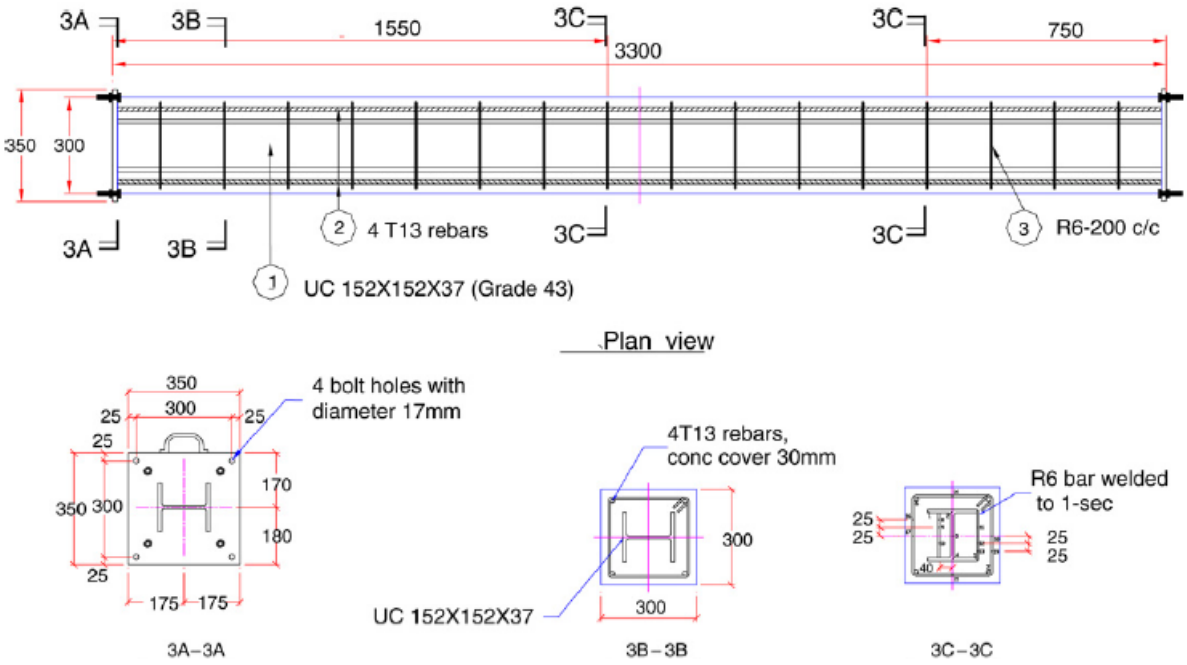

Figure 3. 1 - Specimen details (Huang et al., 2007).

A particular heating curve with two ascending phases was adopted. Different degrees of axial restraint were investigated. The authors ended the column fire resistance reduced under the axial restraint. All columns failed in flexural buckling mode. Moreover, it was observed that all specimens exposed concrete spalling related to the fire heating, which was responsible for a big reduction of the column fire resistance (Figure 3.2).

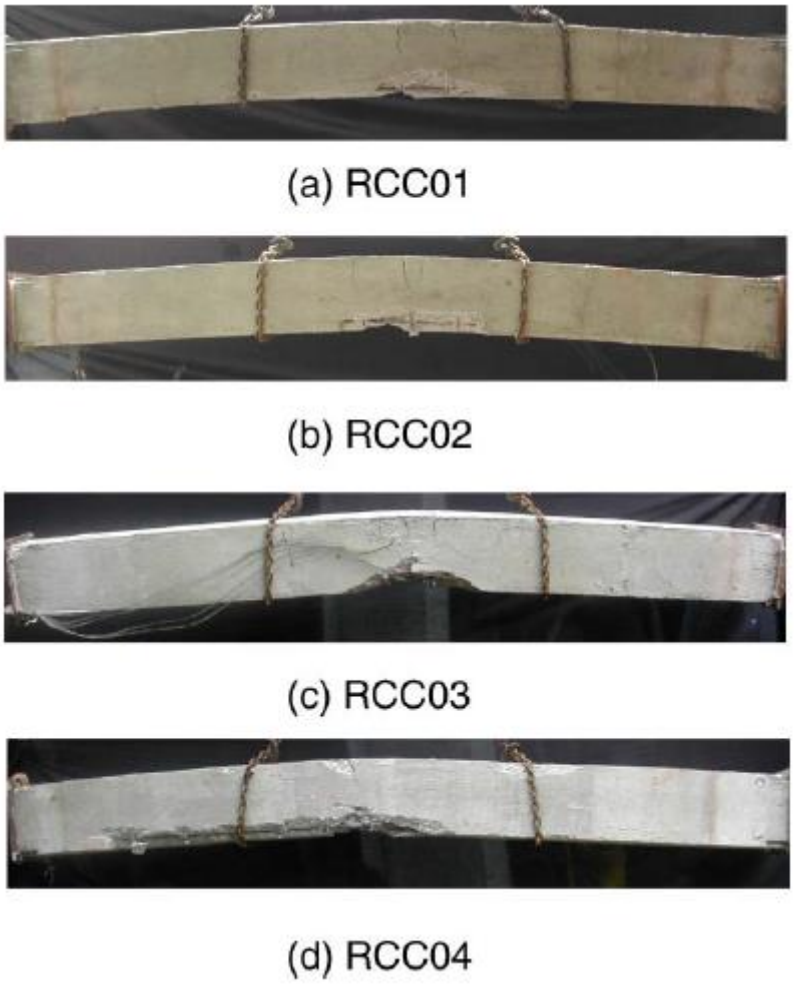

Figure 3. 2 - Pictures of tested specimens (Huang et al., 2007).

A comparison with the fire resistance calculated by Eurocode 4 (EN 1994-1-2, 2005) showed that the predictions of that standard are conservative. All of the mentioned experimental tests reported in these studies were carried out with either pin-ended or built in columns. Usually, real boundary conditions of a column are not pin-ended nor built-in. In real word structure columns are not only submitted to an axial load but also to a rotational restraint load. This fact has not been considered in most of the studies investigated up to

now. The axial restraint is known to have a detrimental effect on the fire resistance of the columns while the rotational restraint may possess a beneficial effect.

In 2013, Lin-Hai Han et al (2013) tested five full-scale circular and square concrete filled stainless steel tubular (CFSST) columns subjected to axial compression under standard fire test conditions see Figure 3.3. The test parameters include load level ranged from 0.15 to 0.45, sectional type both circular and square and columns dimension. A finite element model (FE) was introduced to simulate the temperature development and therefore the structural behaviour of CFSST columns by adopting Program ABAQUS. The results were verified by the present test data. Test results showed that the fire resistance of CFSST columns is considerably influenced by the sectional dimension and load level.

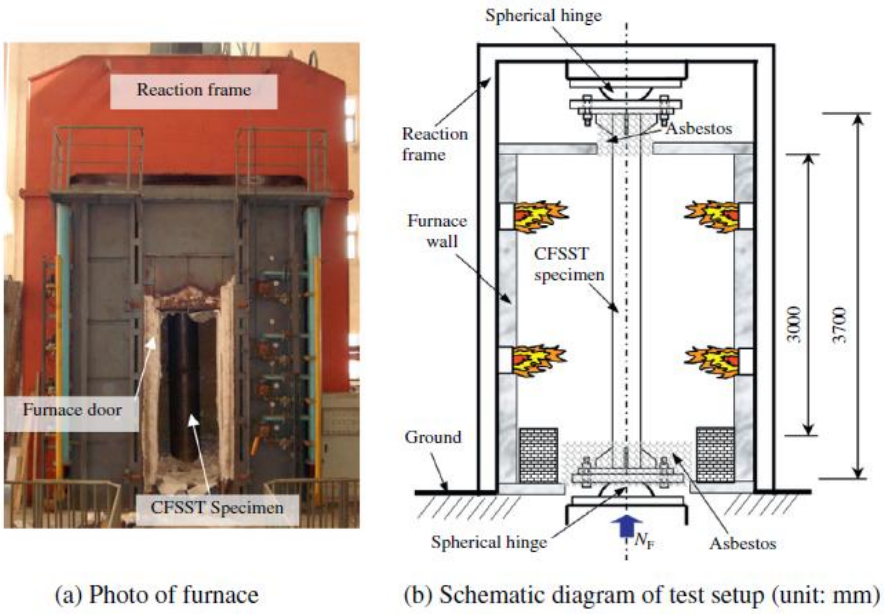

Figure 3. 3 - Fire test setup (Han et al., 2013).

The fire resistance of columns increased from 148 to 220 min when the overall width of the square CFSST column increased from 315 to 630 mm. Moreover, the fire resistance decreased when the load level increased. The use of stainless steel or carbon steel gives different fire performance for CFST columns and CFSST columns under the same fire condition due to the difference in thermal and mechanical properties. Generally, a CFSST column has higher fire resistance compared with its reference CFST counterpart. Supported by the verified FE model, the structural behaviour and failure mechanism of CFSST columns

exposed to fire were analysed. Within the later stage of fire exposure, the analytical results showed that the core concrete carry most of the axial load in the later stage of fire exposure, see Figure 3.4.

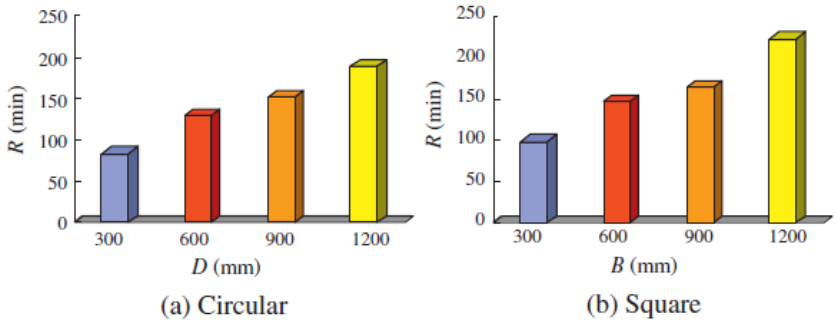

Figure 3. 4 - Influence of sectional dimension (D or B) on fire resistance (R) (Han et al., 2013).

In 2019, Zhou et al (2019) Tested a series of eight circular tubed steel reinforced concrete (CTSRC) stub columns subjected to combined axial loading and fire (see Figure 3.5). The influences of load level and steel tube thickness on the fire resistance of the CTSRC stub columns were investigated. Two similar specimens were tested with the same test scenario to obtain more reliable data. The temperatures in steel and concrete, axial displacement, fire resistance, and failure mode shape were recorded and discussed. In addition, a FE model for simulating the temperature distribution and structural response was established and validated by the test data and used to perform a set of parametric studies. The test results show that under the same load ratio, the increasing cross-sectional dimension and decreasing steel tube thickness will improve the fire resistance of CTSRC stub columns, while the increasing concrete strength has an insignificant influence on it. The cross-sectional dimension has a more significant influence on the temperature distribution than the steel tube thickness and concrete strength. With the increasing cross-sectional dimension, the temperatures of concrete and H-shaped steel reduce. The failure of CTSRC stub columns at elevated temperature is induced by the crushing of concrete inside after the tensile yielding of steel tuber.

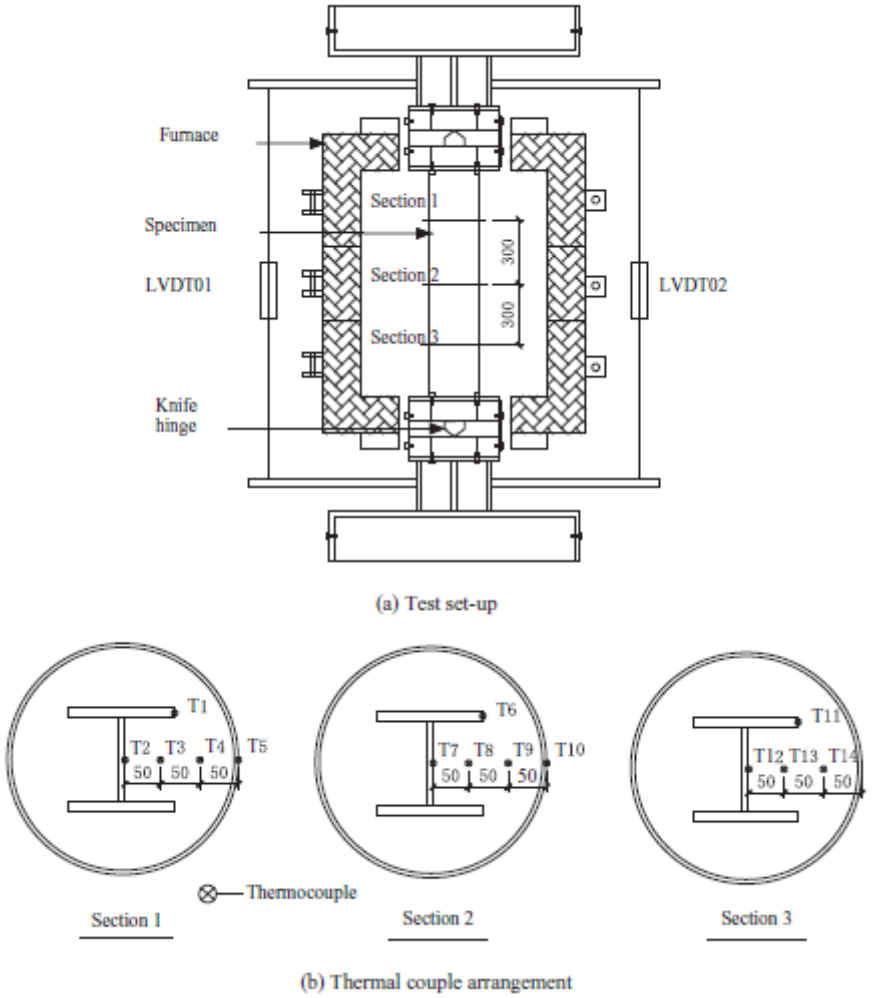

Figure 3. 5 - Schematic diagram of test setup and layout of instrumentations (Zhou et al., 2019).

3.2.2 Numerical research

In 2008, Huang et al. (2008) presented a nonlinear 3-D finite element model for investigating the fire resistance of composite columns with totally encased I-section. The objective of the study is to examine the effects of cross-sectional dimension and load level on column fire resistance.

In this study four groups of columns consisting of square cross-section are used. Their cross-sectional dimensions range from 250×250 to 400×250 mm2, respectively. These columns are subjected to axial compression forces and their four-face exposed to uniform heating. The load levels studied for the composite column are, 0.2, 0.3, 0.4 and 0.5. The numerical

studies showed that under high load levels, columns with small cross-sections have the same fire resistance as suggested by Eurocode 4 (EN 1994-1-2, 2005). However, the increase of cross sectional dimension substantially increases the fire resistance as illustrated in Figure 3.6. To validate and to prove the reliability of the numerical study, four composite columns were tested under transient heating conditions. The finite element analyses were validated against the experimental results. FE predictions of both cross-sectional fire resistance and structural response during heating agreed reasonably well with experimental data. Column failure times are also predicted using a simple method proposed by Eurocode 4 (EN 1994-1-2, 2005). It shows that EN-1994-1-2 predictions agree very well with the FE predictions.

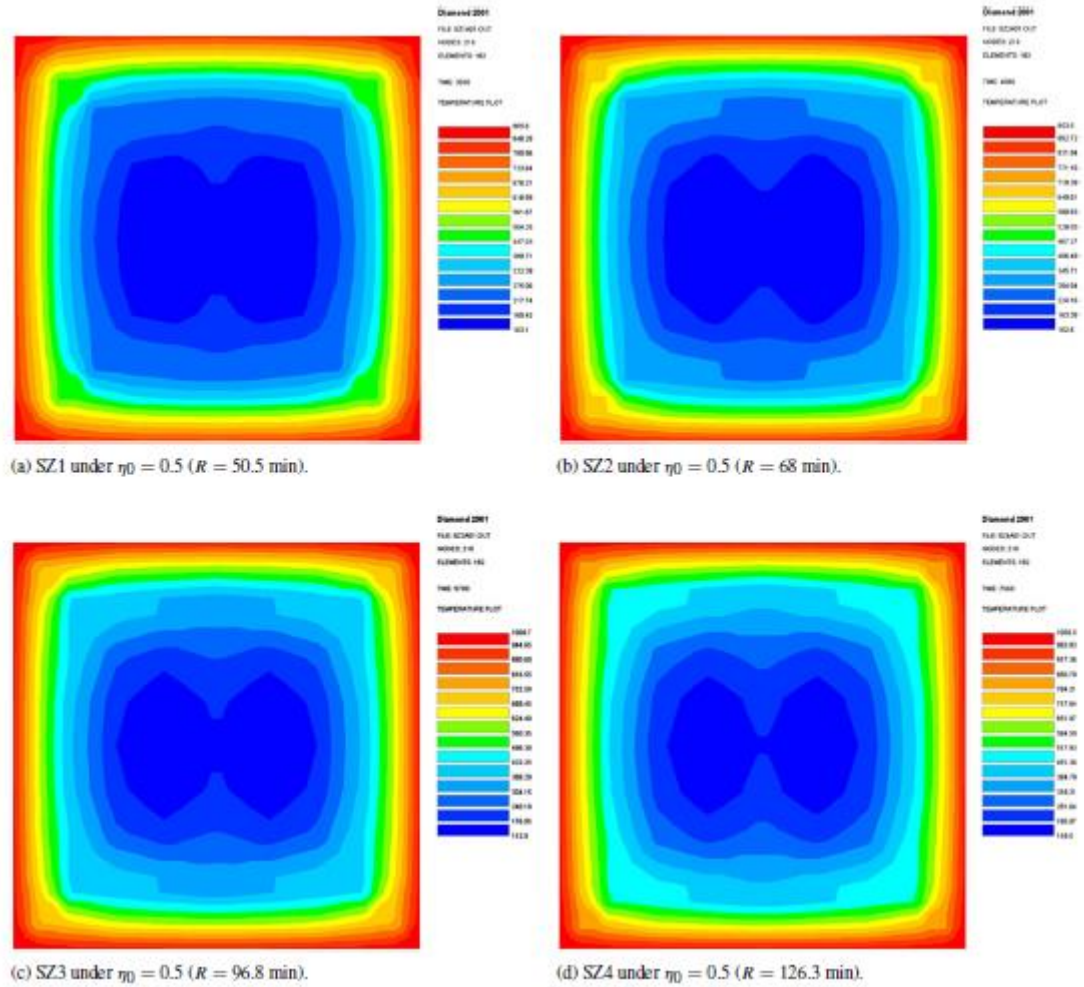

Figure 3. 6 - Cross sectional temperature for four columns under load level of 0.5 at respective failure moment (Huang et al., 2008)..

In 2010, Ellobody and Young (2010) developed a 3D finite element model to investigate the behaviour of concrete encased steel composite columns at elevated temperature see Figure 3.7. The composite columns were pin-ended axially loaded columns, the columns are tested using different cross-sectional dimensions, different structural steel sections, different coarse aggregates and different load ratios during fire. The nonlinear material properties of steel, concrete, longitudinal and transverse reinforcement bars as well as the effect of concrete confinement at ambient and elevated temperatures were used in the finite element models. The initial geometric imperfection was carefully included in the model. In the finite element model, the standard ISO834 is used as a fire source. From the study, authors concluded that the fire resistance of the columns generally increases with the decrease in the column slenderness ratio as well as the increase in the structural steel ratio. It is also shown that the time–axial displacement relationship is considerably affected by the coarse aggregate. The fire resistances of the composite columns obtained from the finite element analyses were compared with the design values obtained from the EN-1994-1-2 for composite columns at elevated temperatures. EN-1994-1-2 shows conservative results for all the concrete encased steel composite columns, except for the columns having a load ratio of 0.5 as well as the columns having a slenderness ratio of 0.69 and a load ratio of 0.4.

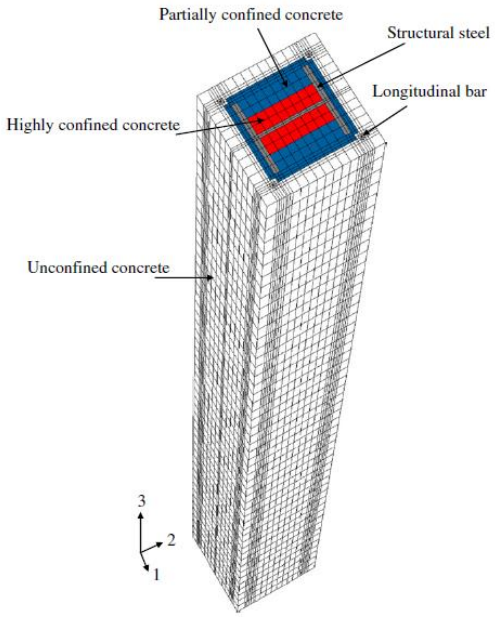

Figure 3. 7 - Finite element model of concrete encased steel composite columns (Ellobody and Young, 2010).

In 2011 Espinos et al (2011) Presented an advanced finite element model in order to study the behaviour of axially loaded concrete filled elliptical hollow section (CFEHS) columns exposed to fire (see Figure 3.8). This study was developed in the framework on previous investigation on concrete filled circular hollow section (CFCHS) columns, both at room temperature and elevated temperature. A parametric study was performed to explore the influence of variation in the global member slenderness, load level, cross-section slenderness and section size. Finally, guidance on the fire design of CFEHS columns is proposed,being recommended to follow the guidelines of Clause 4.3.5.1 in EN-1994-1-2, but employing the flexural stiffness reduction coefficients established by the French National Annex with an equivalent EHS diameter equal to P/π, where P is the perimeter of the ellipse. The results proved that the increase of slenderness and load level decrease the fire resistance of the columns, however the increase of the section factor (*A/V* ratio) increase the fire resistance of the member. The authors notice that the influence of cross-section slenderness and section thickness is not so clear, with opposing trends obtained for stocky and slender columns, which is related to their different failure modes. For that, a comparative study between elliptical and circular concrete filled hollow section columns in fire has also been presented. This study has shown that, for a certain column length and load-bearing capacity, the circular columns attain higher fire resistance than the elliptical columns, with reduced material use. This is due to the lower section factor *A/V* ratio that the circular sections present, which delays the heating up of the column, therefore providing a longer fire resistance period.

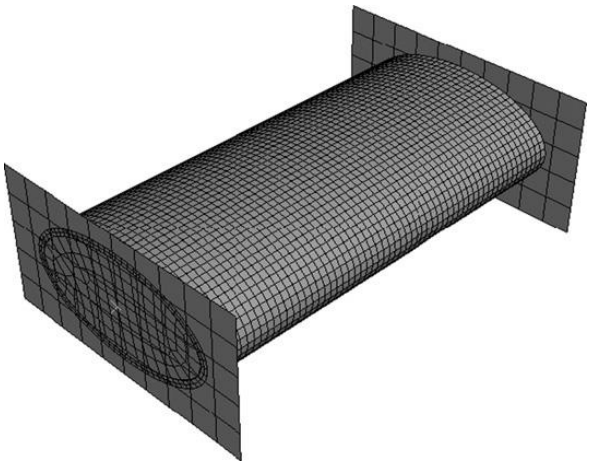

Figure 3. 8 - Three-dimensional finite element model for CFEHS stub columns (Espinos et al., 2011).

In 2019, Kamil et al (2019) Presented a complete and new numerical study on fibre element model (see Figure 3.9) to investigate the fire-resistance of axially loaded rectangular CFST short columns at elevated temperatures considering local buckling. The fire effect problem of a CFST column is solved by using difference finite element methods, to determine the temperature distribution within its cross-section, including an air gap, concrete moisture content and the emissivity of exposure surfaces. The non-linear stress analysis of axially loaded short CFST columns under fire recognizes the stress-strain behaviour of concrete and steel at elevated temperatures. To include the effects of local and post-local buckling on the fire responses of CFST columns, an expression for the initial local buckling and effective widths of steel plates are incorporated in the computational model. The existing experimental and numerical results are utilized to examine the accuracy of the numerical models. The authors did several parametric studies and they conclude that the local imperfection remarkably reduces the ultimate axial loads of CFST rectangular columns at elevated temperatures and it is recommended to be considered in the numerical modelling techniques. The increase of concrete strength, lead to higher ultimate strength of short CFST columns regardless of the fire exposure time. The fire decrease significantly the axial load and initial stiffness of CFST short columns. The computed contribution ratios for steel and concrete as a time function are given in Figure 3.10. It can be observed that the steel contribution ratio decreases with an increase in the time exposure or temperature and eventually the steel tube completely loses its strength. The authors also concluded that, the concrete contribution ratio increases with increasing in the time of fire exposure and the concrete carries the axial load alone after the steel tube completely loses its capacity.

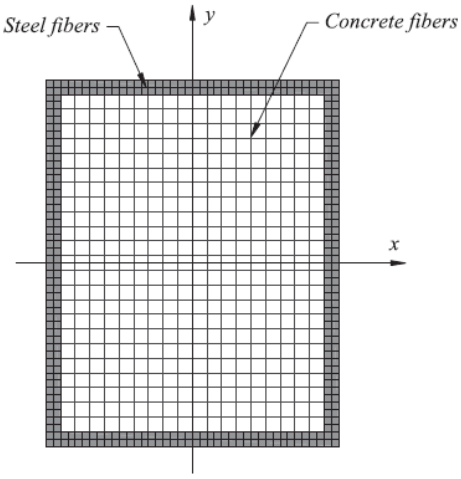

Figure 3. 9 - Typical fibre element discretization (Kamil et al., 2019).

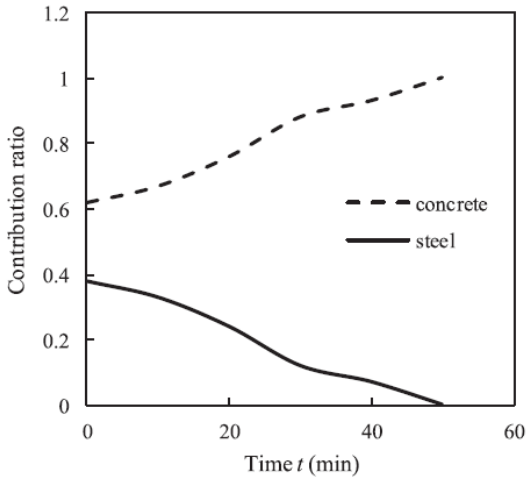

Figure 3. 10 - Steel and concrete contribution ratio as a function of fie exposure time (Kamil et al., 2019).

3.3 Compression and bending

3.3.1 Experimental research

In 2008, Dundar et al (2008) presented an experimental and theoretical study on the behaviour reinforced and concrete-encased composite columns subjected to biaxial bending and axial load. In the experimental part of the study, Figure 3.11 present the diagram of test setup and instrumentation. To determine the ultimate strength capacity, a 12 square and three L-shaped short and slender reinforced concrete columns were analysed. The test results were compared with the theoretical results obtained by the developed computer program which uses various stress–strain models for the confined concrete or unconfined concrete in the compression zone of the member. Finally, the theoretical results obtained using the proposed procedure were also compared with the test results available in the literature for short and slender composite columns. The test results presents that the parameters most effected the ultimate strength capacity of the composite column are the compressive strength of concrete and its corresponding compressive strain. However, the shape of the concrete stress–strain relationship has little effect on the ultimate strength capacity of the composite columns. Consequently, the ratio of computed axial load to experimental load for different cross

section of reinforced and composite column members indicate that the results obtained by the proposed procedure have been in good agreement with the test results of columns subjected to biaxial bending and axial load.

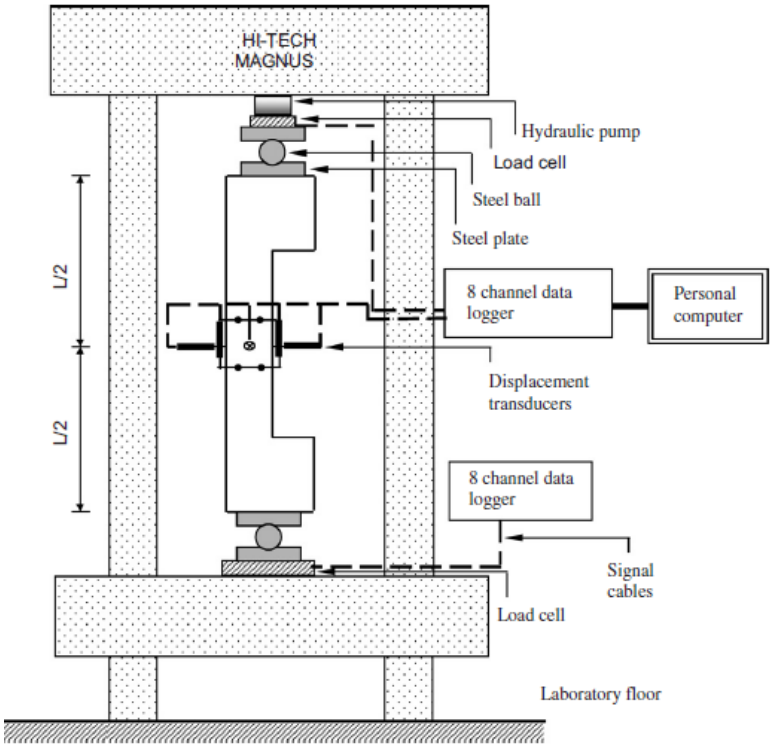

Figure 3. 11 - Diagram of test setup and instrumentation (Dundar et al., 2008).

In 2017, Ren et al (2017) tested the experimental behaviour of Tapered concrete filled steel tubular (CFST) columns under combined compression and bending. A total of twenty-four tapered CFST specimens were tested under combined compression and bending, including twelve square columns and twelve circular ones see Figure 3.12. The test parameters included section type, tapered angle θ, load eccentricity e, slenderness ratio λ and the use of concrete infill have obvious effects on the strength and ductility of the tapered CFST columns. Generally, the results show that for both, square and circular, composite columns, the strength index SI and the ductility index DI decreases with the increasing of tapered angle θ, load eccentricity e as well as slenderness ratio λ With the existence of the concrete core, CFST columns under axial compression is higher than that of CFST columns under combined compression and bending because of existence of the secondary moment caused by eccentricity. A tapered CFST column shows obviously intensive resistance to combined

compression and bending compared with that of a reference hollow tubular member. Finally, a simplified design method for predicting the load carrying capacity of tapered CFST column under combined compression and bending was proposed.

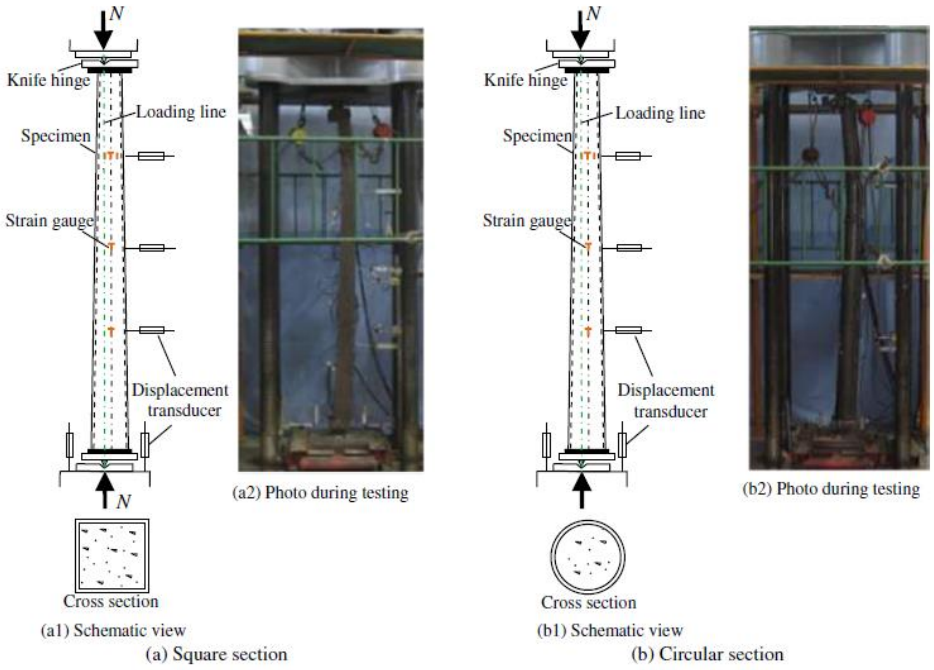

Figure 3. 12 - Test setup for tapered CFST columns (Ren et al., 2017).

In 2019, Guo et al (2019) examines the fire responses of restrained concrete-filled steel tubular (CFST) columns subjected to axial and eccentric loads using high-temperature experiments. In the test procedure authors used a new type of reaction steel frame to simulate the restraint stiffness of the boundary conditions (see Figure 3.13), a set of adjustable knife-edge articulation systems was used to provide the required end eccentricities and the pined-pined ending supports. The use of this type of installation allow to investigate the fire-resistances of CFST columns with finite restraint stiffness and different eccentricities. The test results show that the eccentricity ratios affects the development of the axial deformation. In addition, the bending deformations occurred in the eccentric CFST columns and decreased their elongation, this allowing the thermal reaction forces to decline rapidly if the eccentricity ratios exceeded 0.33. CFST columns should be designed as compressive axial

components or large compressive eccentric components to reduce the thermal reaction forces in small compressive eccentric components exposed to fire. While CFST columns are restrained using the same boundary stiffness conditions, they experience a shorter fire critical time when designed as a small eccentric compressive member. The slenderness ratio influences the bending deformation of the exposed CFST columns to a fire. Low slenderness ratios can reduce the bending deformation and release the reaction forces induced through thermal actions.

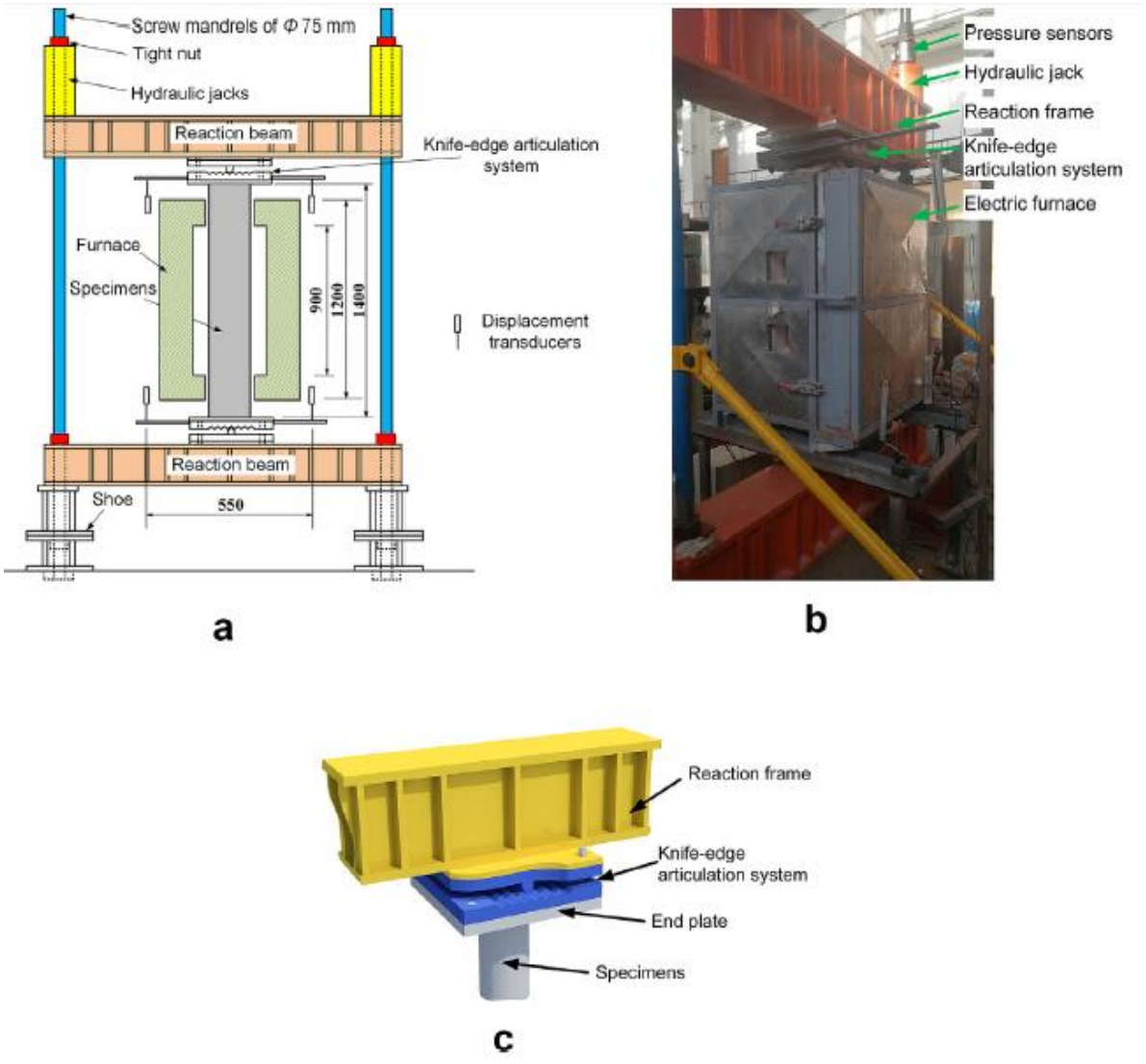

Figure 3. 13 - Details of reaction frame: (a) reaction frame, (b) test setups for fire tests with stronger reaction beams, and (c) knife-edge articulation system (Guo et al., 2019).

3.3.2 Numerical research

In 2009, Schaumann et al (2009) developed a numerical model using the computer program BoFIRE to study the fire behaviour of hollow structural section steel columns filled with high strength concrete (HSS). Though the fire performance of HSS columns filled with normal strength concrete (NSC) is well established, the fire design rules cannot be extended to high strength concrete (HSC) filled steel columns. The numerical study was carried out based on both North American and European material properties. A series of parametric studies was carried out including the type of concrete-filling, moisture content, section size, cross-sectional shape, column slenderness, load eccentricities and concrete compressive strength. The authors conclude that the computer code BoFIRE is capable of modelling the fire response of HSC-filled HSS composite columns. Up to 30 min of fire exposure, the use of HSC as filling in HSS columns is beneficial for non-slender columns with only moderate load eccentricity. Since the disadvantageous load-bearing behaviour of HSC filling increases with rising temperatures, this trend is also valid for higher fire resistance classes. There are variations between the considered European (EU) and North American (NA) material properties resulting in different fire resistance times. The numerical studies showed that North American results are more conservative for increasing concrete strengths and decreasing cross-sectional parameter see Figure 3.14. In general, the results for HSS columns filled with NSC are in fair agreement using the European and North American material properties. In contrast to this, significant differences could be noticed concerning the results for HSC-filling. One of the primary factors that produce these differences is the variation in high temperature material properties of HSC. Hence the authors recommend further research on the high temperature material properties of HSC.

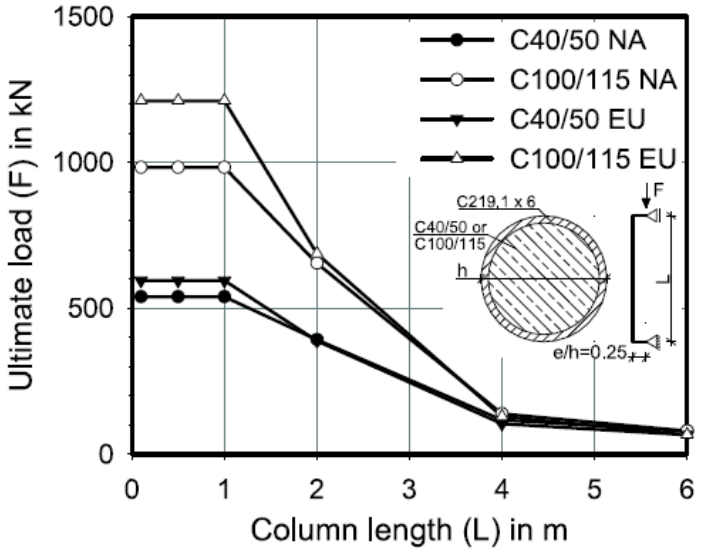

Figure 3. 14 - Ultimate load for eccentrically loaded HSC-filled HSS column using NA and EU HSC material properties at 30 min fire exposure (Schaumann et al., 2009).

In 2016, Mago and Hicks (2016) presented a numerical study on the fire behaviour of slender, highly utilized, eccentrically loaded concrete filled tubular columns. Previously the fire resistance rating was calculated by applying implicit as well as explicit finite element analyses and undertaking sequentially coupled thermal-stress analyses. Initially, published fire tests on concentrically loaded columns as well as columns with a modest load eccentrically ($e/h \leq 0.25$) with e is the load eccentricity and h is the cross section height, the columns were analysed with normal (NSC) and high strength concrete (HSC). A parametric study was undertaken on a composite column using a 400mm square hollow section with a fixed-pinned boundary condition and a relative slenderness at room temperature of 0.6. Load levels of 0.47, 0.35 and 0.24 were considered and, using a constant eccentricity of e/h=0.5, a combination of concentric and eccentric loading was applied to the column, as would occur in real practice. Based on this analysis, the results show that the fire resistance rating FRR reduces significantly as the bending moment increases on the column. Moreover, although the FRR reduced as the load level increased, it was found that for highly loaded columns the FRR were less sensitive to changes in the magnitude of the bending moments (see Figure 3.15). The authors also found that near the top of column the failure mode switched from global buckling to local imperfection when the bending moments in excess of 25% of the

axial force; at this point, the finite element mesh at this location excessively. To remedy this situation, the authors decided to apply more realistic combination of concentric and eccentric loading to the composite column.

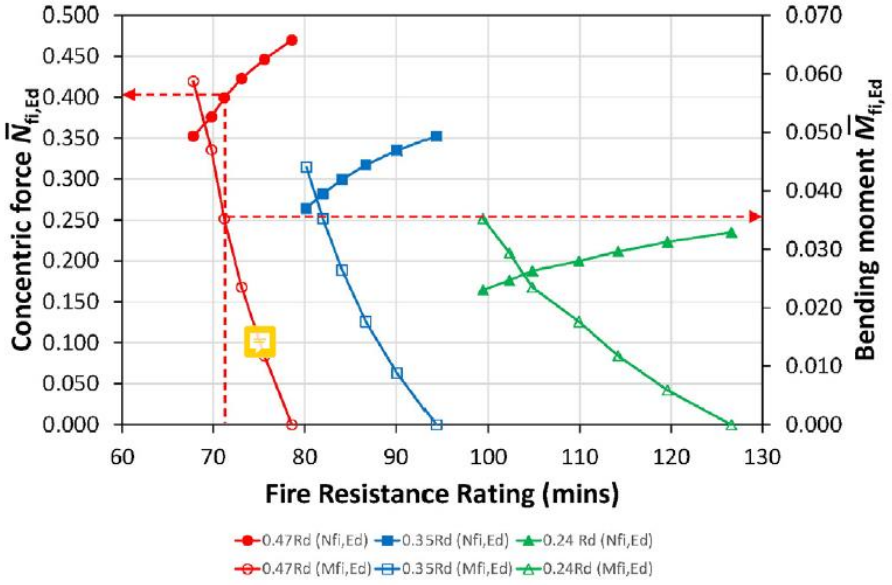

Figure 3. 15 - Concentric force and bending moment versus FRR for the composite column (Mago and Hicks, 2016).

In 2016, Milanović et al (2015) analysed the load-bearing capacity of three types of steel-concrete composite columns under fire. Four different types of columns are analysed see Figure 3.16, three of which are steel concrete composite columns with different cross sections (fully encased steel sections FES, partially encased steel sections PES, and concrete filled tubular sections CFS), while the fourth one is a reinforced concrete column used for comparison. The computer program SAFIR is used for that investigation. The procedure for producing the temperature dependent M-N interaction diagrams of composite columns is based on the simplified method recommended in EN-1994-1-2. The results confirm that the rise of temperature in the composite column cross sections decreases the bearing capacity of cross sections with regard to the axial compression force and biaxial bending. The reduction in bearing capacity depends on the type of cross section, heating time, fire scenario. The highest loss of the M – N bearing capacity was observed in the cross sections where the steel profile is directly exposed to heating, as in PES - partially encased sections. A minimum

reduction in the M–N bearing capacity was observed in sections where the steel profile is protected with concrete lining (FES section). As concrete is characterized by low thermal conductivity, it prevents rapid penetration of temperature into the steel element and reinforcement thus ensuring better behaviour of the column.

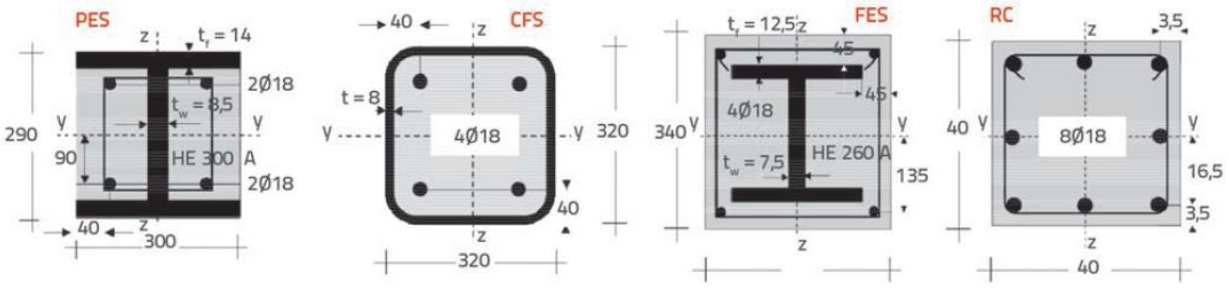

Figure 3. 16 - Cross section geometry of columns (Milanović et al., 2015).

3.4 Conclusion

The behaviour of composite columns subjected to fire has been numerically investigated by several authors, especially in this decade, but even so only a few experimental studies have been published on composite column under fire. The major part of the experimental studies published until now is on hollow steel columns. Load level and eccentricity have a noticeable effect on resulting deformations and fire resistance of composite columns. The higher the load level and the eccentricity, the lower is the fire resistance. Fire induced spalling in concrete significantly affects the thermal and structural response of composite columns, especially those made with hith strength concrete, and leads to lower fire resistance of the column. Eccentrically loaded columns experience higher spalling than that of concentrically loaded columns (Mao and Kodur, 2011). In this chapter, we present the research works dealing with the behaviour of composite steel concrete column at high temperatures by both numerical and experimental investigation.

Chapter 4

ANALYSIS METHODS OF COMPOSITE COLUMNS

4.1 Introduction

Currently, different methods of analysis can be used to assess the thermal behaviour of composite column exposed to fire. Analytical method named simplified calculation methods defined in European standard and numerical simulations named advanced calculation models are treated in this chapter.

The analytical determination of the fire resistance of load bearing structural elements as an alternative to testing has always implicit the uncertainty of the thermal action and mechanical loads to consider in a real fire. Due to high costs, a full scale fire resistance test is usually limited to one test specimen. For this reason, a great amount of research is performed on single elements and sub-frames. An analytical determination of the load bearing capacity of the structural element is based on the characteristic value of the material strength. This gives an analytically determined fire resistance which is lower than the corresponding value derived from a standard fire resistance test. In this chapter, Eurocode 4 (EN 1994-1-2, 2005) is used to determine the load bearing capacity of the composite columns under fire.

In engineering, many practical problems are either extremely difficult or impossible to solve by conventional analytical methods. Finite element methods (FEM) is a versatile numerical method that provides a solution to this problem. The finite element method acts as a link between experimental studies and analytical models, enabling a better understanding of behaviour and experimental control to obtain simplified methods. FEM can easily simulate both material and geometric non-linearity, such as failure and damage of the structures. The modelling composite steel-concrete columns presents a high level of complexity to treat some local phenomena such as cracking of concrete, spalling and the local imperfection and the characterization of the interaction between the surfaces of steel and concrete. The advanced calculation models generally use numerical simulations, generally based on the finite element method. In this case, the calculation tool is essential. Specialized software is available, including: ANSYS, ABAQUS, SAFIR, DIANA, etc. In this study, the finite element software ANSYS (ANSYS 18.2, 2017) is chosen to simulate different types of 3D composite columns under fire conditions. The description of its two models (thermal and mechanical) is invested in this section.

4.2 Simple Calculation Method

The fire resistance of partially encased composite columns under eccentricity of loading can be found using the simplified method given in Eurocode 4 Annex G (EN 1994-1-2, 2005). This method leads to determine the load bearing capacity of PEC column, being calculated from the following equation 4.1:

$$N_{fi,Rd,e} = N_{fi,Rd} \cdot \left(N_{Rd,e} / N_{Rd} \right) \qquad (4.1)$$

Where: $N_{fi,Rd}$ represents the buckling resistance of PEC at elevated temperature, $N_{Rd,e}$ is the buckling resistance of PEC under eccentric loading at ambient temperature and N_{Rd} is the buckling resistance of PEC at ambient temperature.

4.2.1 Buckling resistance of PEC at elevated temperature

This calculation method takes into consideration the effect of the fire in the four components of the cross section. The four components are identified in Figure 4.1 and include: the flange component, the web component, the concrete components and reinforcement components.

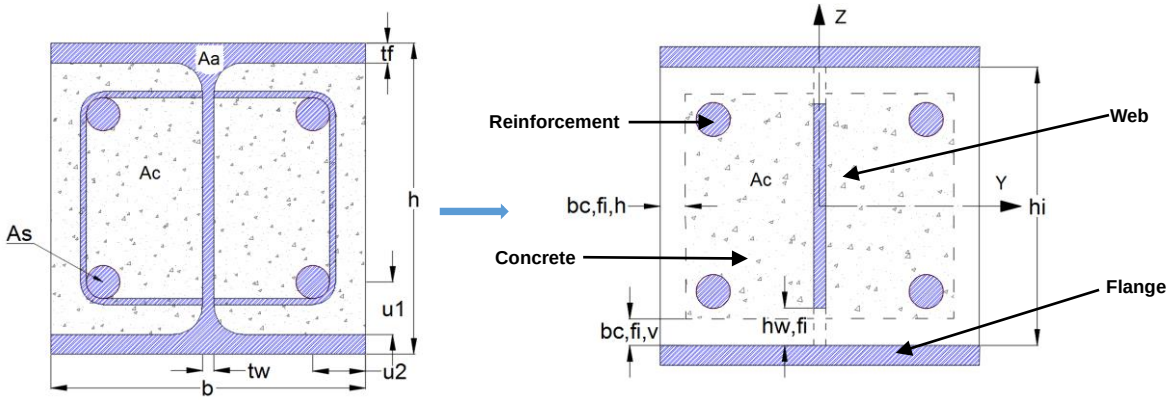

Figure 4. 1 - Reduced cross-section for structural fire design.

4.2.1.1 Flanges of the steel profile

The average flange temperature $\theta_{f,t}$ must be determined according to the next formula. The value depends on the empirical coefficient k_t , the reference value $\theta_{0,t}$ and the section factor A_m/V :

$$\theta_{f,t} = \theta_{0,t} + k_t\left(A_m/V\right) \qquad (4.\ 2)$$

The empirical coefficient is shown in this table:

Table 4. 1 - Parameters for the flange temperature.

Standard Fire Resistance	$\theta_{0,t}\ [m^o C]$	$k_t\ [m^o C]$
R30	550	9,65
R60	680	9,55
R90	805	6,15
R120	900	4,65

The average temperature of the flange allows the calculation of the fire effect on the mechanical properties. This effect is defined by the reduction coefficients, $K_{y,\theta}$ *and* $K_{E,\theta}$, used for the modulus of elasticity and the yield stress, being determined from the following equations:

$$f_{ay,f,t} = f_{ay,f} K_{y,\theta} \qquad (4.\ 3)$$

$$E_{ay,f,t} = E_{ay,f} K_{E,\theta} \qquad (4.\ 4)$$

The plastic resistance to axial compression and the flexural stiffness of the two flanges of the steel profile in the fire situation are determined from the following equations:

$$N_{fi,pl,rd,f} = 2\left(b_{ef}\, f_{ay,f,t}\right)/\delta_{M,fe,a} \qquad (4.\ 5)$$

$$\left(EI\right)_{fi,f,z} = E_{a,f,t}\left(e_f b^3\right)/6 \qquad (4.\ 6)$$

4.2.1.2 Web of the steel profile

The part of the web to be neglected is defined by $h_{w,fi}$. The fire effect is responsible to decrease the height of the resistant web, starting at the inner edge of the flange (see Figure 4.1). This part is determined as follows:

$$h_{w,fi} = 0{,}5\left(h - 2e_f\right)\left(1 - \sqrt{1 - 0.16\left(H_t / h\right)}\right) \qquad (4.\ 7)$$

The parameter H_t is given according to the next table:

Table 4. 2 - Parameter for height reduction of the web.

Standard Fire Resistance	$H_t[mm]$
R30	350
R60	770
R90	1100
R120	1250

The yield stress is modified as follows:

$$f_{ay,w,t} = f_{ay,w,t}\sqrt{1-0.16(H_t/h)} \quad (4.8)$$

The design value of the plastic resistance to axial compression and flexural stiffness of the web for the steel profile in fire situation are determined according to the following equations:

$$N_{fi,pl,rd,w} = \left[ew\left(h-2e_f-2h_{w,fi}\right)\right]f_{ay,w,t}/\delta_{M,fi,a} \quad (4.9)$$

$$(EI)_{fi,w,t} = \left[E_{a,w}\left(h-2e_f-2h_{w,fi}\right)\right]e_w^3/12 \quad (4.10)$$

4.2.1.3 Partially Encased Concrete

An exterior layer of concrete with a thickness $b_{c,fi}$ is going to be neglected in the calculation (see equation 3.12). The thickness $b_{c,fi}$ is given in Table 4.3 and depends on the section factor A_m/V of the entire composite cross-section only for fire ratings 90 minutes and 120 minutes.

Table 4. 3 - Thickness reduction of the concrete area.

Standard Fire Resistance	$b_{c,fi}\ [mm]$
R30	4.0
R60	15.0
R90	$0.5(A_m/V) + 22.5$
R120	$2.0(A_m/V) + 24.0$

The average temperature in concrete $\theta_{c,t}$ is given in Table 4.4 and depends on the section factor A_m/V of the entire composite cross-section at the fire rating class.

Table 4. 4 - Average concrete temperature.

R30		R60		R90		R120	
$A_m/V\left[m^{-1}\right]$	$\theta_{c,t}\left[^{o}C\right]$	$A_m/V\left[m^{-1}\right]$	$\theta_{c,t}\left[^{o}C\right]$	$A_m/V\left[m^{-1}\right]$	$\theta_{c,t}\left[^{o}C\right]$	$A_m/V\left[m^{-1}\right]$	$\theta_{c,t}\left[^{o}C\right]$
4	136	4	214	4	256	4	265
23	300	9	300	6	300	5	300
46	400	21	400	13	400	9	400
		50	600	33	600	23	600
				54	800	38	800
						41	900
						43	1000

The secant modulus of concrete at elevated temperature is obtained from the following expression and is going to affect the effective flexural stiffness:

$$E_{c,\sec,\theta} = f_{c,\theta} / \varepsilon_{cu,\theta} = f_c K_{c,\theta} / \varepsilon_{cu,\theta} \qquad (4.\ 11)$$

The design value of the plastic resistance to axial compression considers the effect of the material temperature and the residual cross section. The effective flexural stiffness of the concrete in the fire situation considers the residual area of concrete. These two parameters are determined from the following expressions:

$$N_{fi,pl,Rd,c} = 0{,}86\left[\left(\left(h-2e_f-2b_{c,fi}\right)\left(b-e_w-2b_{c,fi}\right)\right)-A_s\right]f_{c,\theta}/\delta_{M,fi,c} \qquad (4.\ 12)$$

Where A_s is the cross-section of the reinforcing bars.

$$\left(EI\right)_{fi,c,z} = E_{c,\sec,\theta}\left[\left\{\left(h-2e_f-2b_{c,fi}\right)\left(\left(b-2b_{c,fi}\right)^3-e_w^3\right)/12\right\}-I_{s,z}\right] \qquad (4.\ 13)$$

Where $I_{s,z}$, is the second moment of area of the reinforcing bars related to the central axis Z of the composite cross section.

4.2.1.4 Reinforcing bars

The reduction factor $k_{y,t}$ of the yield stress and the reduction factor $k_{E,t}$ of the modulus of elasticity for the reinforcing bars depend on the fire rating and the position of the reinforcement, being the geometrical average u representative of the distances of the reinforcement to the outer borders of the concrete (see Table 4.5 and Table 4.6).

Table 4. 5 - Reduction factor $k_{y,t}$ for the yield point $f_{s,y}$ of the reinforcing bars.

	Standard Fire Resistance			
u [mm]	R30	R60	R90	R120
40	1	0,789	0,314	0,17
45	1	0,883	0,434	0,223
50	1	0,976	0,572	0,288
55	1	1	0,696	0,367
60	1	1	0,822	0,436

Table 4. 6 - Reduction factor $k_{E,t}$ for the modulus of elasticity of the reinforcing bars.

	Standard Fire Resistance			
u [mm]	R30	R60	R90	R120
40	0,83	0,604	0,193	0,11
45	0,865	0,647	0,283	0,128
50	0,888	0,689	0,406	0,173
55	0,914	0,729	0,522	0,233
60	0,935	0,763	0,619	0,285

The geometrical average u of the axis distances u_1 and u_2 is obtained from $u = \sqrt{u_1.u_2}$, being u_1 the distance from the outer reinforcing bar to the inner flange edge in [mm] and u_2 is the distance from the outer reinforcing bar to the concrete surface [mm]. There are a few restraints to the calculation of the geometrical average u, see next equations.

$$(u_1 - u_2) > 10mm, \qquad then \qquad u = \sqrt{u_2(u_2 + 10)} \tag{4. 14}$$

$$(u_2 - u_1) > 10mm, \qquad then \qquad u = \sqrt{u_1(u_1 + 10)} \tag{4. 15}$$

The design value of the plastic resistance to axial compression and flexural stiffness of the reinforcing bars takes into account the effect of the temperature into the mechanical properties in fire condition and are obtained as follows:

$$N_{fi,pl,Rd,s} = A_s k_{y,t} f_{s,y} / \delta_{M,fi,s} \tag{4. 16}$$

$$(EI)_{fi,s,z} = k_{E,t} E_s I_{s,z} \tag{4. 17}$$

The partial safety factor can be considered equal to 1.

4.2.1.5 Calculation of the axial buckling load at elevated temperatures

The fire resistance of the composite column in axial compression (buckling load) shall be obtained from the following equation:

$$N_{fi,Rd} = \chi . N_{fi,pl,Rd} \qquad (4.\ 18)$$

Where: χ is the reduction coefficient for buckling curve *c*, depending on the non-dimensional slenderness ratio $\overline{\lambda_\theta}$ and $N_{fi,pl,Rd}$ is the design value of the plastic resistance of the cross section to axial compression under fire.

The axial plastic resistance under fire $N_{fi,pl,Rd}$ of the cross-section calculated according to following equation.

$$N_{fi,pl,Rd} = A_f . f_{ay,f,\theta} / \gamma_{Mfi,a} + A_w . f_{ay,w,\theta} / \gamma_{Mfi,a} + A_c . f_{c,\theta} / \gamma_{Mfi,c} + A_s . f_{ay,s,\theta} / \gamma_{Mfi,s} \qquad (4.\ 19)$$

Where A_i is the area of each element *i* of the cross-section and subscript "*f* " "*w*" "*c*" "*s*" refers to the four components: flange, web, concrete and reinforcement respectively, $f_{i,\theta}$ is the yield stress of each component at elevated temperature, and $\gamma_{M,fi}$ is the partial factor of each material in fire situation.

The stability of PEC requires the calculation of the critical load and the effective flexural stiffness. These quantities depend on the temperature effect, the elastic modulus and the second order moment of area of each component (flange; web; concrete; reinforcement), according to equation (4.20).

$$(EI)_{fi,eff,z} = \varphi_{f,\theta}(EI)_{fi,f,z} + \varphi_{w,\theta}(EI)_{fi,w,z} + \varphi_{c,\theta}(EI)_{fi,c,z} + \varphi_{s,\theta}(EI)_{fi,s,z} \qquad (4.\ 20)$$

In this equation, $(EI)_{fi,eff,z}$ represents the effective flexural stiffness of the composite section in fire, $(EI)_{fi,f,z}$ represents effective flexural stiffness of the flange, $(EI)_{fi,w,z}$ represents effective flexural stiffness of the web, $(EI)_{fi,c,z}$ represents the effective flexural stiffness of the concrete and $(EI)_{fi,s,z}$ represents the effective flexural stiffness of reinforcement. The contribution of each part is going to be weighted according to φ factors, a reduced modulus

of elasticity and a reduced cross-section. These values depend on the fire rating, as expressed in the following table:

Table 4. 7 - Reduction coefficients for bending stiffness around the week axis.

Standard fire resistance class	$\varphi_{f,\theta}$	$\varphi_{w,\theta}$	$\varphi_{c,\theta}$	$\varphi_{s,\theta}$
R30	1,0	1,0	0,8	1,0
R60	0,9	1,0	0,8	0,9
R90	0,8	1,0	0,8	0,8
R120	1,0	1,0	0,8	1,0

Once the effective flexural stiffness is calculated, the Euler buckling load or elastic critical load in fire situation is obtained as follows:

$$N_{fi,cr,z} = \pi^2 / L_\theta^2 \times (EI)_{fi,eff,z} \qquad (4.\ 21)$$

Where: L_θ is the buckling length of the column in fire situation.

The non-dimensional slenderness ratio $\bar{\lambda}_\theta$ is calculated according to equation (4.22).

$$\bar{\lambda}_\theta = \sqrt{N_{fi,pl,R} / N_{fi,cr,z}} \qquad (4.\ 22)$$

Where: $N_{fi,pl,R}$ is the value of $N_{fi,pl,Rd}$ when the safety factors $\gamma_{M,fi,a}$, $\gamma_{M,fi,s}$ and $\gamma_{M,fi,c}$ are taken equal to 1.

4.2.2 Buckling Resistance of PEC under Eccentric Loading at Ambient Temperature

Initially, the resistance of the cross-section is determined using an interaction diagram between the axial load resistances and bending moment resistance as given by (EN 1994-1-1, 2004). The diagram is shown schematically in Figure 4.2, where $N_{pl,Rd}$ is the axial squash capacity (Point A), and $M_{pl,Rd}$ is the plastic moment capacity (Point B). Although the shape of the interaction diagram is similar to that of the reinforced concrete columns which is strictly curved, it may be approximated to a series of straight lines. Point C is established by the application of the moment $M_{pl,Rd}$ and a resultant axial capacity of the concrete alone $N_{pm,Rd}$, Point D by the moment capacity $M_{max,Rd}$ under 0,5 $N_{pm,Rd}$.

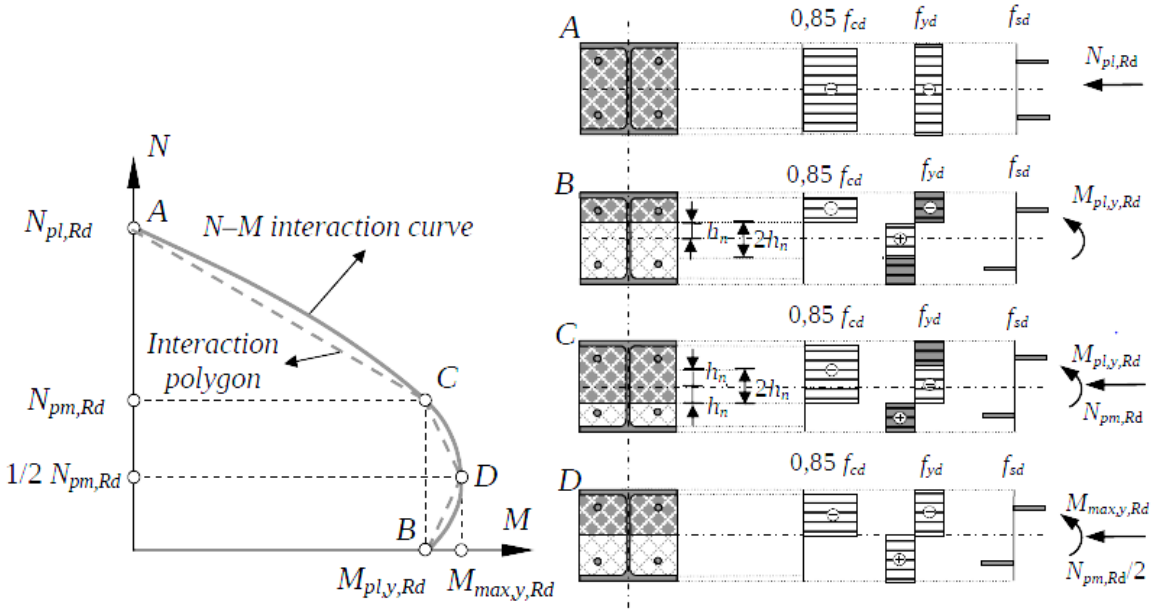

Figure 4. 2 - Simplified interaction curve and corresponding stress distributions.

4.2.2.1 Axial load capacity, $N_{pl,Rd}$ [Point A]

This is given by the sum of the individual components due to the steel section, the concrete and the reinforcement (see Figure 4.3 (a)). So, in general $N_{pl,Rd}$ is given by:

$$N_{pl,Rd} = A_a . f_y / \gamma_a + A_c . 0{,}85 . f_{c,} / \gamma_c + A_s . f_s / \gamma_s \qquad (4.\ 23)$$

Where A_a is the area of the steel section and f_y is the yield strength, A_c is the concrete area and f_{ck} is the characteristic cylinder strength, A_s is the area of the reinforcement and f_{sk} is the characteristic strength.

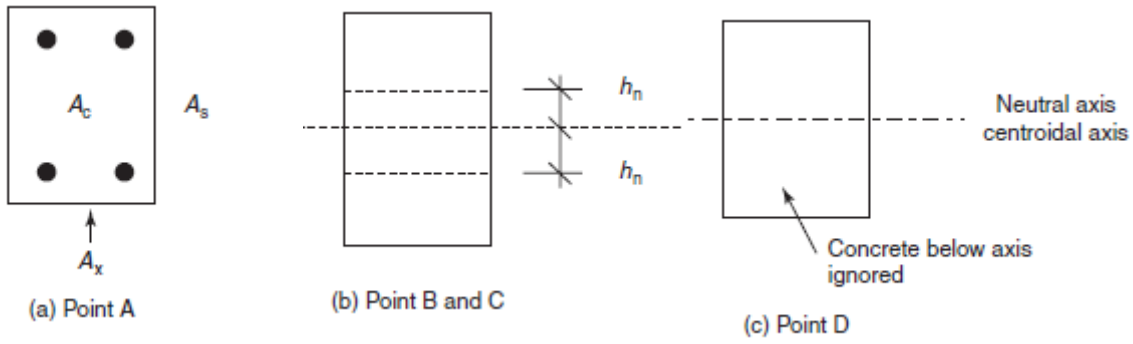

Figure 4. 3 - Calculation of section capacities.

4.2.2.2 Calculation of $M_{pl,Rd}$ [Point B]

For the typical section given in Figure 4.3 (b), the forces in the flanges and the reinforcement cancel out, and thus the tension force in the web must balance the compression block in the concrete. It is therefore straightforward to determine the height of the web h_n above the centroid axis. Equating compressive and tensile forces gives:

$$h_n = \frac{N_{pm,Rd} - A_{s,n.}(2.f_{sd} - 0{,}85 f_{cd})}{2b_c.0{,}85.f_{cd}. + 2.t_w.(2.f_{yd} - 0{,}85.f_{cd})} \qquad (4.\ 24)$$

Where $N_{pm,Rd}$ is given by Eq. (3.26)

The plastic moment capacity is determined by taking moments about the centroid axis of the section. The moment capacity $M_{pl,Rd}$ is thus given by

$$M_{pl,Rd} = M_{\max,Rd} - .M_{n,Rd} \qquad (4.\ 25)$$

The values of $M_{n,Rd}$ and $M_{max,Rd}$ are given by equations (4.28) and (4.29), respectively.

4.2.2.3 Determination of $N_{pm,Rd}$ [Point C]

This can be done by noting that the neutral axis shifts from h_n above the centroid axis to the same distance below it (Figure 4.3 (b)), $N_{pm,Rd}$ is determined from horizontal force equilibrium recognizing that the forces in the steel flanges and reinforcement cancel out, that is the axial load is carried by the concrete alone. The area of the concrete A_c is given by:

$$A_c = b.h - 2.t_f.b - t_w.(h - 2.t_f) - 4.\pi.r^2 \qquad (4.\ 26)$$

Where b ; h; t_f; t_w; and r are the section geometry, and $N_{pm,Rd}$ is given by

$$N_{pm,Rd} = A_c.0{,}85.f_{ck} / \gamma_c \qquad (4.\ 27)$$

The moment capacity $M_{n,Rd}$ is given by

$$M_{n,Rd} = h.h_n^{\,2}.f_y \qquad \text{case of} \quad (h_n < t_w). \qquad (4.\ 28)$$

4.2.2.4 Determination of $M_{max,Rd}$ [Point D]

For this case when an axial force of $0{,}5N_{\mathrm{pm,Rd}}$ acts the neutral axis coincides with the centroid axis (Figure 4.3 (c)), and thus $M_{max,Rd}$ is simply given by the sum of the plastic moment capacities of the reinforcement, the steel section and the concrete above the centroid weak axis. $M_{max,Rd}$ is given by:

$$M_{\max,Rd} = w_{pl,a} f_{yd} + w_{pl,s} f_{sd} + w_{pl,c} f_{ck} / 2 \tag{4.29}$$

Where $W_{pl,a}$ is the plastic section modulus for the steel section, $W_{pl,c}$ is the plastic section modulus for the concrete section and $W_{pl,s}$ is the plastic section modulus for the rebars.

4.2.2.5 Determination of the load bearing capacity $N_{Rd,e}$

The greatest first-order bending moment is multiplied by a factor k_n given by:

$$K_n = \frac{\beta}{1 - N_{ed}/N_{cr}} \geq 1{,}0 \tag{4. 29}$$

Where:

$$\beta = 0{,}66 + 0{,}44.\frac{M_1}{M_2} \geq 0{,}44 \tag{4. 30}$$

M_2 and M_1 are the applied external moments from first order or second-order global analysis.

$$\chi = \frac{N_{Rd}}{N_{pl,RD}} \text{ (Calculated From resistance to axial compression).} \tag{4. 31}$$

And

$$\chi_d = \frac{N_{ed}}{N_{pl,RD}} \tag{4. 32}$$

Where: χ_d is the parameter representing the axial load, N_{ed} is applied eccentric load. $N_{pl,Rd}$ is the axial plastic resistance of the cross section.

$$\chi_n = \chi\left(1 - \frac{M_1}{M_2}\right)/4 \tag{4. 33}$$

The column has sufficient resistance if the design moment M_{sd} is smaller than the resistance moment M_{adm}:

$$M_{sd} = N_{ed}.\delta.K_n < M_{adm} = 0{,}9.\nu.M_{pl,Rd} \quad (4.\ 34)$$

Where

$$\upsilon = \upsilon_d - \upsilon_k \frac{\chi_d - \chi_n}{\chi - \chi_n} \quad (4.\ 35)$$

υ_d and υ_k correspond of the projection of χ and χ_n in the M-N iteration curve respectively.

We increase the applied eccentric load N_{ed} by a constant load N ($N_{ed} = N_{ed} + N$) while the condition of the resistance of the column is not satisfied, the final value of the applied load N_{ed} is the load bearing capacity under eccentric loading ($N_{Rd,\delta} = N_{ed}$).

4.2.3 Buckling resistance of PEC at ambient temperature

The buckling resistance of the composite column in axial compression can be obtained from Eurocode 4 (EN 1994-1-1, 2004) and can be written as follows.

$$N_{Rd} = \chi.N_{pl,Rd} \quad (4.\ 36)$$

Where: $N_{pl,Rd}$ is the plastic resistance to compression of a composite cross-section and should be calculated by adding the plastic resistances of its components (steel (a); reinforcement (s); concrete (c)):

$$N_{pl,Rd} = A_a.f_{yd} + 0{,}85.A_c f_{cd} + A_s.f_{sd} \quad (4.\ 37)$$

Where: A_i is the area of the components and f_i is the yield strength of the components.

χ is the reduction factor for the relevant buckling mode given by Eurocode 3 (EN 1993 -1-1, 2005) and can be deduced according to the relevant relative slenderness $\bar{\lambda}$.

$$\bar{\lambda} = \sqrt{N_{pl,R}/N_{cr}} \quad (4.\ 38)$$

Where: $N_{pl,R}$ is the value of the plastic resistance $N_{pl,Rd}$ when the safety factors are taken equal to the unity and N_{cr} is the Euler bucking load calculated by the following formula:

$$N_{cr} = \pi^2 / L^2 \times (EI)_{eff} \quad (4.\ 39)$$

Where: $(EI)_{eff}$ is the effective flexural stiffness and L is the buckling length of the column.

$$(EI)_{eff} = E_a I_a + E_s I_s + K_e E_{cm} I_c \quad (4.\ 40)$$

Where: K_e is a correction factor equal to 0,6.

I_a, I_c and I_s are the second moments of area of the structural steel section, the un-cracked concrete section and the reinforcement respectively with the regard to the bending plane being considered. E_a E_s and E_{cm} are the modulus of elasticity of steel, reinforcement and concrete respectively.

As can be seen, when the eccentricity of loading is considered, the method of Eurocode 4 (EN 1994-1-2, 2005) becomes relatively complex for an everyday practice and it needs necessarily the computer programming. An advanced calculation method is developed based on finite elements approximation using ANSYS 18.2 (ANSYS 18.2, 2017) to determine the thermal behaviour of PEC under eccentric loading.

4.3 Advanced Calculation Method

A numerical finite element model was used for predicting the behaviour of composite columns when exposed to fire up to 120 min. ANSYS 18.2 was used to perform the numerical modelling analysis (ANSYS 18.2, 2017). After a convergence test, the mesh size used for finite element approximation is defined between 20 mm to 30 mm (see Figure 4.4). The simulation method is based on uncoupled thermal and mechanical analysis. The first step in the method solves the nonlinear transient thermal analysis and defines the temperature of the elements under fire (Fellouh et al., 2017). The thermal results applied for the mechanical analysis as a thermal load at different fire rating classes (R30, R60, R90 and R120). The second step considers the nonlinear incremental solution method to find the buckling resistance of the composite columns for specific fire rating periods. The model is a full three dimensional model, based on a perfect contact between the materials.

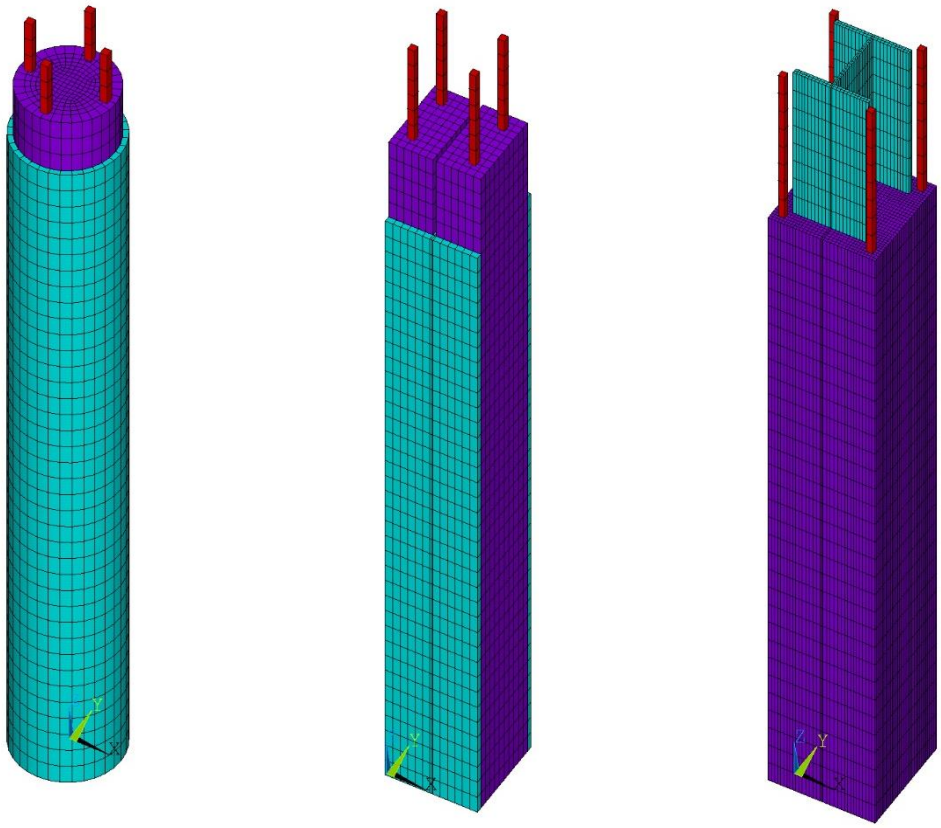

Figure 4. 4 - Finite element approximation for the different composite columns.

4.3.1 Elements used in the numerical models

Different types of elements are going to be applied to solve the thermal and the mechanical analysis. These elements are defined in the data base of the software ANSYS. The elements were selected according to the simulation needs, using the lower order finite elements available.

The finite element SHELL131 is used to model the steel profile for the thermal analysis, see Figure 4.5. The element has a 3-D layered shell element having in-plane and through-thickness thermal conduction capability. The element has four nodes with up to 32 temperature degrees of freedom at each node. The conducting shell element is applicable to a 3-D, steady-state or transient thermal analysis (ANSYS 18.2, 2017). The element SHELL131 switched to SHELL181 from thermal to mechanical model. SHELL181 is suitable for analysing thin to moderately-thick shell structures (like steel profile). It is a four-node element with six degrees of freedom at each node: translations in the x, y, and z

directions, and rotations about the x, y, and z axes. SHELL181 is well-suited for linear, large rotation, and/or large strain nonlinear applications. Change in shell thickness is accounted for nonlinear analysis. In the element domain, both full and reduced integration schemes are supported (ANSYS 18.2, 2017).

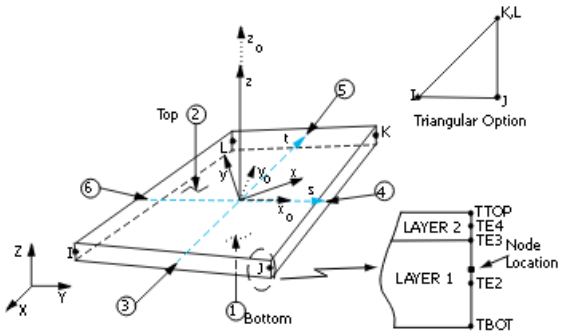

Figure 4. 5 - Finite element geometry of SHELL131.

The finite element SOLID70 is used to model the concrete. The element has a 3-D thermal conduction capability, SOLID70 has 8 nodes with a single degree of freedom, temperature at each node. The element is used to a 3-D transient thermal analysis (see Figure 4.6). The element also can compensate for mass transport heat flow from a constant velocity field. The element uses linear interpolating functions, but it is able to use 2x2x2 integration point (full integration). The element SOLID70 replaced by SOLID65 to model the mechanical behaviour of the concrete. SOLID65 is used for the 3-D modelling of solids with or without reinforcing bars (rebar). The solid is capable of cracking in tension and crushing in compression. The element is defined by eight nodes having three degrees of freedom at each node: translations in the nodal x, y and z directions. Up to three different rebar specifications can be defined. This element uses linear interpolating function, but it is able to use 2x2x2 integration points (full integration) or 1 integration point (reduced integration) (ANSYS 18.2, 2017).

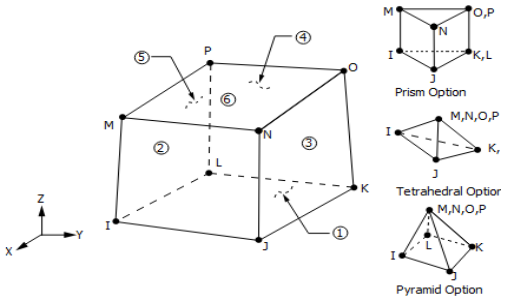

Figure 4. 6 - Finite element geometry of SOLID70.

The finite element LINK33 is used to model the reinforcement. This element has the ability to conduct heat between its nodes which are applicable to the transient thermal analysis. The element has a single degree of freedom, temperature at each node (see Figure 4.7). The conducting bar is the element which uses a linear interpolating functions and only one integration point. The element LINK33 switched to LINK180 from thermal to mechanical model. LINK180 is a 3-D spar that can model trusses and bars. The element is a uniaxial tension compression with 3 degrees of freedom in each node (translations in each direction of the coordinate system), as illustrated in Figure 4.7. The element is able to work in elastic, plastic and large deflection. The element uses linear interpolating functions and only 1 integration point (ANSYS 18.2, 2017).

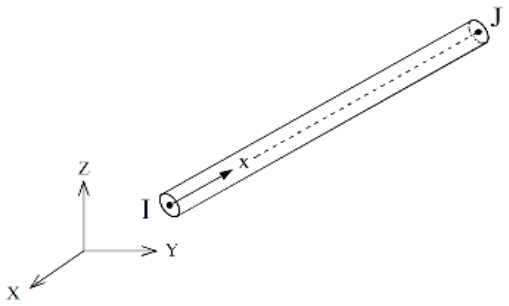

Figure 4. 7 - Finite element geometry of LINK33.

4.3.2 Thermal analysis

The thermal solution was considered transient and nonlinear, using an incremental procedure with a time step of 60 second, but it may decrease to 1 s. Four sides of the cross section were heated by the fire source ISO-834 (ISO834-1, 1999) up to 120 min. The thermal analysis was considered with radiation and convection heat transfer using standards coefficients from

Eurocede 1 (EN 1991-1-2, 2009). The finite element method requires the solution of equation 4.41 in the internal domain of the composite column and equation 4.42 in the external surface when exposed to fire. In these equations: T represents the temperature of each material; $\rho(t)$ defines the specific mass; $C_p(T)$defines the specific heat; $\lambda(T)$ defines the thermal conductivity; α_c specifies the convection coefficient; T_g represents the gas temperature of the fire compartment using standard fire ISO 834 (ISO834-1, 1999) around the cross section, Φ specifies the view factor; ε_m represents the emissivity of each material; ε_f specifies the emissivity of the fire; σ represents the Stefan-Boltzmann constant.

$$\nabla \cdot (\lambda_{(T)} \cdot \nabla T) = \rho_{(T)} \cdot C_{p(T)} \cdot \partial T / \partial t \qquad (\Omega) \tag{4. 41}$$

$$(\lambda_{(T)} \cdot \nabla T) \cdot \vec{n} = \alpha_c (T_g - T) + \Phi \cdot \varepsilon_m \varepsilon_f \cdot \sigma \cdot (T_g^4 - T^4) \qquad (\partial\Omega) \tag{4. 42}$$

A perfect contact is assumed between the rebars and concrete in this analysis. The criterion for convergence uses a tolerance value of the heat flow, smaller than 0.1% with a minimum reference value of 1x10-6. Figure 4.8 shows a temperature distribution for the composite columns after 120 min of fire.

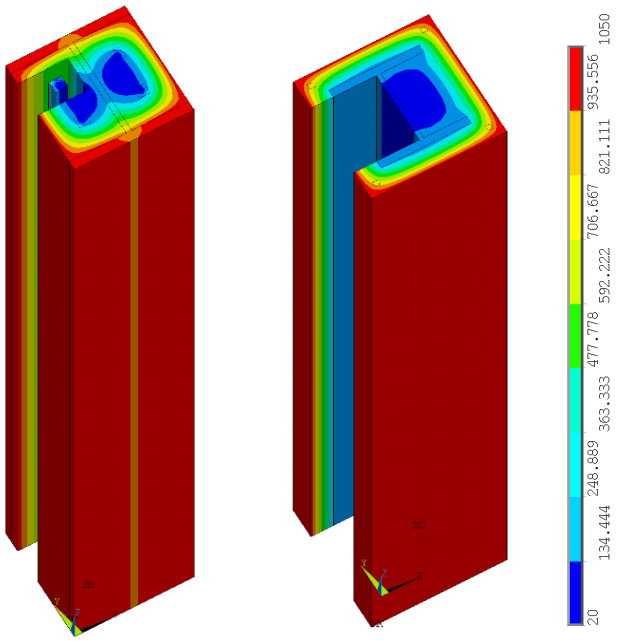

Figure 4. 8 - Temperature field for the composite columns after 120 min.

4.3.3 Mechanical analysis

For the mechanical non-linear analysis, an imperfection is applied to update the geometry of the column. The geometric imperfections were defined based on the instability mode shape defined in the elastic buckling analysis. In this model, in order to avoid convergence difficulties due to the localized effect of the loading and supports, a rigid plate modelled with SOLID185 was applied to both ends of the columns (see Figure 4.9). To model the pin-pin ended boundary condition for the composite column, two mid line nodes of the rigid loading plate are restrained in X and Y direction, and the mid height node of the PEC is restrained in the Z direction to prevent any displacement of the column (displacement controlled) as illustrated in Figure 4.9. Based on a nonlinear material model, the Arc-length solution method is used in this study, an incremental eccentric load (N_e) is applied on the top and the bottom of a rigid plate equal to (N_{rd} / 2) / 1000. In case of convergence difficulties, a minimum and maximum incremental load of 0.01xN_e and 10xN_e are used in the solution methods, being the convergence criterion based on displacement, with a convergence tolerance of 5% *N*.

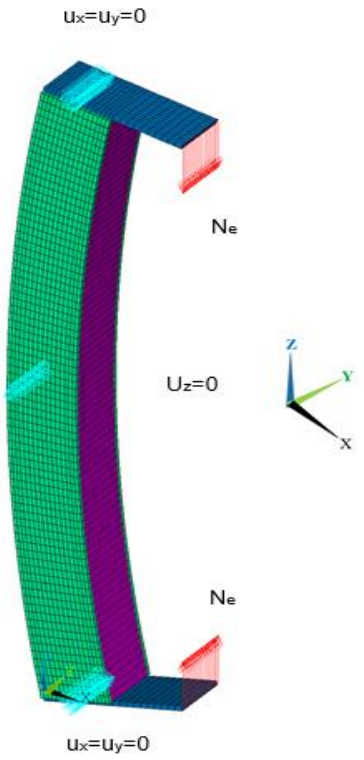

Figure 4. 9 - Numerical model, discretization and boundary conditions.

4.4 Conclusion

This chapter focused on two methods of analysis used to assess the fire resistance of the composite columns. The first method is the analytical method which uses simplified calculations rules and simplified formulae obtained from EN 1994-1-2. It consists of the determination of reduction buckling coefficients used to verify the buckling. The second method of analysis, known as advanced calculation method based on the finite element method according to the software ANSYS to evaluate the mechanical performance of the composite structures. The simulation method is based on uncoupled thermal and mechanical analysis.

Chapter 5

THERMAL AND MECHANICAL BEHAVIOUR OF COMPOSITE COLUMNS SUBJECTED TO AXIAL LOAD

5.1 Introduction

It is well known that the type of concrete and the section type have considerable effect on the thermal and mechanical behaviour of the composite columns (Fellouh et al., 2020). This chapter include two part of study, the first one investigate the effect of concrete type on the thermal and mechanical behaviour. The second part deals about the effect of the section shape on the loading bearing capacity of the composite columns. In this section, two types of concrete (HSC-NSC) are considered for the composite columns to compare the thermal and mechanical properties of the composite columns. As example two different columns are selected, notably HEB160 profile totally encased with concrete [TEC] and HEB 220 profile partially encased with concrete [PEC] as illustrated in Figure 4.1 and Figure 4.2. This type of composite column usually is found in composite structures of four to ten story. For the second part of this study three deferent composite columns having the same mechanical properties are examined in order to known their effect in load bearing capacity in fire condition. This columns are named: Partially encased column [PEC]; totally encased column [TEC] and Concrete field tubular column [CFT].

5.2 Thermal and mechanical behaviour of the composite columns

The two columns mentioned above were exposed to fire according to the standard fire curve ISO834 fire (ISO834-1, 1999). The boundary conditions are pinned in both ends with column height of 3 m. this case of boundary is the most comment in the practice. Properties for steel were assumed from S275 grade and B500 grade for profile and rebars respectively, while grade C20/25 (NSC) and grade C80/95 (HSC) were assumed for concrete. The physical and the mechanical properties of the materials of the columns are summarised in the next tables:

Table 5. 1 - Mechanical characteristics of concrete C20/25.

$f_{ck}\,[MPa]$	$f_{ck,cube}\,[MPa]$	$f_{cm}\,[MPa]$	$f_{ctm}\,[MPa]$	$E_{cm}\,[GPa]$	$\varepsilon_{c1}\,[‰]$	$\varepsilon_{cu1}\,[‰]$
20	25	28	2,2	30	2,0	3,5

Table 5. 2 - Mechanical characteristics of concrete C80/95

f_{ck} [MPa]	$f_{ck,cube}$ [MPa]	f_{cm} [MPa]	f_{ctm} [MPa]	E_{cm} [GPa]	ε_{c1} [‰]	ε_{cu1} [‰]
80	95	88	4,8	42	2.4	5

PEC and TEC composite section are shown in Figure 5.1 and figure 5.2 and their geometrical characteristics are presented in Table 5.3 and Table 5.4 respectively.

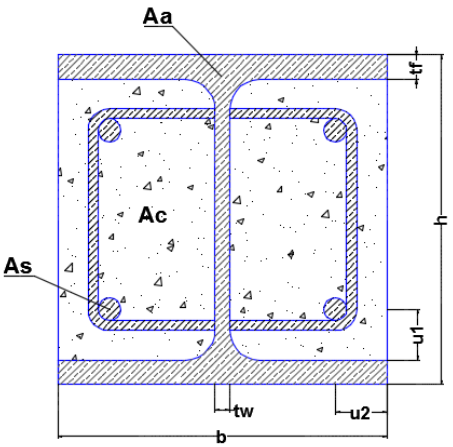

Figure 5. 1 - Cross section model for partially encased column.

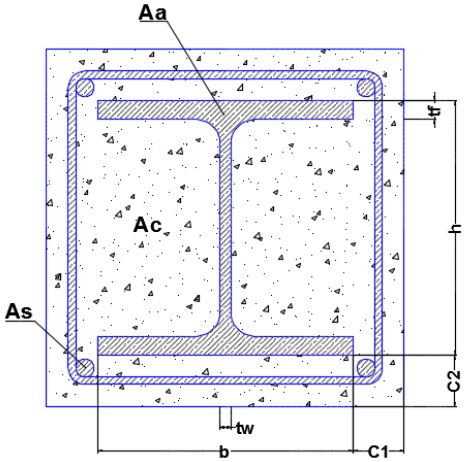

Figure 5.2- Cross section model for totally encased column.

Table 5. 3 - Section properties for partially encased columns.

Profile	*b [mm]*	*h [mm]*	t_w *[mm]*	t_f *[mm]*	*N° of bars*	u_1 *[mm]*	u_2 *[mm]*	ϕ_s *[mm]*
HEB220	*220*	*220*	*9.5*	*16*	*4*	*50*	*50*	*25*

Table 5. 4 - Section properties for totally encased columns.

Profile	*b [mm]*	*h [mm]*	t_w *[mm]*	t_f *[mm]*	c_1 *[mm]*	c_2 *[mm]*	*N° of bars*	ϕ_s *[mm]*	u_1 *[mm]*	u_2 *[mm]*
HEB160	*160*	*160*	*8*	*13*	*50*	*50*	*4*	*12*	*30*	*30*

5.2.1 Influence of the concrete on the temperature distribution

5.2.1.1 Partially encased concrete for normal and high strength concrete

The temperature evolution of the PEC columns having the same cross section geometries for NSC and HSC are illustrated in Figure 5.3 and Figure 5.4 respectively. These two type of

concrete are chosen to show the importance of concrete in protecting the column section against the fire. Three different position from the cross section are selected to estimate the temperature evolution (Flange; Web; Concrete). As seen in Figure 5.3, the temperature in the flange is greater than that of the concrete. However, the temperature in the web is approximately the same as it is in the normal strength concrete, due to the presence of concrete protection between the flanges. The difference of the temperature between the flange and the concrete is attributed to the larger thermal conductivity of the steel with the regard to the concrete and the lower specific heat of the steel compared with concrete (seen in chapter two). This may affect the loadbearing capacity of the composite column. On the other hand, a slight difference between the temperature in the web profile and the concrete is observed for high strength concrete as shown in Figure 5.4. This is probably related to the high strength concrete characteristics. The change of the heating rate observed both the flange and the web of the steel profile in the range temperature of 750 °C and 800 °C, is due to the allotropic phase transformation from the ferrite phase to the austenitic phase, see Figure 2.19.

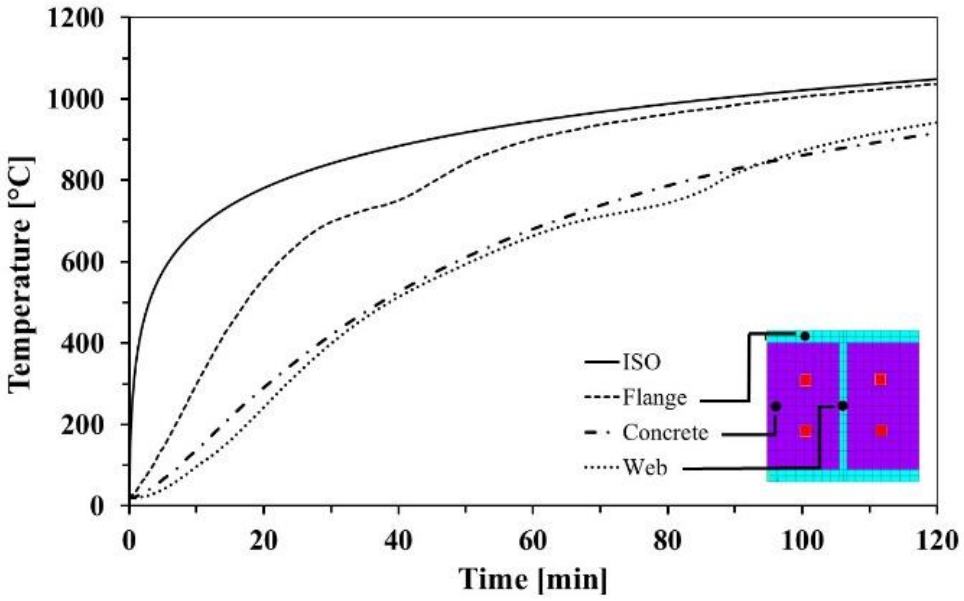

Figure 5.3- Comparison of temperature evolution in PEC with NSC.

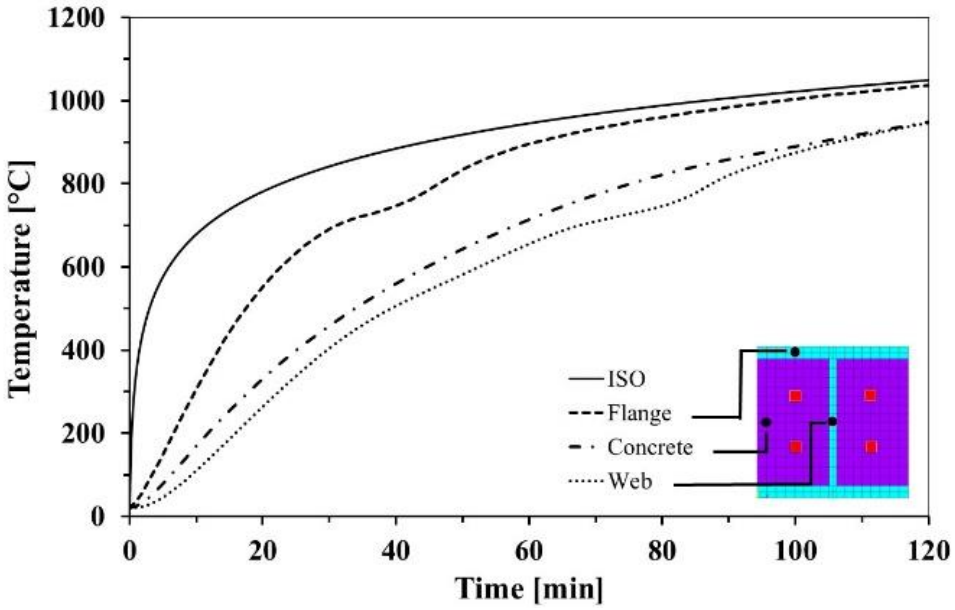

Figure 5.4- Comparison of temperature evolution in PEC with HSC.

The temperature distribution in PEC section due to fire is plotted in Figure 5.5 and Figure 5.6 corresponding to normal and high strength concrete respectively. The difference between the maximum and minimum temperature depends on the concrete type. The results found that the use of HSC reduces the level of fire protection with the regard to NSC in approximately 74 °C of difference between minimum and maximum temperature, after 120 min of fire exposure. This behaviour is justified by the high thermal conductivity and the low specific heat of HSC. It is concluded that the steel profiles heat faster when HSC is used. It is to be noted that the impact of fire on the PEC section is more pronounced for HSC than NSC.

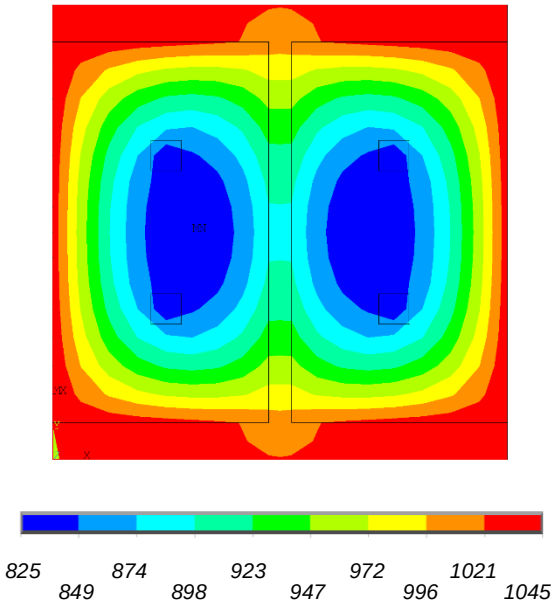

Figure 5.5 - Temperature distributions after 120 min for PEC with NSC.

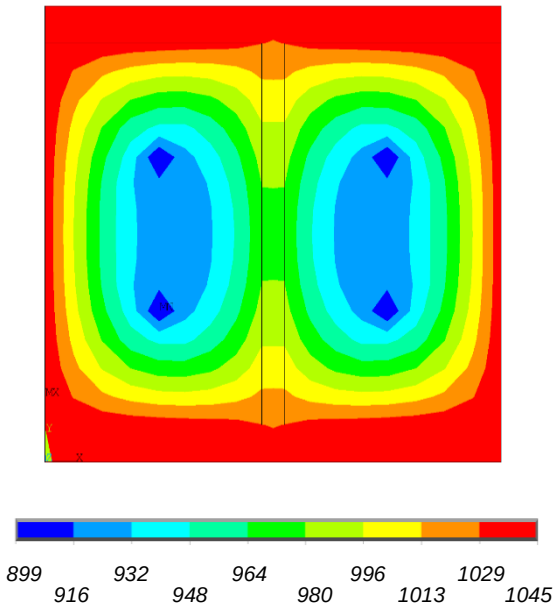

Figure 5.6 - Temperature distributions after 120 min for PEC with HSC.

5.2.1.2 Totally encased concrete for normal and high strength concrete

The temperature evolution of the TEC columns (TEC HEB160) with different types of concrete (NSC, HSC) is depicted in Figure 5.7 and Figure 5.8 respectively. From Figure 5.7 the concrete indicate the highest temperature when compared with steel profile, because the concrete is directly exposed to fire, however the steel profile present a less temperature due to the concrete cover protection. It is evident that the web less affected by the fire than the flange because of its fairest position from the external exposition aria. The maximum temperature in the flange of the composite column reaches 577.74°C for NSC and 650.99°C for HSC after 120 min of fire exposure. This suggests that NSC protects steel profile better than HSC.

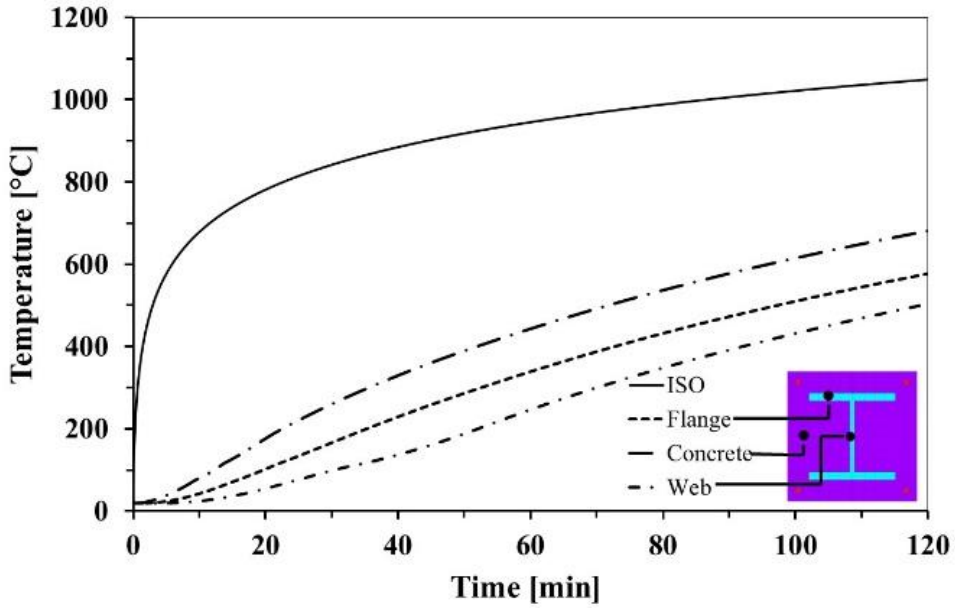

Figure 5.7- Comparison of temperature evolution in TEC with NSC.

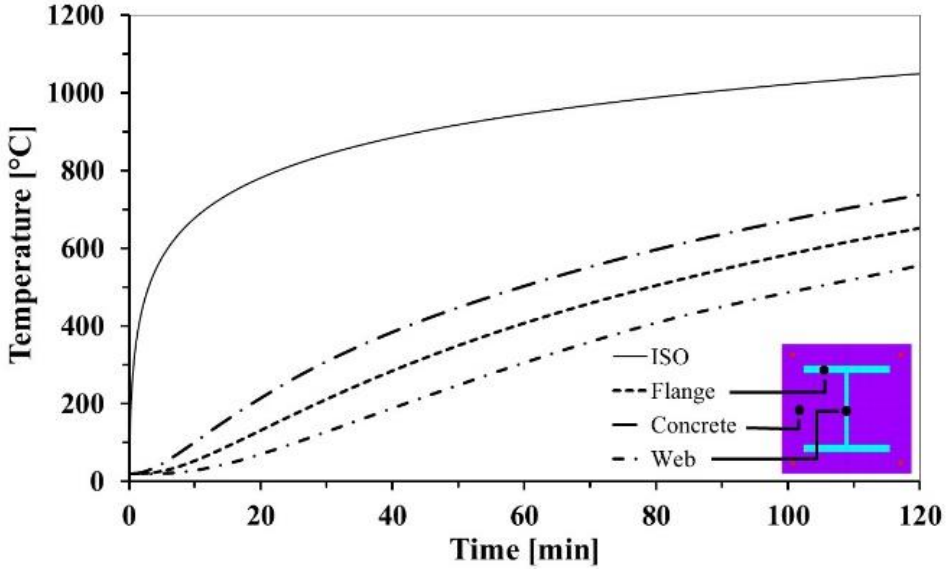

Figure 5.8- Comparison of temperature evolution in TEC with HSC.

The temperature distribution in TEC section is represented in Figure 5.9 and Figure 5.10. According to the thermal simulation, the temperature field increase with increase of time exposure. The results found show that the HSC heat faster than NSC because of its high

thermal conductivity. The difference between the minimum temperature on NSC and that of HSC is 52°C after 120 min of fire exposition. However, the cover thickness of concrete increases the fire protection of profile, therefore TEC presents higher fire protection than PEC, moreover the concrete corner shows higher temperature caused by the heat transfer from two sides.

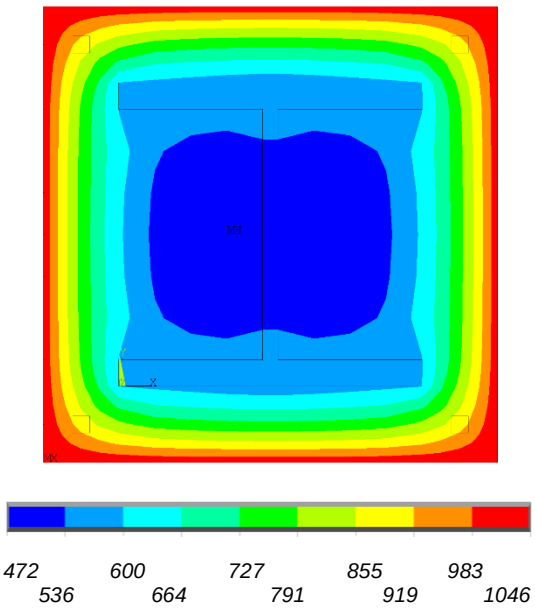

Figure 5.9- Temperature distributions after 120 min for TEC with NSC.

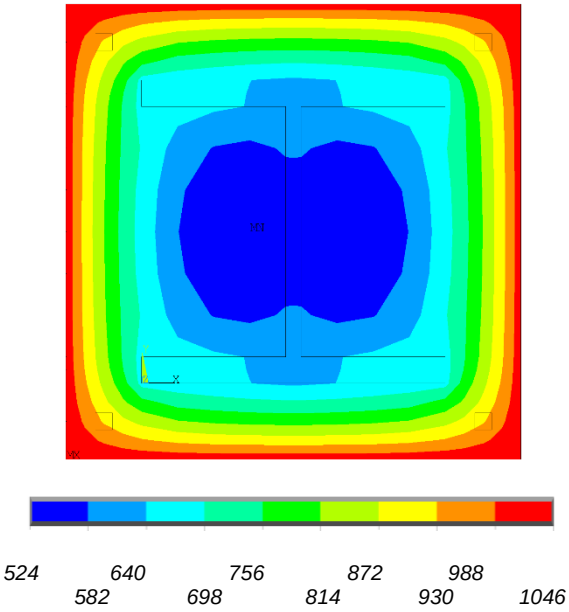

Figure 5.10- Temperature distributions after 120 min for TEC with HSC.

5.2.2 Linear bucking load of the composite columns for different cross sections

The static linear analysis is the basis for the Eigen buckling analysis. This numerical solution of a linear buckling analysis assumes that everything is perfect and therefore the linear buckling load of the composite column is greater than the real buckling load because of the imperfection are not taking into account. Figure 11 presents the buckling mode shape of composite columns for the linear analysis. The figure display the maximum displacement on the mid height of the column without exceeding 1 mm. The displacement scaling is increased by the software ANSYS in order to bring an idea about buckling mode shape.

PEC TEC

Figure 5.11- Linear buckling deformed shape example

The results of linear buckling load for both PEC and TEC under fire are illustrated in Figures 5.12 ; 5.13 ; 5.14 and 5.15 according to normal and high strength concrete. In these figures the composite columns cross section where varied from HEB 160 to HEB 200 profile. As it is expected, the linear buckling load of the composite column increases with the increase of the cross section dimension especially at ambient temperature (without fire). It is noticed that the impact of fire on the fire resistance of the PEC section is very important regardless their different cross section dimension. This behaviour is due to the absence of the concrete protection. The rate of deterioration of the buckling load for the composite column HEB200 with NSC from ambient temperature to fire rating class R30 is around 80 %. Furthermore it seems that the composite column with TEC section is less influenced by the fire compared with that of the PEC section. The rate of deterioration is around 43 % for the column HEB 200 made from NSC after 30 min of fire. This results is related to the presence of the concrete

around the steel profile. The buckling load results for the composite columns with HSC are high with the regard to those of the NSC at low fire exposure time (R30, R60). This observation is reversed at high fire exposure time (R90, R120). For instance R30 the load bearing capacity reach 1.54 e+6 N for the column with HEB 200 with NSC, however for the correspondent column with HSC the load bearing capacity reach 1.99 e+6 N.

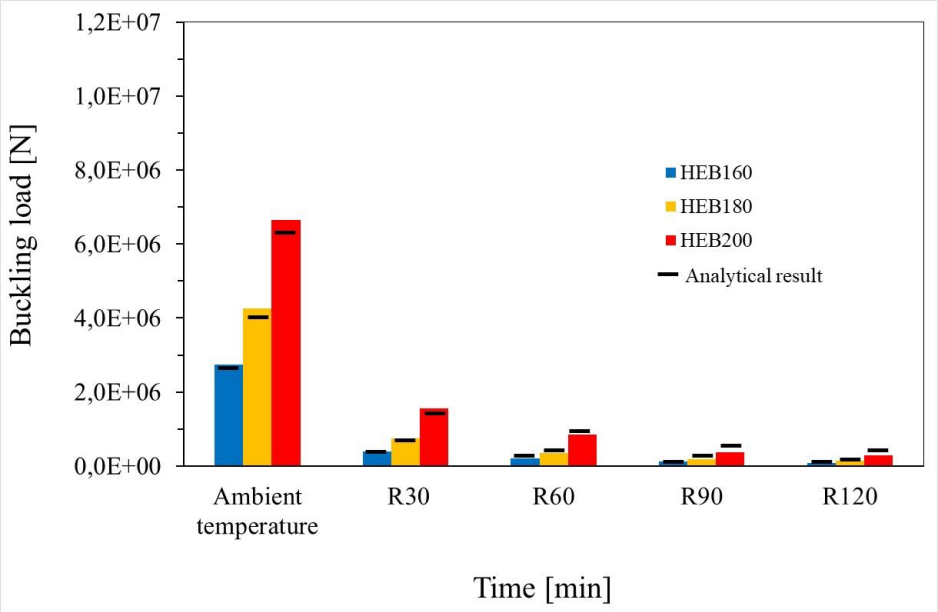

Figure 5.12- Linear buckling load of PEC composite columns made NSC.

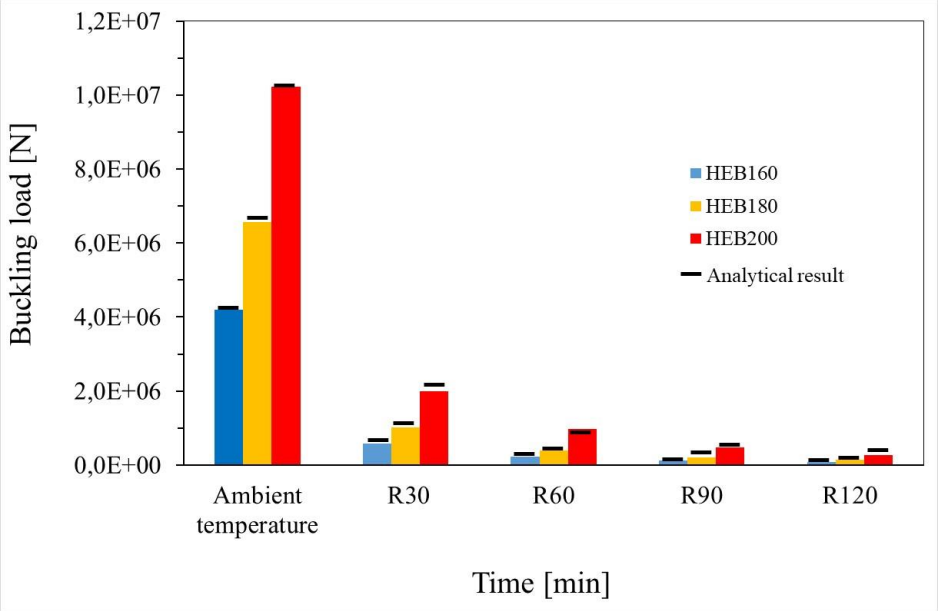

Figure 5.13- Linear buckling load of PEC composite columns made HSC.

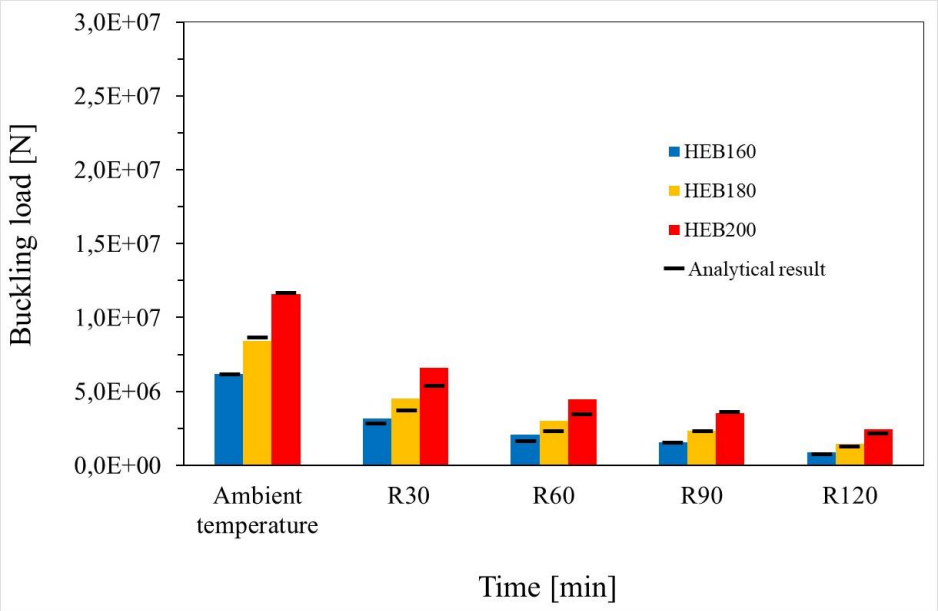

Figure 5.14- Linear buckling load of TEC composite columns with NSC.

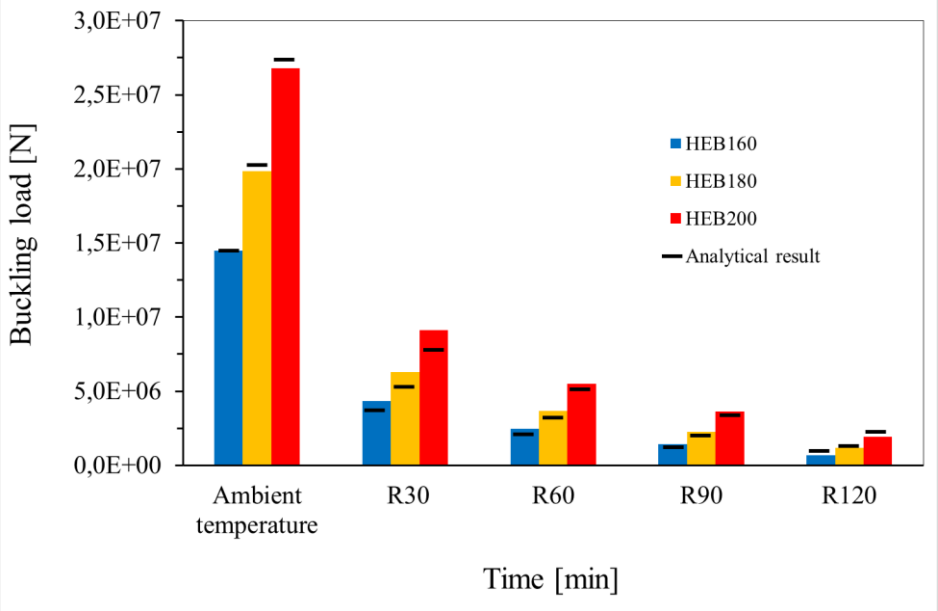

Figure 5.15- Linear buckling load of TEC composite columns with HSC

5.2.3 Verification of the numerical results

In order to validate the linear buckling results, a comparison between the numerical results and the analytical results according to Eurocode 4 (EN 1994-1-2, 2005) are presented in this

section for both column section (PEC and TEC) respectively. The most of the results found in Figure 5.16 for different cross section and different fire rating class are regrouped close to the continuous line (equal coefficient correlation r=1). The numerical result agree fairly with the analytical result. It is suggested that the fear results is obtained in the region situated between -15% and +15%. Beyond 15% the results found are considered conservative. Bellow the interrupted line (-15%) the obtained results are assumed to be unsafe. The results of TEC section obtained by the numerical method are close to those of the analytical method despite the results are little bite greater comparatively to the results of the PEC section as shown in Figure 5.17.

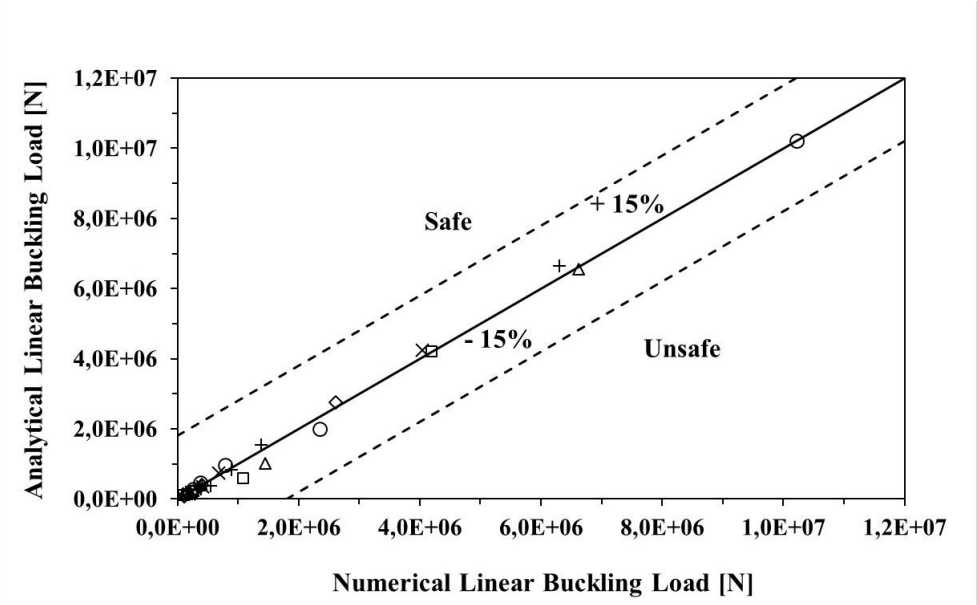

Figure 5.16- Comparison of the numerical results of the PEC composite columns against the analytical results.

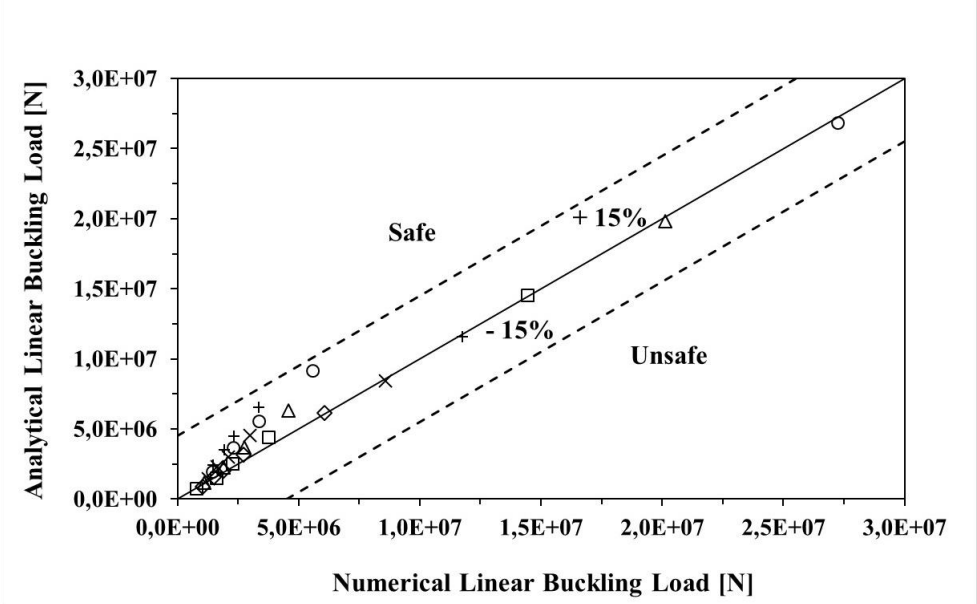

Figure 5.17- Comparison of the numerical results of the TEC composite columns against the analytical results.

5.2.4 Non-linear buckling loading

For non-linear behaviour, the imperfection is considered in the analysis. This imperfection is based on the Eigen buckling model duly scaled to the maximum considered displacement. For most of the real-world structures, the maximum imperfection is taken equal to L/150 (L height of the column) as recommended by EN-1993-1-1 in section 5-3-2 for buckling curve C (EN 1993 -1-1, 2005). The buckling load of the composite columns at elevated temperature is depend on the cross section area, materials strength and time-temperature history. Figure 5.18 and Figure 5.19 shows the variation of the buckling load of composite columns as a function of the fire exposure time. The buckling load decreases with increase of the fire exposure time regardless the material type. The reduction in buckling load is more pronounced for HSC than for NSC. This is probably due to the high thermal conductivity of HSC. A decrease of around 35% in loadbearing capacity between the two materials is found at ambient temperature indicating the best structural performances of PEC composite column with HSC. However, after approximately 60 min under fire, the two materials reach the same value of buckling load, see Figure 5.18. For TEC section (Figure 5.19), a difference of around 55% in loadbearing capacity is observed between both materials at room temperature, this may be associated with the high amount of concrete used and consequently related to

the mechanical properties of each material (see Figure 2.28 and Figure 2.30). After 30 min of fire, the two composite columns loses their mechanical performance and reaches approximately the same loadbearing capacity, and this indicate the bad fire resistance of composite column made with HSC. Similar results was also observed at high-strength concrete encased steel composite columns reported by Cheng et al (2004) and Li et al (2021). The loadbearing capacity reductions for all columns after 90 min of fire are: 88%; 82%; 89% and 72% for PEC HSC; PEC NSC; TEC HSC and TEC NSC respectively. From the comparison between the results, it is clear that the TEC composite column with NSC present the higher fire resistance. The TEC composite column with HSC present the lower fire resistance.

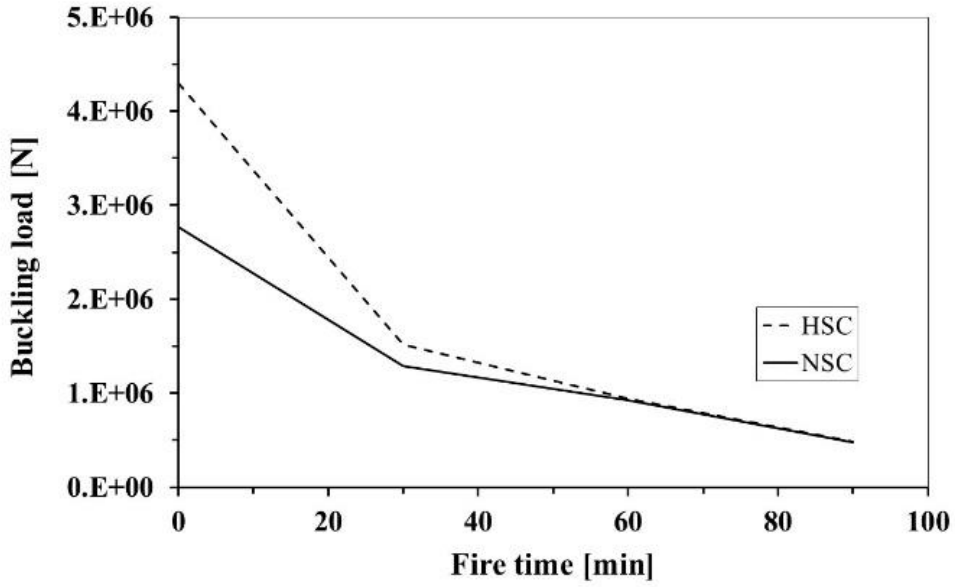

Figure 5.18- Comparison result of buckling load for PEC.

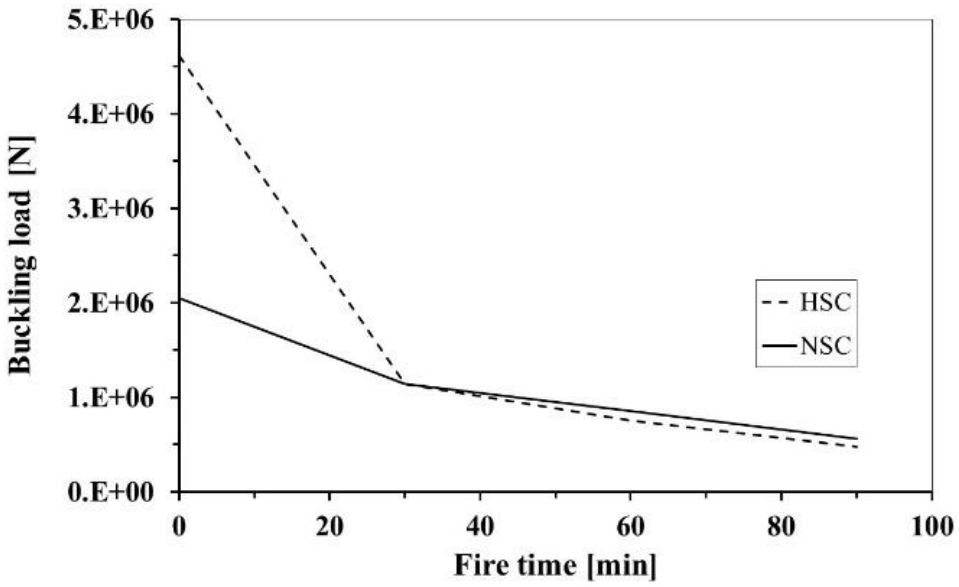

Figure 5.19- Comparison result of buckling load for TEC.

The lateral displacement versus loadbearing capacity is illustrated in Figure 5.20 and Figure 5.21 for PEC and TEC respectively. These graphs show that the lateral displacement at the mid-height of the column increases with the increase of the axial load up to the maximum loadbearing capacity. The Figure 5.20 indicates that at low fire exposure time, column made with HSC presents a high buckling load with regard to NSC. However, at elevated fire exposure time, the behaviour is reversed. It is thought that this is attributed to the difference in the thermal behaviour of the two materials. The loadbearing capacity of PEC column made with HSC exceeds approximately that of NSC about 15% at R30. After 90 min of fire, this difference is reduced. Under fire and regardless the exposure time, the deflection in column made with HSC is smaller than that of NSC (around 25%) because of the stress-train relationship of each material (ductility).

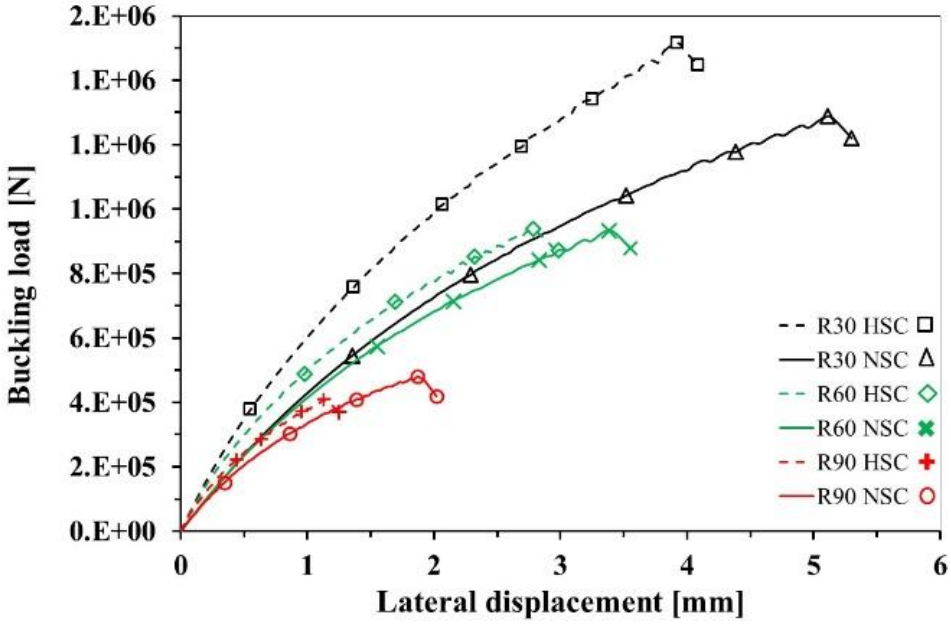

Figure 5.20- Lateral displacement-Load curve for PEC.

In Figure 5.21 it is shown the loadbearing capacity of the TEC section as a function of the lateral displacement versus. It can be seen that the use of NSC provides a deflection larger than when using HSC (about 60% of difference), which may be beneficial for evacuating the occupants in fire accident (safety case). Also this may be useful for continuous structures; the elements continue to support the external loads without collapse and this is due to the load redistribution within the structure (Hoang, 2010). In such situation, the maximum loadbearing capacity of materials is not as important as the ductility. According to Figure 5.20 and Figure 5.21, it can be seen that the lateral displacement of the composite columns is relatively small, even the solution method accounts for large displacement theory. This is mainly due to the high stiffness of the composite column. Such behaviour for composite elements is found elsewhere in the literature (An and Han, 2014; Chicoine et al., 2002). In this study, concrete material is assumed to have a non-linear behaviour without cracking or crashing, therefore the failure mode is due to the loss of stability of the composite column.

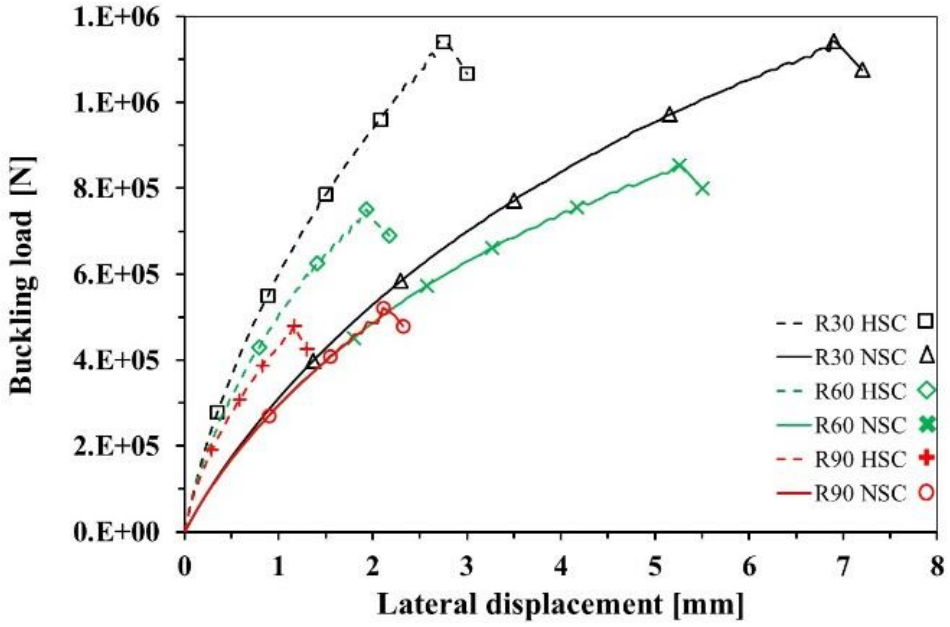

Figure 5.21- Lateral displacement-Load curve for TEC.

5.2.5 Verification of the Advanced Method Result

The buckling load results found using the finite elements simulation are compared with those obtained by simple calculation method (EN 1994-1-1, 2004; EN 1994-1-2, 2005) and presented in Table 5.5, for room temperature conditions and fire. The current field of the calculation method is limited to concrete grade between C20/25-C50/60. So, only the results for NSC will be compared in this section. The numerical and analytical results of the buckling load column are compared in load bearing capacity. At ambient temperature the PEC section present a loadbearing capacity of 2763900 N and 2700000 N using the numerical method and the analytical method respectively. Moreover, at elevated temperature (R90) the PEC composite column display a loadbearing capacity of 481539 N and 502166 N using the numerical method and the analytical method respectively. It can be seen that most of the simulation results are in agreement with that of the simplified method with a difference smaller than 5%.

In the same context, the numerical results of the TEC composite column are in agreement with those of the analytical method at ambient temperature. However, at elevated temperature R60 and R90 the TEC section present a difference of 16% and 32% respectively.

It is to be noted that the average temperature in TEC section is deduced from the finite element method and used in the simplified method, because the simplified method does not include formulas to calculate the average temperature in TEC composite column. The higher differences between the analytical and the numerical results for TEC section maybe attributed to the combination of both methods in the analysis of the behaviour of the composite column. However, the temperature evaluation of the PEC section is calculated according to Annex G (EN 1994-1-2, 2005). The mechanical performances (load bearing capacity) of the columns at room temperature are reduced more than twice after 30 min of fire exposure. This confirms the importance to consider the fire conditions in the design of composites structures.

Table 5. 5 - Buckling load, comparison between the numerical and analytical results.

Fire rating class		*Numerical results Nfi,rd[N]*	*Analytical results Nfi,rd[N]*	*Difference %*
PEC	*t=0*	*2763900*	*2700000*	*02 %*
	R30	*1287687*	*1307070*	*01 %*
	R60	*925564*	*889214*	*04 %*
	R90	*481539*	*502166*	*04 %*
TEC	*t=0*	*2050180*	*2176987*	*05 %*
	R30	*1142300*	*1136519*	*01 %*
	R60	*855109*	*1024813*	*16 %*
	R90	*560810*	*833524*	*32 %*

5.3 Influence of the section shape of the composite columns on the fire resistance

Three composite column having different cross-section where selected to assess the effect of the cross section shape on the load-bearing capacity under fire. These cross sections are namely: partially encased steel column (PEC) HEB 300 with an additional 4Ø25 reinforcement; totally encased steel column (TEC) HEB 260 profile and concrete filled tubular column (CFT) profile 323.9 with an additional 4Ø16 reinforcement, see Figure 5.22. The analyses of the columns where performed about the minor axis (z-z). The geometrical properties of the different composite column sections are taken so that to have the same load bearing capacity at ambient temperature, see figure 5.22. The load bearing capacity value of a given PEC section is determined according to the analytical formulae (EN 1994-1-2, 2005) at ambient temperature. The load bearing capacity of the other section (TEC, CFT) are calculated by varying gradually the dimensions of the section till to get the same value of

the PEC section. This value is found approximately equally to 5.2 e+6 N. All the composite columns have the same mechanical properties i;e : concrete C30/37, Steel S275 and reinforcement grade B500.

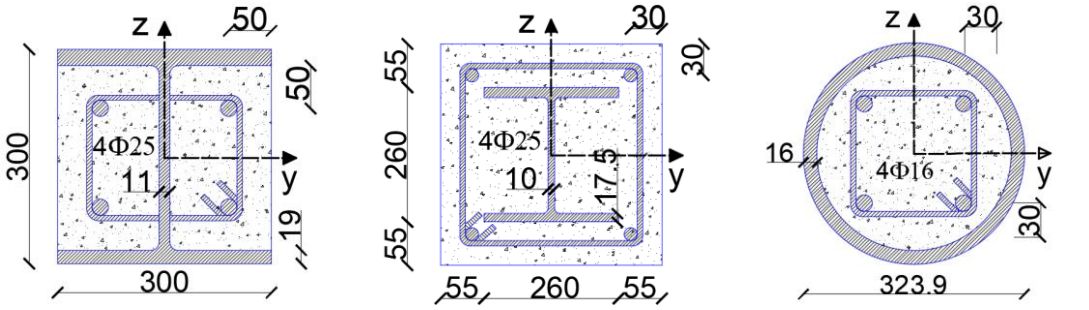

Partially encased Column **Totally encased column** **Concrete field tubular column**

Figure 5.22- Dimension of the three different cross sections composite columns.

The analyses was performed using the software ANSYS (ANSYS 18.2, 2017) to define the temperature fields and the mechanical behaviour of the three different cross sections. It is noted that the composite columns where exposed to ISO-834 (ISO834-1, 1999) standard fire from all four sides.

5.3.1 Temperature distribution of the different composite columns sections

The time dependent temperature fields of the examined cross sections obtained by the software ANSYS are presented in Figure 5.23. This analyses aims to investigate the influence of the different composite column sections on the thermal behaviour. The composite column was heated according to ISO standard fire up to 120 min. the temperature distribution for the different cross sections columns where plotted using the software ANSYS at low and the high fire rating class (R30 and R120) are exposed in this section. In general the results show significantly different average temperature reached in the cross sections. The PEC composite column reached the highest average temperature (737 °C) with the respect to the other sections seems its steel profile is subjected directly to fire. However, the TEC composite column presents the lowest average temperature which is 610 °C after 120 min under fire. Moreover, the minimum temperature represented by the bleu aria in the TEC section is 26.96 °C, which is the lower value regarding the corresponding bleu aria for the other section.

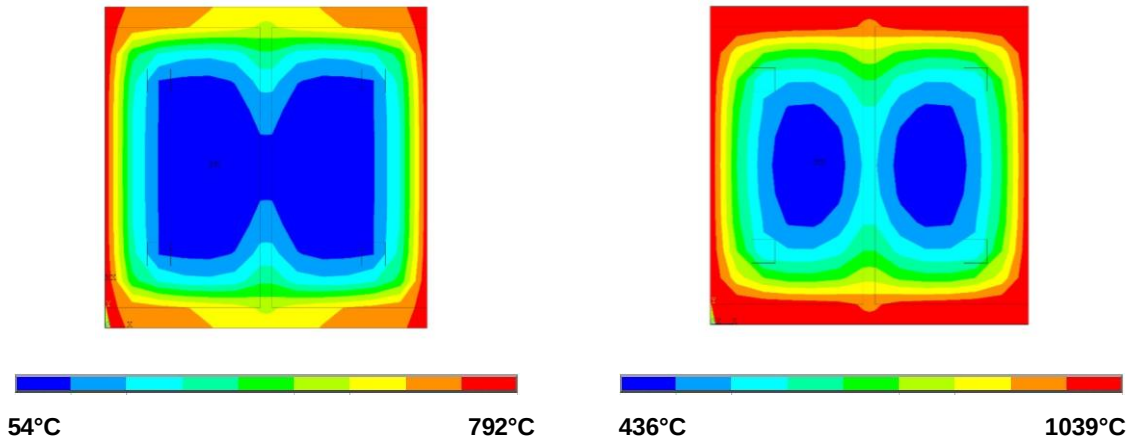

(a) PEC 30 min T=428.29°C **(b) PEC 120 min T=737.95°C**

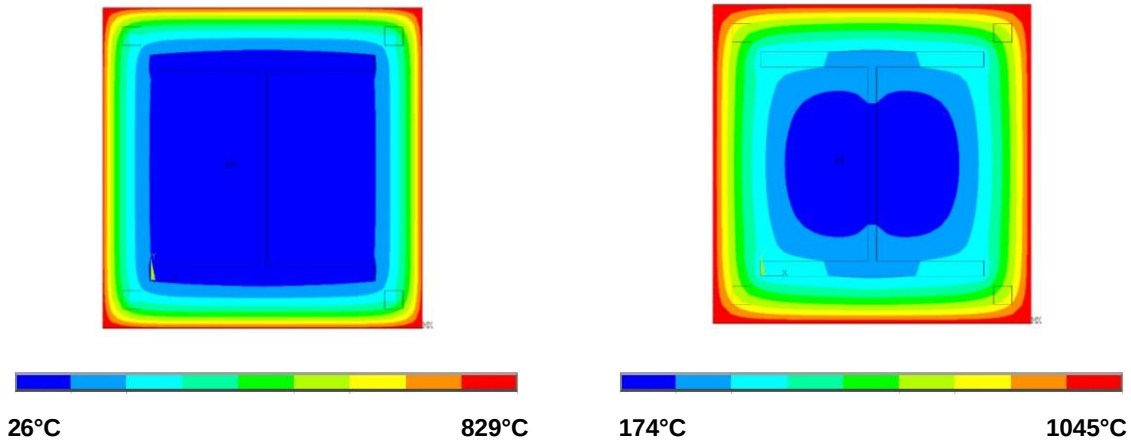

(c) TEC 30 min T=428.46°C **(d) TEC 120 min T=610.28°C**

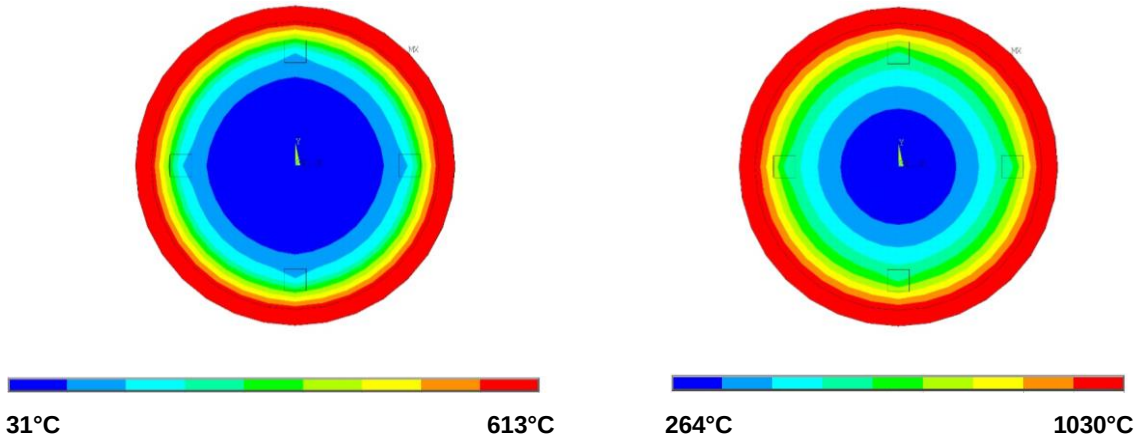

(e) CFT 30 min T=359.04°C **(f) CFT 120 min T=647.59°C**

Figure 5.23 - Temperature distribution for different cross sections composite columns.

The totally encased composite column resist better to fire because of the cover concrete protection. Otherwise, the CFT resists to fire better than the PEC columns because the concrete inside section is confined by the tube steel profile which has reduce the fire impact.

It is to be noticed that the weak point for the PEC section is situated in the core of the PEC section. This problem is due to the fact that the flange of the PEC which is not entirely protected by the concrete is joined with the web leading to a heat transfer, as a result the temperature of the core section is enhanced.

To better understand the thermal behaviour of the different section type, the average temperature of each section is plotted as a function of the fire exposure time in Figure 5.24. The average temperature for all sections increases with the increase of the fire exposure time. In general, the temperature variation of the three different sections includes two stages. In the first stage (the first few minute) the rate of temperature rise increases fast. The second stage start after 10 min; 20 min and 37 min for the TEC; PEC and CFT section respectively.

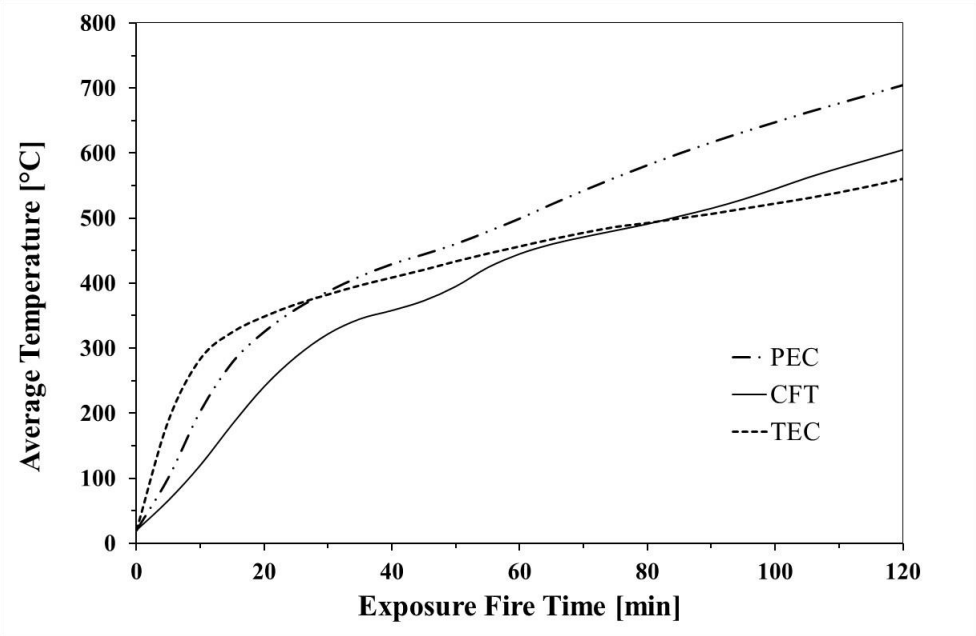

Figure 5.24- Average temperature evolution versus exposure fire time for the different cross sections composite columns.

The rise of the temperature rise in this stage is slow. After 120 min under fire, the TEC section displays the lowest average temperature than that of the CFT section and finely that of the PEC section. The thermal behaviour in the first stage is mostly influenced by the ISO fire. The difference in the rate of the temperature rise between the different sections may be probably attributed to the amount and the thermal characteristics of the materials. In the second stage, the temperature rise is decreasing a little bit because of the composite material

that constitutes the sections. Columns at elevated temperature. At the end of the second stage the difference in the average temperature between the different sections is related to the thermal conductivity of each material and the presence of the concrete. In addition the steel profile and the steel tube of the PEC and the CFT respectively are subjected directly to fire. So the average temperature in these sections becomes highly related to the bad thermal performances of the steel. This figure highlights very well the importance of the concrete in the composite columns at fire accident regarding the thermal behaviour as found by Milanović et al (2015).

5.3.2 Load bearing capacity of the different composite columns sections

The load bearing capacity curves for the three types of columns were plotted as a function of the fire exposure time period of standard fire exposure according to the advanced calculation method as shown in Figure 5.25. It is observed that the Mechanical properties of constitutive materials are reduced considerably by the fire action, which results in a low load bearing capacity of all columns with regard to that under ambient temperature. The TEC composite column present the highest fire resistance compared with other columns especially between R30 and R90. This result may be related to the best thermal behaviour of the TEC column due to its concrete cover. However, the CFT column presents the lowest buckling load because of the low fire performance of its steel profile, which is directly exposed to fire. When the PEC column compared to the CFT column it is demonstrated that the PEC column behave better than CFT column because it is reported that the square section shape resist better than the circular section shape (Rodrigues and Laim, 2017). At R90, the columns reach a very low level of load bearing capacity, seems the temperature at this rate is very high and all the materials component lost their performance. For that the three composite columns converge to the same value of buckling load. The composite column with TEC section can supports a load bearing capacity of 2.5 MN up to 60 min under fire, however for approximately the same value of load bearing capacity the column with CFT section can support only 30 min under fire.

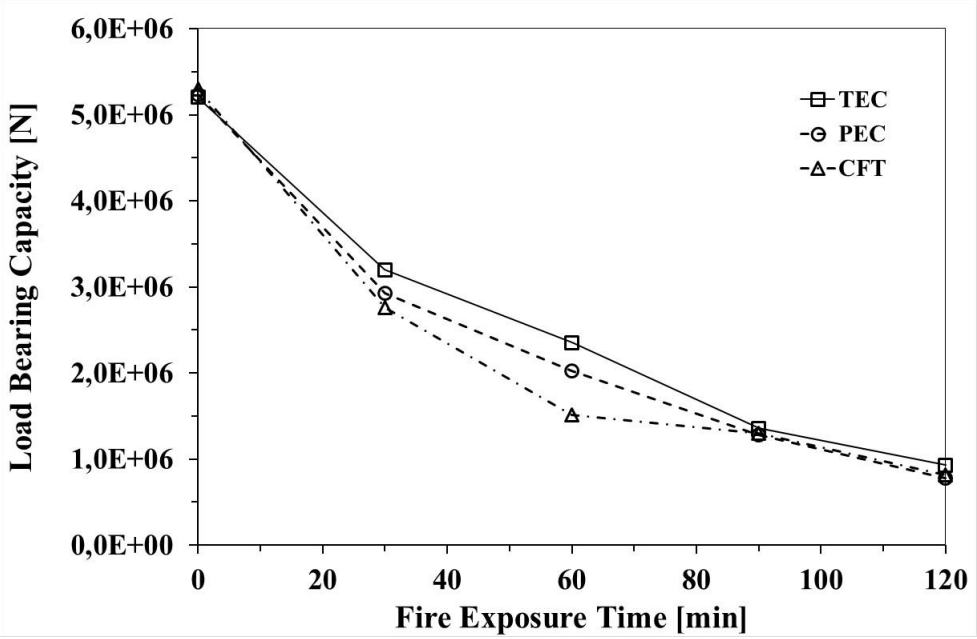

Figure 5.25- Load bearing capacity of composite columns at different fire rating class..

5.4 Conclusion

The linear and non-linear behavior of composite columns in fire situation was investigated according to the advanced and simplified calculation method. The main variable in this study where: the concrete strength and the composite column shape. A several calculations where performed to assess the thermal and mechanical behavior of the composite column including the temperature evolution and the load bearing capacity and the following conclusions can be made:

- The use of analytical method is limited to normal strength concrete. For high strength concrete we need to use a numerical model such as ANSYS to describe the linear the non-linear behaviour of composite columns under fire.
- The use of HSC in composite column reduces the level of fire protection with the respect to NSC. This behaviour is attributed to the high thermal conductivity and the low specific heat of HSC.
- By doing a comparison between three different composite column sections, it is found that TEC composite column present the lowest average temperature after 120 min under fire. This section resist batter to fire because of the concrete cover.

- The average temperature variation of the three different sections includes two different stages. In the first stage the rate of temperature rise increases fast. In the second stage the temperature rise is slow.
- The linear buckling load of the composite column increases with the increase of the cross section dimension especially at ambient (without fire).
- The rate of deterioration of the linear buckling load for the PEC composite column made with NSC is around 80 % when the temperature increases under 30 min of fire. It is also found that the composite column with TEC section is less influenced by the fire compared with that of the PEC section.
- The results of the linear buckling show that the use of HSC presents a high value of load bearing capacity at low fire exposure time (R30, R60). However at high fire exposure time the results of the load bearing capacity for NSC are better than those of the HSC.
- The results of linear calculation for TEC section obtained by the numerical method are close to those of the analytical method despite the results are a little bit greater comparatively to the results of the PEC section.
- The non-linear analyses shows that the use of HSC concrete is beneficial for composite columns regarding its best performance at low fire exposure time. However, this behaviour is not observed at higher exposure time.
- The buckling load results indicate that the use of HSC concrete in composite columns shows a higher degradation at elevated exposure time compared with NSC concrete, particularly when using totally encased column (TEC).
- The mechanical performance (loadbearing capacity) in composite columns at ambient temperature are reduced more than twice after 30 min of fire exposure. This confirms the importance to consider the fire conditions in the design of composites structures.
- NSC in composite structures provides more deflections than HSC (about 60% of difference), which may be useful during fire accident (safety level).
- The TEC composite column present the highest fire resistance compared with other columns especially between R30 and R90. This result may be related to the best thermal behaviour of the TEC column due to its concrete cover.
- The CFT column presents the lowest buckling load because of the low fire performance of its steel profile, which is directly exposed to fire.

- The composite column with TEC section can supports a load bearing capacity of 2.5 MN up to 60 min under fire, however for approximately the same value of load bearing capacity the column with CFT section can support only 30 min under fire.

Chapter 6

THERMAL AND MECHANICAL BEHAVIOUR OF COMPOSITE COLUMNS SUBJECTED TO COMBINED COMPRESSION AND BENDING

6.1 Introduction

In most structures with portal frame, compression load in columns are applied with bending moments (eccentric loading), which may create instability problems, particularly in fire accident. In this work, a numerical investigation was carried out to simulate the fire behaviour of composite column subjected to combined compression and bending. The main variable in this part of study where: the buckling length with 3, 4.5 and 6m, the load eccentricity about the week axis (e function of b) with e=50%*b; e=100%*b and e=150%*b, where e is the applied load eccentricity and b is the dimension of the section base, finally the reinforcement incorporated into the concrete. This analysis lead to a determination of the axial load and the bending moment, which allowed finding the M-N interaction curve, this later aids to verify the safety of the composite column section. It is to be noted that the analysis was performed using the advanced method according to the software ANSYS (ANSYS 18.2, 2017) and the verification was done using the simplified method according to the standard Eurocode 4 (EN 1994-1-2, 2005).

6.2 Effect of eccentricity on the load bearing capacity of the composite columns

6.2.1 M-N interaction diagram at ambient temperature

M-N interactive curves were developed to present the combined compression-bending resistance of columns in a single figure. The axial load (*N*) versus the bending moment (*M*) are represented by Y axis versus X axis respectively, the interior of the m-n interaction diagram indicate the safety region and the exterior the unsafety region. A PEC section with HEB300 profile is selected for the determination of the interaction curves diagram. The steel profile is S 275 grade and the rebars are B500 grade, while concrete is C30/37. Such characteristics of the section are commonly in practice, see Figure 6.1.

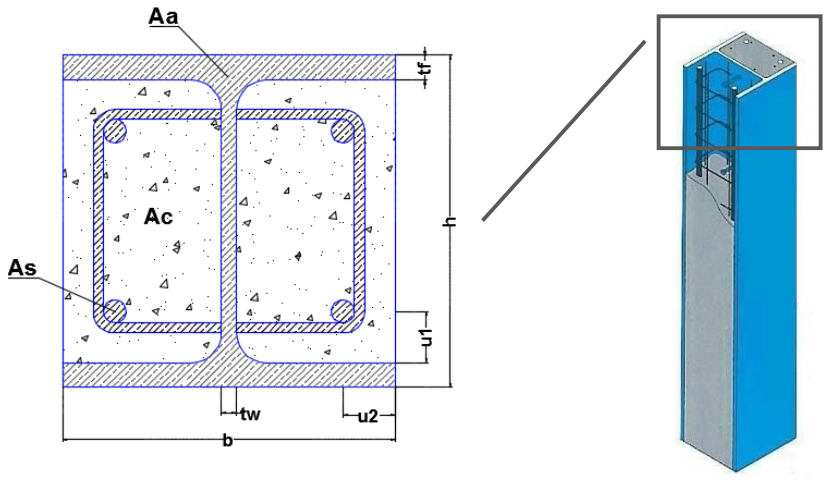

Figure 6. 1 - Cross section example of PEC column.

The M-N interaction diagram determined by both advanced and simplified method presented in Figure 6.2 for a different eccentricities (*e*0 mm; *e*150 mm; *e*300 mm; *e*450 mm). The buckling length where taken 3 m. It can be seen that in general, when the eccentricity of loading is involved, the bearing capacity of the column is decreased.

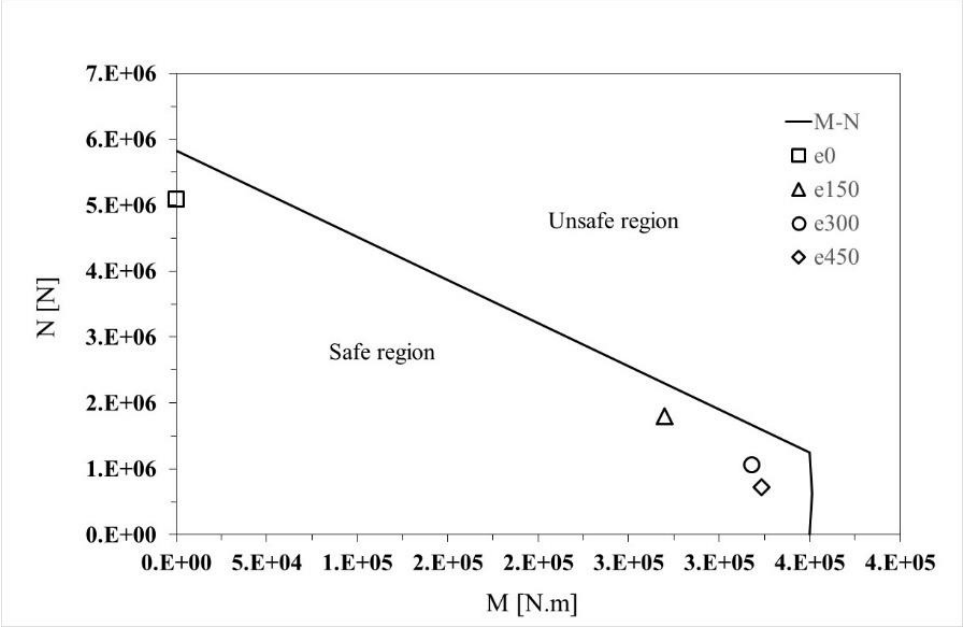

Figure 6. 2 - Interaction M-N curve for uniaxial bending PEC HEB300 3m.

The M-N interaction curves of PEC columns with different cross-sections are displayed in Figure 6.3 at ambient temperature. We found that there are significant differences in M-N interaction curves, indicating that the cross-sectional type affects columns load bearing

capacity under eccentric loading. The M-N interaction curves capacity decrease with the decrease of the cross section geometries.

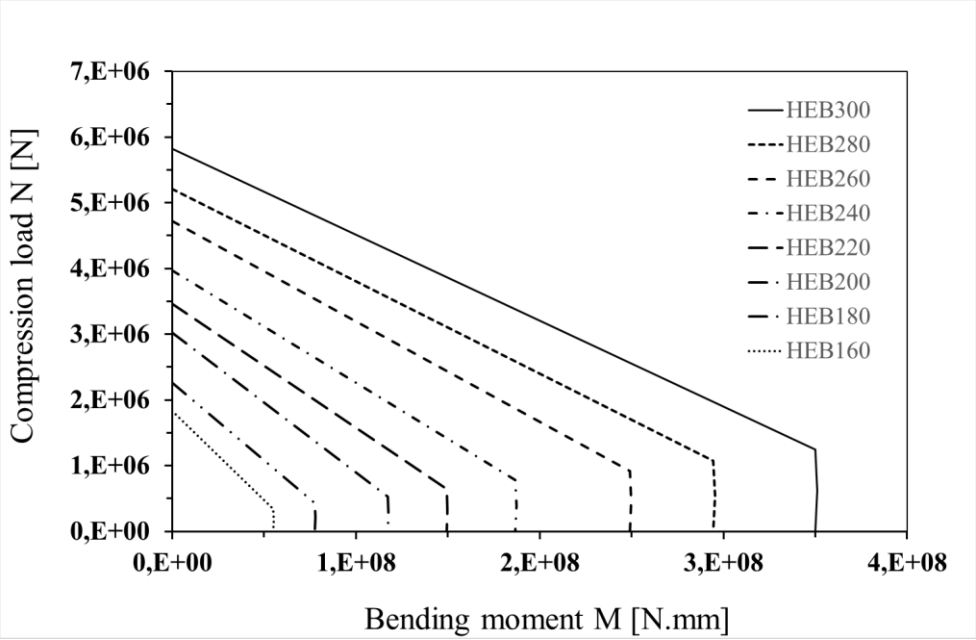

Figure 6. 3 - M-N interaction diagram for different cross section.

6.2.2 M-N interaction diagram at fire situation

Figure 6.5 shows the variation of buckling resistance of PEC columns depending on the fire exposure time and eccentricity of the load, using both analytical and numerical method. The buckling load decreases with the increase of fire exposure time and the level of eccentricity. It is known that the high temperatures caused by fire effect, affects considerably the mechanical properties of the materials component. Consequently, the region limited by the axial force and by the bending moment bearing capacity of the columns is reduced, resulting in a change of the M-N interaction diagrams (load bearing capacity). It is clear from Figure 6.5 that EN-1994-1-2 results agree fairly with the results of the finite elements model (ANSYS results), particularly at higher fire rating class (R60-R90-120), however at low fire exposure time (R30), the analytical method presents higher unsafe results when applying an eccentric loading (unsafe case). It is thought that the average temperature in the core concrete reached 216 °C after 30 min of fire exposure (R30) estimated by the analytic method. However at this fire rating class (R30) the temperature depends of the position of the node

in the concrete material, calculated by the numerical method. The temperature varies from the surface to the core concrete from 64°C to 792 °C respectively (see Figure 6.4). It is clear that the average temperature given by the analytical and the numerical method are not closes to each other, which may explain the unsafety result found. Espinos et al (2014) found in his study cared out on axial and eccentric loaded composite column that the EN-1994-1-2 method give unsafety results for the axial loaded column at elevated temperature).

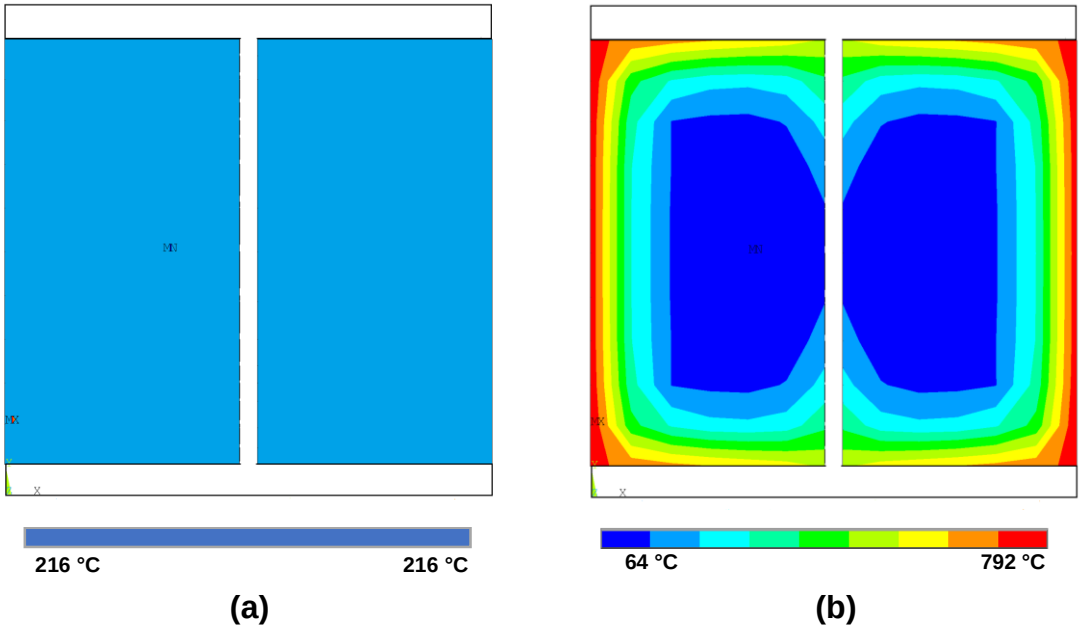

Figure 6. 4 - (a) Temperature distribution in concrete by analytical method; (b) Temperature distribution in concrete by numerical method

For the other fire rating class (R60; R90; R120) it is thought that the fire exposure time is enough to the heat to be spread in all parts of the concrete, as a result the average temperature estimated by the numerical method will be approximately the same as calculated by the analytical method. This may explain the close results in the numerical and analytical methods.

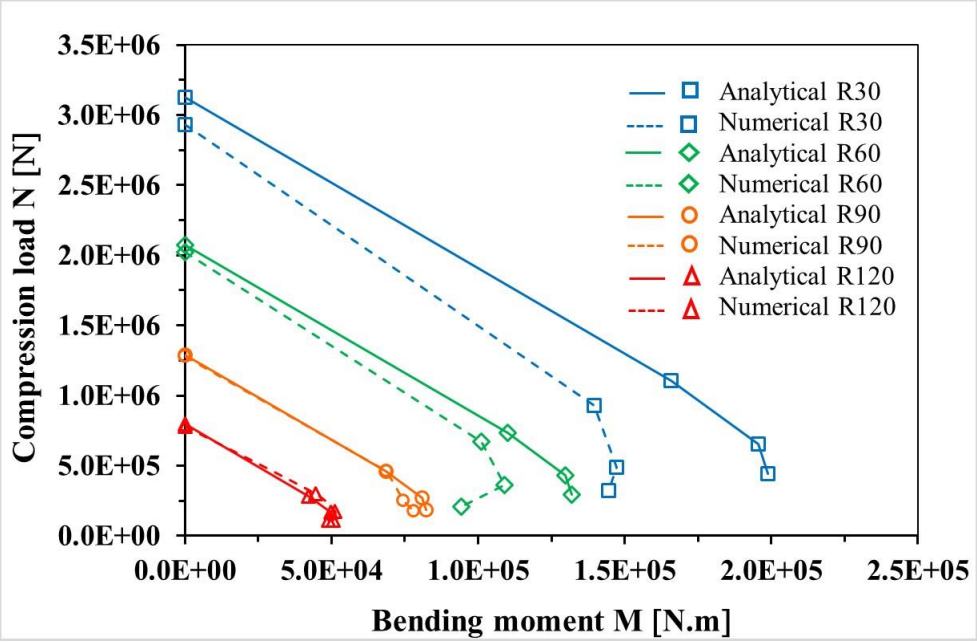

Figure 6. 5 - M-N interaction diagram for different fire rating class.

6.2.3 Compression Load versus Lateral Displacement

The effect of varying the eccentricity of the load for same height (3m) is plotted in Figure 6.6. It is to be noted that the variation of eccentricity has a significant influence on the load capacity as found elsewhere (Won et al., 2016). For stance the variation of the eccentricity of 150 mm to 300 mm leads to reduction of the load capacity of 50 %, however, its effect is less pronounced on the displacement.

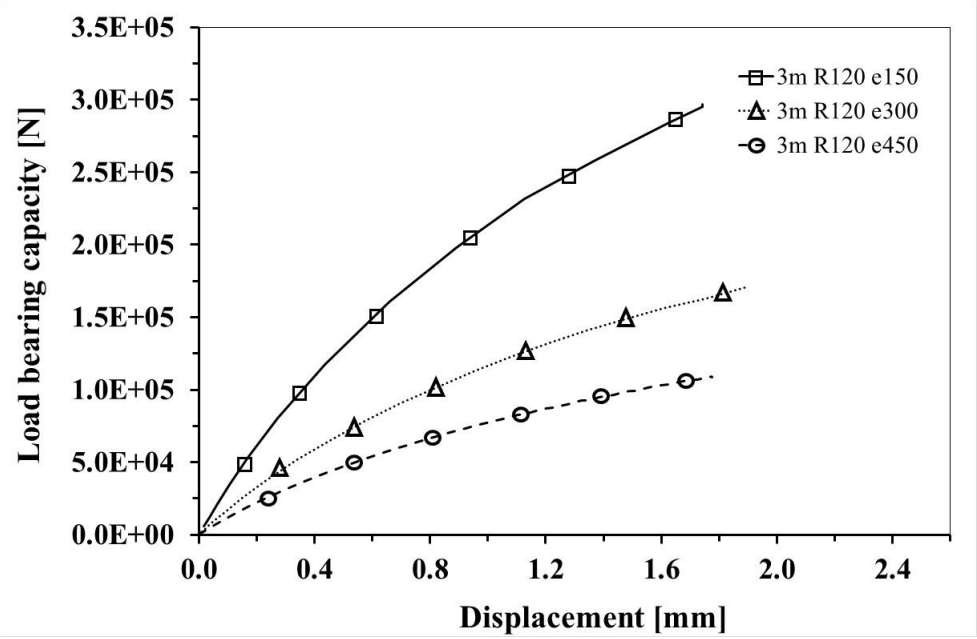

Figure 6. 6 - Displacement versus load capacity with column height of 3m and 120 min of fire.

6.3 Effect of buckling length on the fire resistance of composite columns

6.3.1 M-N interaction curve

The effect of the buckling length on the M-N interaction diagram evaluated with both methods is illustrated in Figure 6.7 for 120 min. As expected, the M-N values decrease with the increase of the buckling length of the composite column, especially for the column with 3 m height, the moment resistance decreases after reaching its maximum value. It is clear from the Figure 6.7 that the results found with the numerical method agree fairly with those calculated of the analytical when considering different buckling length.

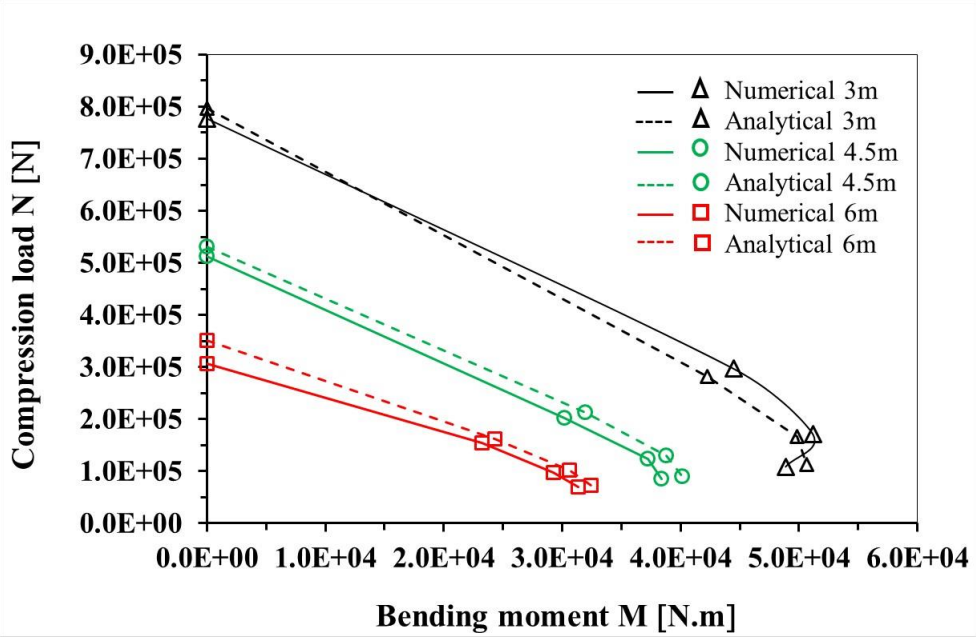

Figure 6. 7 - M-N interaction diagram for different column slenderness.

6.3.2 Compression Load versus Lateral Displacement

The variation of compression load with the lateral displacement in the mid-height of the column is represented in Figure 6.8 for high fire rating (R120). It is shown in Figure 6.8 that the lateral displacement increases with the increase of the compression load, for the same buckling length. When increasing the buckling length of the column, the load capacity is reduced and the displacement is highly increased. The comparison the figure 6.6 and figure 6.8 indicate that the eccentricity has more influence in the load capacity then the buckling length. In practical design of composite structure, it is more interesting to consider the effect of eccentric loading then the effect the slenderness.

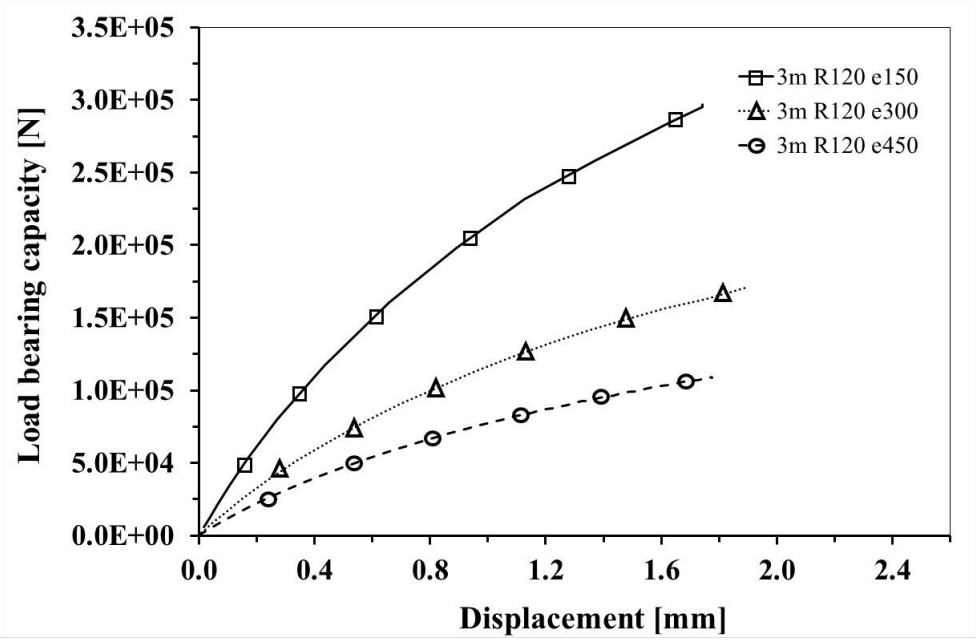

Figure 6. 8 - Displacement versus load capacity with e=450mm and 120 min of fire.

6.4 Buckling load bearing capacity

Figure 6.9 shows the variation of the load bearing capacity of the composite column (3 m high) as a function of the fire exposure time under axial compression and combined compression and bending. Composite columns display a reduction of the buckling load with the increase of the fire exposure time as a result of the deterioration of the mechanical properties of the materials. The PEC composite column loaded by an axial compression resists better to the fire than the composite column under an eccentric loading. For instance, the load bearing capacity of the composite column under axial compression load at R120 is 7.77 E5 *N*, however that of the composite column under combined compression and bending R60 is only 6.73 E5 *N*. In case of fire accident, the composite column designed to resist to buckling at R120 under compression without eccentricity will be similar to the column subjected to an eccentric loading at R60; the fire rating is reduced at more than half.

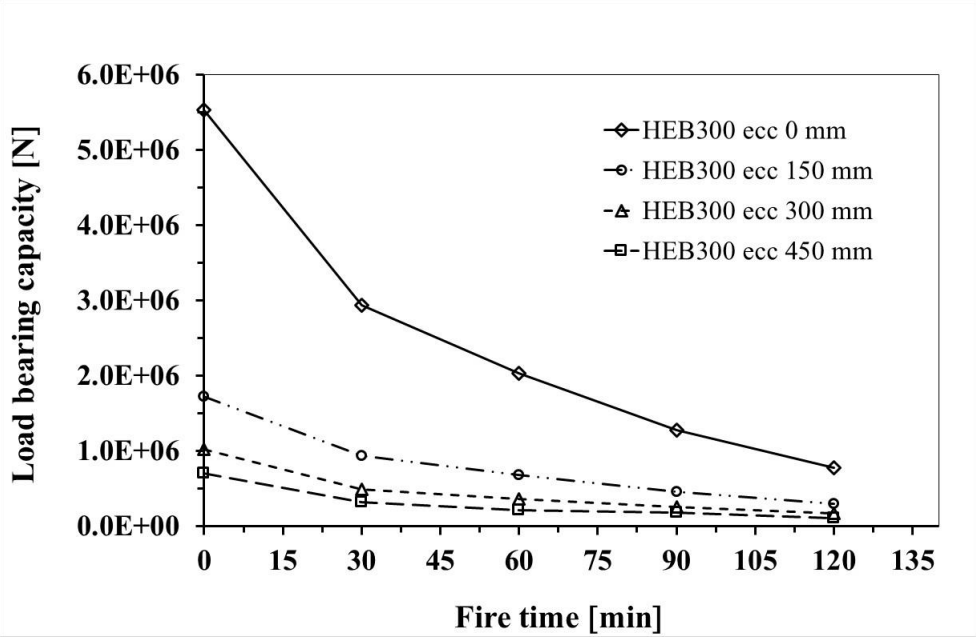

Figure 6. 9 - Fire time versus load capacity in PEC.

The variation of the load bearing capacity versus eccentricity for ambient and elevated temperature is illustrated in Figure 6.10. The load bearing capacity at the different temperature decreases with the increases of the eccentricity. It can notice when applying a bending moment with compression on the composite column, a strong reduction in the load capacity is observed (similar to the result of Ren et al (2017)), but with the increase of fire rating, a slight reduction is noted. The effect of eccentricity on the load bearing capacity of the composite column is less pronounced with the increase of the fire rating class. According to the Figure 6.10 the load bearing capacity become very weak in the presence of the eccentric loading and the fire accident (about 87 % and 85 % load capacity reduction for the eccentricity and fire effect respectively) this is why it is recommended to avoid as possible eccentric loading in construction building.

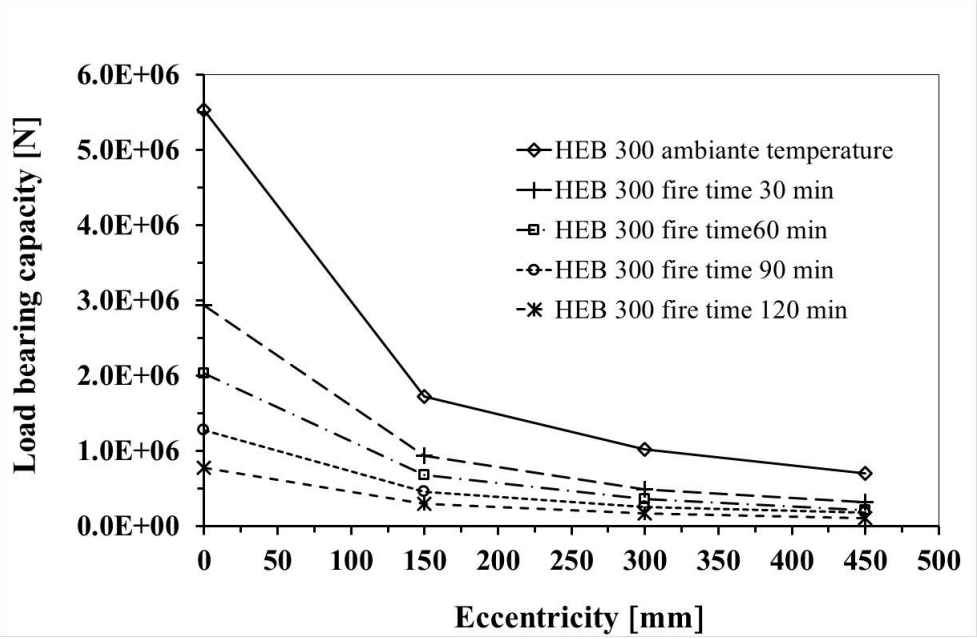

Figure 6. 10 - Eccentricity versus load capacity in PEC.

6.5 Reinforcement Contribution of Composite Column in Fire Resistance

The temperature distribution in PEC composite column with and without rebars is plotted in Figure 6.11 using the advanced numerical method (ANSYS). According to both cross section, the difference between the minimum temperatures is 5°C after 120 min. The results show that including rebars in composite column increases slightly the level of fire protection as found by Ukanwa et al (2017). It is observed that the presence of reinforcement has modified the temperature distribution of the cross section.

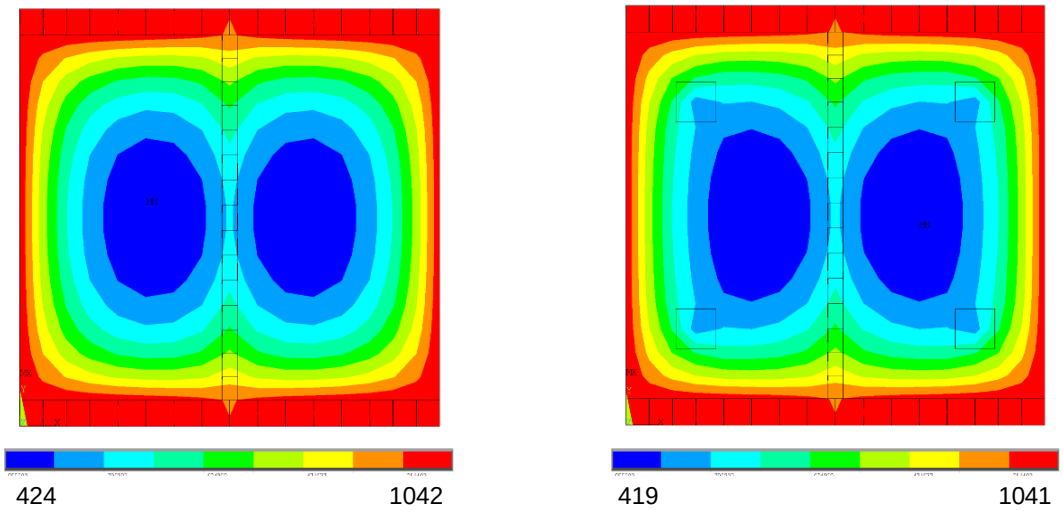

Figure 6. 11 - (a) Temperature distribution in PEC without rabars at R120; (b) Temperature distribution in PEC with rabars ϕ25 at R120

The effect of the reinforcement on the load capacity for the same geometrical cross section (PEC HEB300) incorporating different rebar's diameter (ϕ0, ϕ10, ϕ25), is illustrated in Table 6.1. The results found indicate that the load capacity of the PEC column increases with the increase of the reinforcement content. So it is clear that the reinforcement has a greater contribution when the column is subjected to eccentric loading than when it is under axial compression as shown in Table 1 (expressed by the difference in percentages). This results is found elsewhere (MacGregor and Bartlett, 2000). This is maybe related to the good compression strength of concrete in case of axial loading, which does not need reinforcement (see Figure 6.12 (a)). However, in case of combined compression and bending the concrete section may suffer from the tension stress, which explains the importance of the presence of the reinforcement (see Figure 6.12 (b)). For a given reinforcement the loading eccentricity has a more pronounced effect on plain concrete than the reinforced concrete.

Table 6. 1 - Effect of reinforcement on the load bearing capacity of the composite column.

Eccentricity	Load bearing capacity [N]			Difference in [%]		
e [mm]	⌀0	⌀10	⌀25	⌀0/⌀10	⌀10/⌀25	⌀0/⌀25
0	7.40E+05	7.45E+05	7.77E+05	0.61	4.33	4.96
150	2.47E+05	2.67E+05	2.97E+05	7.78	11.43	20.11
300	1.40E+05	1.51E+05	1.71E+05	8.25	12.96	22.27
450	9.29E+04	9.95E+04	1.09E+05	7.15	9.09	16.89

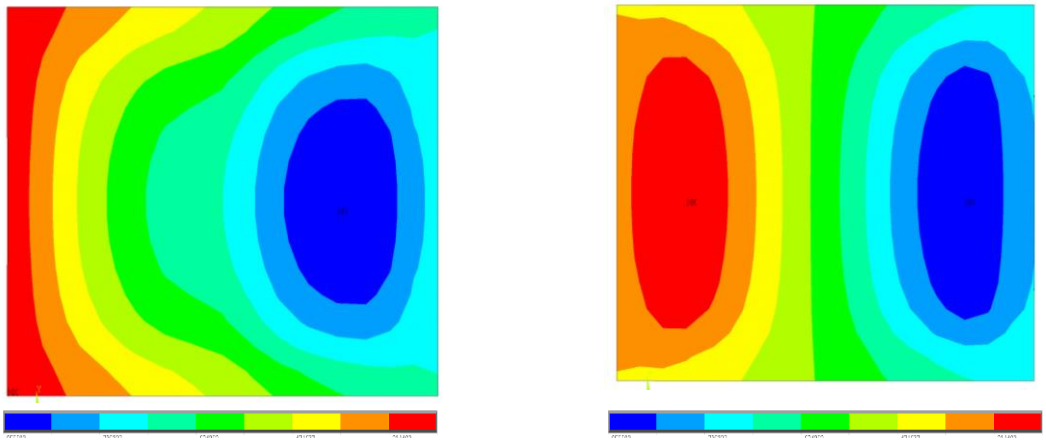

Figure 6. 12 - (a) Stress in PEC under centric compression load; (b) Stress in PEC under eccentric loading.

6.6 Fire scenario effect

A fire scenario is a detailed description of a fire incident. Scenarios are particularly suited to examine conditions and events taken together, and fire scenarios describe all essential elements of a fire incident. The components which make up the events and conditions of a fire scenario may include events such as ignition, fire spread, smoke production, intensity and fire protection etc. The fire scenarios have a significant effect on the behaviour of steel and composite structures (Dwaikat et al., 2011; Jiang et al., 2014). It follows that the thermal behaviour of a composite column depends on the fire scenario to which it is subjected. To reproduce the fire scenarios most commonly encountered in composite column, two parametric study were investigated in this work. The first one deals about the different fire scenarios exposed to the composite column sides, and the second one considers the intensity of fire along the column height.

6.6.1 Fire scenario according to the exposed side of the column

The PEC composite column HEB 300 used in this analysis to study the different fire scenario, the column is heated up to 120 min according to ISO-834 fire source (see Figure 6.13). In addition to the generalized fire (scenario 1, Figure 6.13 a)), three other scenarios are chosen, scenario 2 according to Figure 6.13 b) where the two concrete sides are protected, scenario 3, Figure 6.13 c) where the two steel sides are protected and the scenario 4 where

one side of steel profile is protected and the other three sides exposed to fire, see figure 6.13 d).

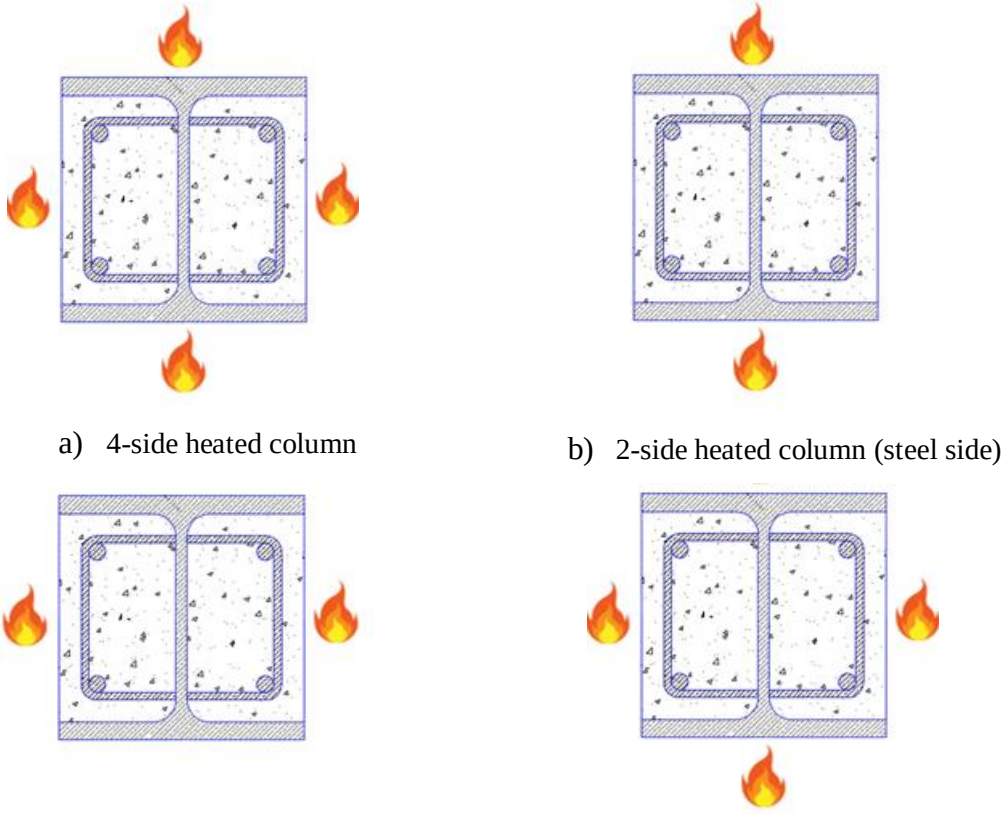

a) 4-side heated column

b) 2-side heated column (steel side)

c) 2-side heated column (concrete side)

d) 3-side heated column

Figure 6. 13- Different cases of fire scenario on the column sides.

6.6.1.1 Thermal response

The results of the thermal analysis of the fire scenario after 120 minutes of a standard fire ISO834 is presented in Figure 6.14. The Figures 6.14 a, b, c and d show the thermal results in the cross sections for the fire scenario 1; 2 ; 3 and 4 respectively. It can be observed that the maximum temperature of the fire scenario 1 reaches a very high value (1039 °C) compared with the other fire scenario. Regarding the exposed parts of the steel profile (fire scenario 2), especially the flanges, the steel profile temperature field increases fast and reaches a high temperature but less than that of the fire scenario 1. However, in fire scenario 3, where the two concrete sides are exposed to fire, this leads to much lower temperatures in the composite column especially in the web and the core of the cross section, because of the concrete protection. The highest temperature obtained on the heated side of column at 120

min of fire exposure is about 1028 °C. It is to be noted that the region of the highest temperature in fire scenario 3 is the smallest. This is attributed to the insulation effect of concrete and to the unheated flange steel side. The last scenario (scenario 4) shows the same thermal behaviour on the two concrete exposed side as scenario 3. However the other exposed side indicates the highest temperature about 1039 °C.

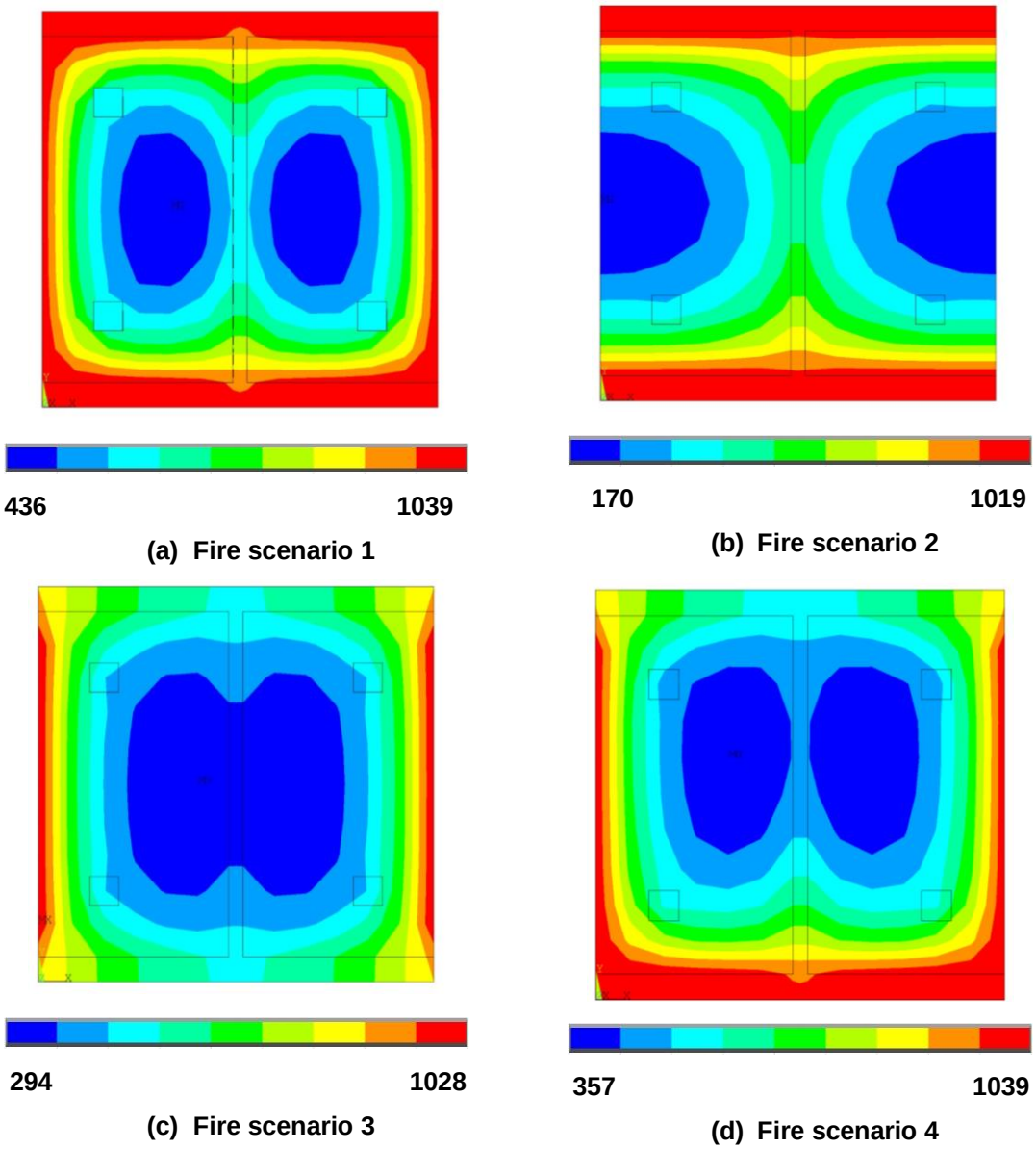

Figure 6.14- Temperature distribution after 120 min of fire for the three different fire scenarios.

This thermal behaviour is observed by other research work (Mao and Kodur, 2011). It can be seen that the minimum temperature is only 170 °C corresponding to the fire scenario 2, the other fire scenario (1, 3 and 4) indicate the minimum temperature 436 °C , 294 °C and

357 °C respectively. The region of the minimum temperature in the cross section is reduced as the increase of the exposed fire side.

The measured temperature in the middle column cross section for the various fire scenarios is plotted as a function of fire time in Figure 6.15. This point represent farthest point from the fire. It can be seen that the four fire scenario increases with the increase of the fire exposure time. There is an important difference between the ISO-834 temperature and the temperature of the four fire scenario attributed to the position of the external fire source and the middle -point of the cross section respectively. The temperature of the fire scenario 1 (generalized fire) shows the highest temperature because their four sides are exposed to fire. Despite the 3-sides composite column exposed to fire (fire scenario 4), the temperature in the middle point of the cross section of fire scenario 2 is higher than that of fire scenario 4. This is because in fire scenario 2 the two side exposed to fire are made from steel, however in fire scenario 4 there is only one side made from steel and the other two sides made from concrete. It is to be concluded that the temperature in the middle point of the cross section increased with increase of the exposed sides if the sides are made from the same materials.

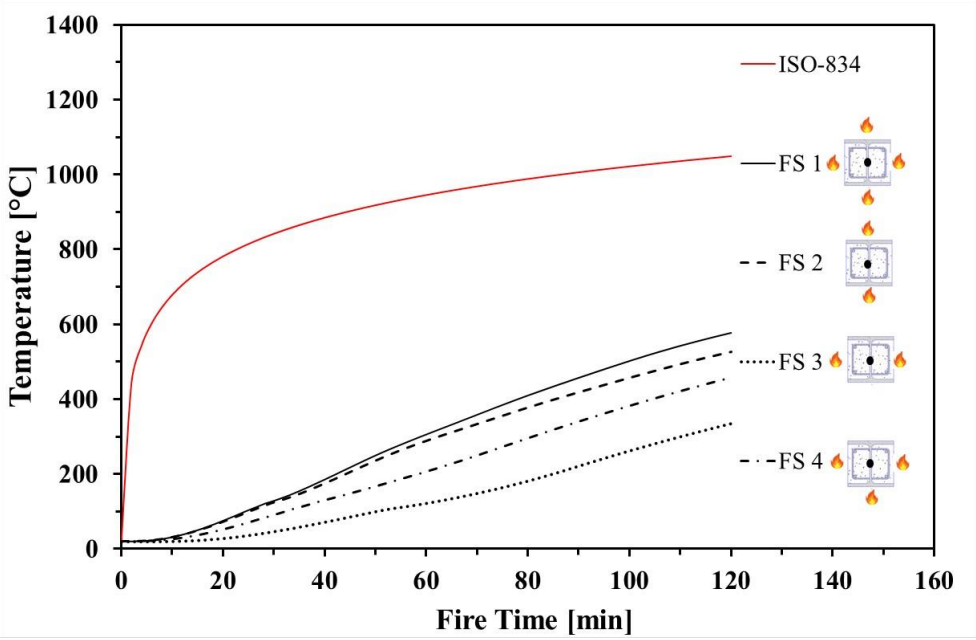

Figure 6.15- Temperature evolution in the middle point of the cross section for the different fire scenarios.

6.6.1.2 Load bearing capacity

The load bearing capacity of the four different fire scenarios is plotted as a function of the eccentricity at fire rating class R120 in Figure 6.16. It can be seen that when the two concrete sides are exposed to fire (fire scenario 3), the composite column presents a high load bearing capacity value. This results is found elsewhere (Mao and Kodur, 2011). However for the other fire scenario (1,2 and 4) it is observed that the load bearing capacity is clearly reduced with the regard to that of the scenario 3. Moreover, the composite column has approximately the same value of load bearing capacity if at least one steel side is exposed to fire. The load bearing capacity reaches the same value for at the eccentricity of 450 mm for all the fire scenarios. This observation probably attributed to the compressed concrete of the cross section. It is to be noticed that the area of the compressed concrete is reduced as the increase of the eccentricity (increase of the bending moment). However the tensile concrete is increasing but this concrete dos not attribute to in the load bearing capacity. In fire accident even the steel profile is protected by the concrete the load bearing capacity of the composite column is affected if the compression load is accompanied by the bending moment.

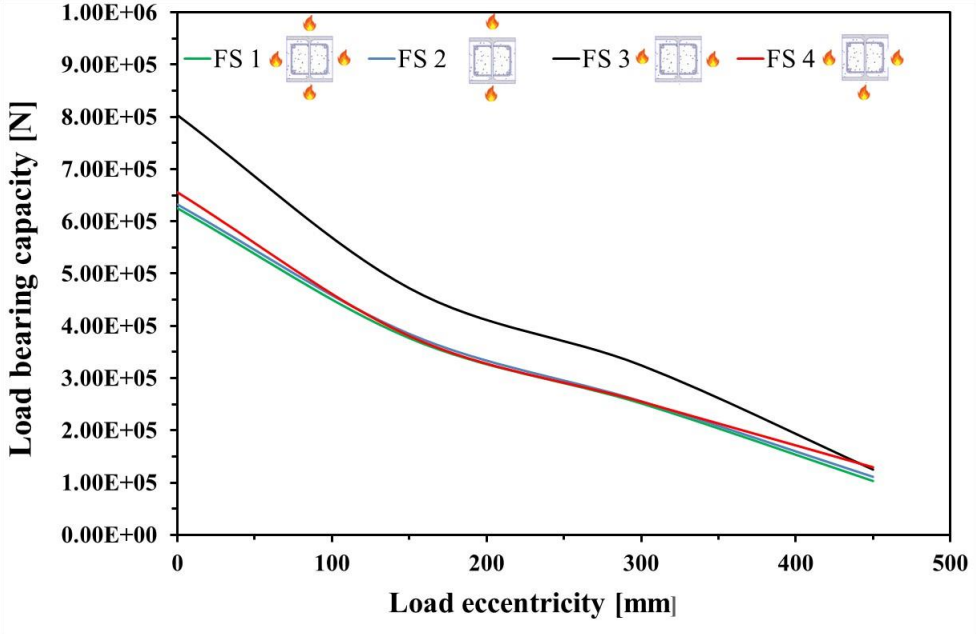

Figure 6.16- Load bearing capacity of composite column at different fire scenarios.

The load bearing capacity versus the lateral displacement of the mid height of the column presented in Figure 6.17. It is observed from the curves that the load capacity increase with

the increase of the displacement up to the maximum load capacity. The results show that the curve of fire scenario 3 present the highest load bearing capacity and the highest ductility for compression loading, this related to the axially loaded condition and to the low temperature reaches in that fire scenario. The column subjected to combined compression and bending loading present a low bearing capacity because the presence of the bending moment. When the composite column subjected to eccentric load and to very high temperature (fire scenario1) the ductility increase and the column present the lowest bearing capacity. There is a difference of 28% between fire scenario 3 and fire scenario 1 load capacity for compression loading, however this difference reduced to 21% when the column exposed to combined compression and bending.

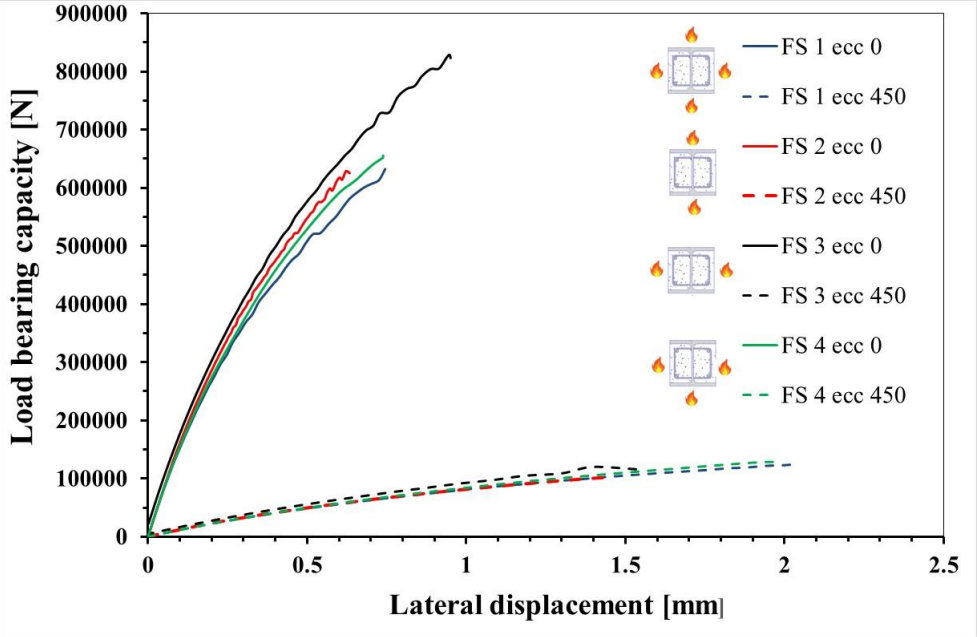

Figure 6.17- The Load bearing capacity versus the lateral displacement of the mid height of the composite column at 120 of fire.

6.6.2 Fire scenario according to the heated part of the column

The parameter considered in this section takes into account the partial and the total protection of the composite column. The protection may be made from a substance like intumescent coating (Mesquita et al., 2009), gypsum plate, Stucco plaster and bricks. Three fire scenarios can be happened in fire accident as illustrated in Figure 6.18; notably fire scenario 1 which is the generalized fire; fire scenario 2 in which the upper part of column is fully protected

against the fire and the rest of column is without protection, and fire scenario 3 in which the first upper 1 m is exposed to ISO-834 fire source and the following 2 meters are subjected to 2/3 and 1/3 ISO-834 fire source respectively. It is to be noted that the four composite column sides are exposed to fire. In this fire scenarios we are looking to the effect of the fire exposure on the thermal and mechanical behaviour when the intensity of the fire is varied along the height of the column.

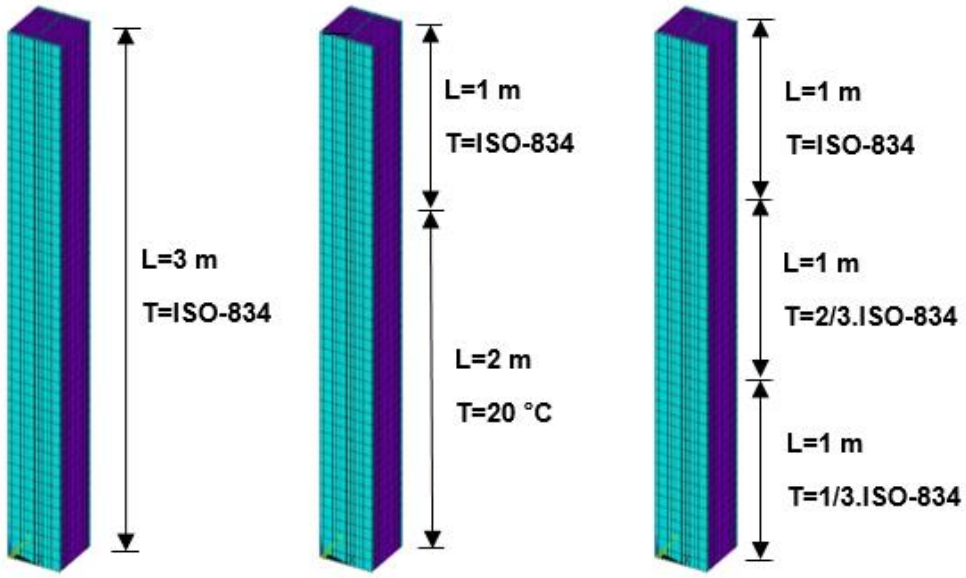

a) Fire scenario 1 b) Fire scenario 2 c) Fire scenario 3

Figure 6.18- Different cases of heated part of the composite column.

6.6.2.1 Thermal response

Temperature distribution after 120 min of fire exposure for the different fire scenarios are plotted in the Figure 6.19. The results show a significant difference in the temperature depending of the heated part of the column. The column exposed to fire scenario 1 presents the highest temperature distributed over the entire length of the column, because it has no fire protection. The temperature distribution is low as the fire protection is found on the column (see Figure 6.19 b)). However, in fire scenario 3 (Figure 6.19 c)) the temperature distribution is reduced progressively as the column part is far from the fire source. Same result is found by Kim et al (2007).

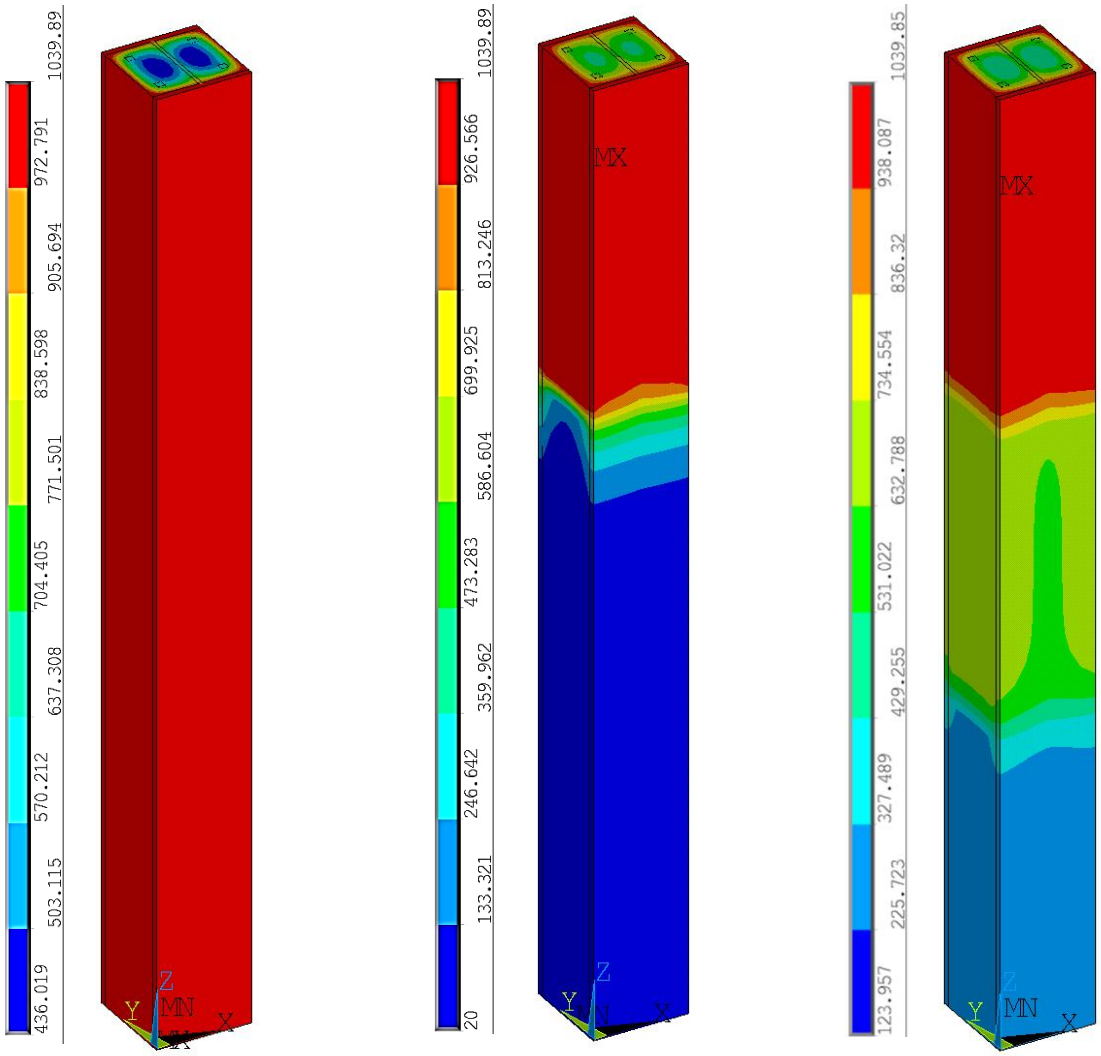

a) Fire scenario 1 b) Fire scenario 2 c) Fire scenario 3

Figure 6.19- Temperature distribution after 120 min of fire exposure for the different fire scenarios.

6.6.2.2 Load bearing capacity

Figure 6.20 shows the load bearing capacity versus the lateral displacement curves obtained from the axial compression (ecc =0 mm) and the combined compression and bending (ecc= 450 m) after 120 min of fire exposure for the three different fire scenarios. It can be observed that the type of fire scenario has an influence on the deformation of the column when the column subjected to concentric compression. The lateral displacement in fire scenario 2 does not exceed 0.3 mm, however the lateral displacement in the other scenarios reaches 0.7 mm. it is to be thought that the column in fire scenario 1 is entirely exposed to fire (very high

temperature) and as a result the deformation is the largest (in agreement with Kardomateas et al (2009)). Otherwise the lateral displacement of the column in fire scenario 2 is less because some part of the column is protected from the fire. When the column subjected to eccentric loading, this leads to a high lateral displacement depending on the composite column heated part. When the composite column subjected to compression loading accompanied with bending moment the load bearing capacity is strongly reduced.

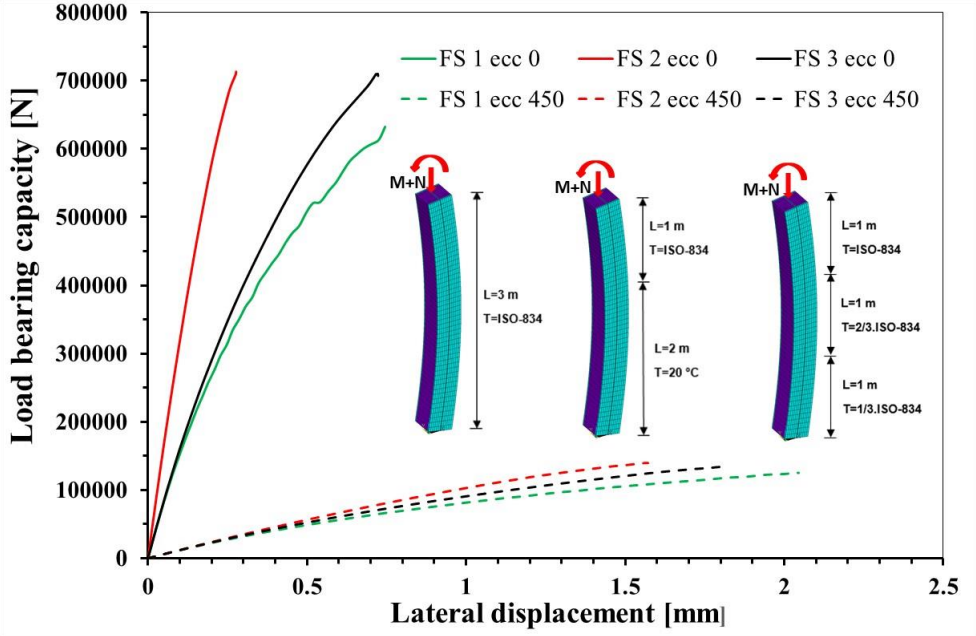

Figure 6.20- load bearing capacity versus the lateral displacement after 120 min of fire exposure for the different fire scenarios.

The results found from Figure 6.20 indicate that the load capacity of the PEC column is high as the temperature corresponding to the fire scenario is low increases. There is not a great difference of the load capacity between the three fire scenario for both concentric and eccentric loading (about 10 %). However the difference of the load capacity is very important between concentric and eccentric loading (around 80 %). The effect of the kind of loading on the mechanical behaviour is more influencing than that the effect of the fire scenario.

6.7 Conclusion

The fire resistance of partially encased composite columns under combined compression and bending moment was investigated using analytical and numerical method. The following conclusions can be made:

- The use of a three dimensional numerical model (ANSYS) allowed to describe easily the thermal behaviour of PEC columns under eccentric loading with the regard to the analytical method, which is based on three complex steps.
- For the fire rating R30, the analytic method presents a conservative result of approximately 45% when applying an eccentric loading.
- There is a good agreement between the two methods particularly at high temperature.
- In this study the presence of the load eccentricity has found to have more effect on the loadbearing capacity than the slenderness of the composite column.
- Introducing a bending moment on the top of the column may have the same effect as the fire.
- The reinforcement has a slight influence on the temperature evolution, moreover the reinforcement have a great contribution on the load capacity, especially in combined loading for compression and bending.
- The temperature in the middle point of the cross section increased with increase of the exposed sides if the sides are made from the same materials.
- When only the two concrete sides are exposed to fire, the partially encased composite column presents a high load bearing capacity value.
- The composite column has approximately the same value of load bearing capacity if at least one steel side is exposed to fire.
- The column exposed to generalized fire presents the highest temperature distributed over the entire length of the column, because it has no fire protection.
- The lateral displacement on the composite column is large as the column is entirely exposed to fire. Otherwise, the lateral displacement is low if a part of the column is protected.
- The effect of the kind of loading on the mechanical behaviour is more influencing than that the effect of the fire scenario.

CONCLUSIONS

The aim of this work is to develop an efficient Non-linear 3-D finite element model to investigate the behaviour of axially loaded and eccentrically loaded (combined compression and bending) of different composite column types; partially encased column, totally encased column and concrete field tubular column exposed to fire. The Numerical results are compared and validated with those of the analytical results.

The main variables in this study were: concrete strength, composite column shape, buckling length, load eccentricity, time of fire exposure and fire scenario. After performing several calculations, the following conclusions can be made:

- The use of analytical method is limited to normal strength concrete. For high strength concrete, we need to use a numerical model such as ANSYS to describe the linear the non-linear behaviour of the composite columns under fire.
- The use of HSC in composite column reduces the level of fire protection with the respect to NSC. This behaviour is attributed to the high thermal conductivity and the low specific heat of HSC.
- By doing a comparison between three different composite column sections, it is found that TEC composite column presents the lowest average temperature and the highest fire resistance compared with other columns. This section resists better to fire because of the concrete cover.
- The results of the linear buckling show that the use of HSC presents a high value of load bearing capacity at low fire exposure time (R30, R60). However, at high fire exposure time, the results of the load bearing capacity for NSC are better than those of the HSC.
- The non-linear analysis shows that the use of HSC concrete is beneficial for composite columns regarding its best performance at low fire exposure time. However, this behaviour is not observed at higher exposure time. The results indicate that the use of HSC concrete in composite columns shows a higher degradation at elevated exposure time compared with NSC concrete.
- The mechanical performance (load bearing capacity) in composite columns at ambient temperature are reduced more than twice after 30 min of fire exposure. This confirms the importance to consider the fire conditions in the design of composites structures.
- NSC in composite structures provides more deflections than HSC (about 60% of difference), which may be useful during a fire accident (safety level).

- The CFT column presents the lowest buckling load because of the low fire performance of its steel profile, which is directly exposed to fire. The composite column with TEC section can supports a load bearing capacity of 2.5 MN up to 60 min under fire, however for approximately the same value of load bearing capacity, the column with CFT section can support only 30 min under fire.
- The use of a three dimensional numerical model (ANSYS) allowed to describe easily the thermal behaviour of PEC columns under eccentric loading with the regard to the analytical method, which is based on three complex steps.
- For the fire rating R30, the analytic method presents a conservative result of approximately 45% when applying an eccentric loading. There is a good agreement between the two methods particularly at high temperature.
- In this study, the presence of the load eccentricity has found to have more effect on the load bearing capacity than the slenderness of the composite column. Introducing a load eccentricity on the top of the column may have the same a reducing effect on the load bearing capacity as the fire.
- The reinforcement has a slight influence on the temperature evolution, moreover the reinforcement have a great contribution on the load capacity, especially in combined compression and bending.
- When only the two concrete sides are exposed to fire, partially encased composite column presents a high load bearing capacity value. The effect of the kind of loading on the mechanical behaviour is more influencing than that of the effect of the fire scenario.

REFERENCES

ANSYS®, Academic Research, Release 18.2, Help System, Element reference, ANSYS, Inc, 2017.

An, Y. F., and Han, L. H. (2014). Behaviour of concrete-encased CFST columns under combined compression and bending. Journal of Constructional Steel Research, 101, 314-330.

Espinós Capilla, A. (2012). Numerical analysis of the fire resistance of circular and elliptical slender concrete filled tubular columns (Doctoral dissertation, Editorial Universitat Politècnica de València).

Correia, A. J. P. D. M. (2012). Fire resistance of steel and composite steel-concrete columns (Doctoral dissertation).

Arioz, O. (2007). Effects of elevated temperatures on properties of concrete. Fire safety journal, 42(8), 516-522.

Benlakehal, N., Kassoul, A., Piloto, P. A. G., and Bouchair, A. (2017). Time resistance of industrial steel portal frames with haunches under fire. Asian Journal of Civil Engineering (BHRC), 18, 993-1008.

Bihina, G., Zhao, B., and Bouchaïr, A. (2013). Behaviour of composite steel–concrete cellular beams in fire. Engineering Structures, 56, 2217-2228.

Cheng, F. P., Kodur, V. K. R., and Wang, T. C. (2004). Stress-strain curves for high strength concrete at elevated temperatures. Journal of Materials in Civil Engineering, 16(1), 84-90.

Chicoine, T., Tremblay, R., Massicotte, B., Ricles, J. M., and Lu, L. W. (2002). Behavior and strength of partially encased composite columns with built-up shapes. Journal of Structural engineering, 128(3), 279-288.

Correia, A. J. M., and Rodrigues, J. P. C. (2011). Fire resistance of partially encased steel columns with restrained thermal elongation. Journal of Constructional Steel Research, 67(4), 593-601.

Dai, X. H., and Lam, D. (2012). Shape effect on the behaviour of axially loaded concrete filled steel tubular stub columns at elevated temperature. Journal of Constructional Steel Research, 73, 117-127.

Dong, Y., and Prasad, K. (2009). Experimental study on the behavior of full-scale composite steel frames under furnace loading. Journal of structural engineering, 135(10), 1278-1289.

Dundar, C., Tokgoz, S., Tanrikulu, A. K., and Baran, T. (2008). Behaviour of reinforced and concrete-encased composite columns subjected to biaxial bending and axial load. Building and environment, 43(6), 1109-1120.

Dwaikat, M. M. S., Kodur, V. K. R., Quiel, S. E., and Garlock, M. E. M. (2011). Experimental behavior of steel beam–columns subjected to fire-induced thermal gradients. Journal of Constructional Steel Research, 67(1), 30-38.

Ellobody, E., and Young, B. (2010). Investigation of concrete encased steel composite columns at elevated temperatures. Thin-Walled Structures, 48(8), 597-608.

El-Tawil, S., and Deierlein, G. G. (1999). Strength and ductility of concrete encased composite columns. Journal of Structural engineering, 125(9), 1009-1019.

EN 1991-1-2. (2009). Eurocode 1: Actions on structures - Part 1-2: General actions - Actions on structures exposed to fire. Brussels: European Committee for Standardization.

EN 1992-1-1. (2004). Eurocode 2: Design of concrete structures - Part 1-1: General rules and rules for buildings. Brussels: European Committee for Standardization.

EN 1992-1-2. (2004). Eurocode 2: Design of concrete structures - Part 1-2: General rules structural fire design. Brussels: European Committee for Standardization

EN 1993 -1-1. (2005). Eurocode 3: Design of steel structures Part 1-1: General rules and rules for buildings. Brussels: European Committee for Standardization.

EN 1993-1-2. (2005). Eurocode 3: Design of steel structures - Part 1-2: General Rules-Structural fire design, Brussels: European Committee for Standardization.

EN 1994-1-1. (2004). Eurocode 4: Design of composite steel and concrete structures - Part 1-1: General rules and rules for buildings. Brussels: European Committee for Standardization.

EN 1994-1-2. (2005). Eurocode 4: Design of composite steel and concrete structures - Part 1-2: General rules - Structural fire design. Brussels: European Committee for Standardization.

Espinos, A., Gardner, L., Romero, M. L., and Hospitaler, A. (2011). Fire behaviour of concrete filled elliptical steel columns. Thin-walled structures, 49(2), 239-255.

Espinós, A., Romero, M. L., Portolés, J. M., and Hospitaler, A. (2014). Ambient and fire behavior of eccentrically loaded elliptical slender concrete-filled tubular columns. Journal of constructional steel research, 100, 97-107.

Fellouh, A., Benlakehal, N., Piloto, P., Ramos, A., and Mesquita, L. (2017). Load carrying capacity of partially encased columns for different fire ratings. Fire Research, 1(1).

Fellouh, A., Bougara, A., Piloto, P. A., & Benlakehal, N. (2020). Non-linear buckling analysis of composite columns made from high and normal strength concrete under fire. Asian Journal of Civil Engineering, 21(1), 17-27.

Feng, M., Wang, Y. C., and Davies, J. M. (2004). A numerical imperfection sensitivity study of cold-formed thin-walled tubular steel columns at uniform elevated temperatures. Thin-Walled Structures, 42(4), 533-555.

Feng, M.Q., Wang, Y.C., and Davies, J.M. (2001). Behaviour of short thin-walled channel columns at elevated temperatures. Proceedings of the International Seminar on Steel Structures in Fire, Shanghai.

Gernay, T. (2016). Fire performance of columns made of normal and high strength concrete: A comparative analysis. In Key Engineering Materials (Vol. 711, pp. 564-571). Trans Tech Publications Ltd.

Guo, Z., Wang, X., Zhang, X., Song, J., and Li, C. (2019). Effects of boundary restraints on concrete-filled steel tubular columns with reinforcements exposed to fire. Thin-Walled Structures, 142, 52-63.

Han, L. H., Chen, F., Liao, F. Y., Tao, Z., and Uy, B. (2013). Fire performance of concrete filled stainless steel tubular columns. Engineering Structures, 56, 165-181.

Han, L. H., Li, W., and Bjorhovde, R. (2014). Developments and advanced applications of concrete-filled steel tubular (CFST) structures: Members. Journal of constructional steel research, 100, 211-228.

Han, L. H., Yang, Y. F., and Xu, L. (2003). An experimental study and calculation on the fire resistance of concrete-filled SHS and RHS columns. Journal of constructional steel research, 59(4), 427-452.

Heskestad, G., and Hamada, T. (1993). Ceiling jets of strong fire plumes. Fire Safety Journal, 21(1), 69-82.

Hoang, H. (2010). Structural continuity effects in steel frames under fire conditions (Doctoral dissertation, Worcester Polytechnic Institute).

Huang, Z. F., Tan, K. H., and Phng, G. H. (2007). Axial restraint effects on the fire resistance of composite columns encasing I-section steel. Journal of Constructional Steel Research, 63(4), 437-447.

Huang, Z. F., Tan, K. H., Toh, W. S., and Phng, G. H. (2008). Fire resistance of composite columns with embedded I-section steel—Effects of section size and load level. Journal of Constructional Steel Research, 64(3), 312-325.

Ibáñez Usach, C. (2016). Fire response analysis of circular concrete filled tubular columns and the effects of axial and rotational restraints (Doctoral dissertation, Universitat Politècnica de València).

ISO834-1 (1999). Fire resistance tests - Elements of building construction – Part 1: General requirements for fire resistance testing, International Organization for Standardization, Switzerland.

Jiang, J., Li, G. Q., and Usmani, A. (2014). Influence of fire scenarios on progressive collapse mechanisms of steel framed structures. Steel Construction, 7(3), 169-172.

Jiang, Y., Silva, A., Castro, J. M., Monteiro, R., and Silvestre, N. (2017). Experimental and Numerical Assessment of the Behaviour of RuCFST Members under Monotonic and Cyclic Bending. In 16th World Conference on Earthquake Engineering.

Kamil, G. M., Liang, Q. Q., and Hadi, M. N. (2019). Numerical analysis of axially loaded rectangular concrete-filled steel tubular short columns at elevated temperatures. Engineering Structures, 180, 89-102.

Kardomateas, G. A., Simitses, G. J., and Birman, V. (2009). Structural integrity of composite columns subject to fire. Journal of composite materials, 43(9), 1015-1033.

Kim, J., Lee, S. W., and Kwon, S. (2007). Time-to-failure of compressively loaded composite structures exposed to fire. Journal of composite materials, 41(22), 2715-2735.

Klabník, M., and Králik, J. (2017). Equivalent stress and strain of composite column under fire. Procedia engineering, 190, 522-529.

Kodur, V. (2014). Properties of concrete at elevated temperatures. International Scholarly Research Notices, 2014.

Kodur, V., and Khaliq, W. (2011). Effect of temperature on thermal properties of different types of high-strength concrete. Journal of materials in civil engineering, 23(6), 793-801.

Kodur, V. K. R., Wang, T. C., and Cheng, F. P. (2004). Predicting the fire resistance behaviour of high strength concrete columns. Cement and Concrete Composites, 26(2), 141-153.

Lacki, P., Derlatka, A., and Kasza, P. (2018). Comparison of steel-concrete composite column and steel column. Composite Structures, 202, 82-88.

Li, S., Liew, J. R., Xiong, M. X., and Lai, B. L. (2021). Experimental investigation on fire resistance of high-strength concrete encased steel composite columns. Fire Safety Journal, 121, 103273.

Liu, C., Wang, Y., Liu, X., Yang, D., and Du, X. (2017). State-of-the-Art of Research on Damage Mechanism and Mechanical Property of the Composite Structures after Exposure to Fire. The Open Civil Engineering Journal, 11(1).

Luccioni, B. M., Figueroa, M. I., and Danesi, R. F. (2003). Thermo-mechanic model for concrete exposed to elevated temperatures. Engineering Structures, 25(6), 729-742.

MacGregor, J. G., and Bartlett, F. M. (2000). RC: Mechanics and design. first Canadian edition. Scarborough (Ontario): Prentice-Hall Canada Inc, 173-300.

Mago, N., & Hicks, S. J. (2016). Fire behaviour of slender, highly utilized, eccentrically loaded concrete filled tubular columns. Journal of Constructional Steel Research, 119, 123-132.

Malhotra, H. L., and Stevens, R. F. (1964). FIRE RESISTANCE OF ENCASED STEEL STANCHIONS. proceedings of the Institution of Civil Engineers, 27(1), 77-98.

Mao, X., and Kodur, V. K. R. (2011). Fire resistance of concrete encased steel columns under 3-and 4-side standard heating. Journal of constructional steel Research, 67(3), 270-280.

Mesquita, L. M., Piloto, P. A., and Vaz, M. A. (2009). Intumescent coating modelling based on small scale experimental tests. In III Conferência Nacional em Mecânica de Fluidos, Termodinâmica e Energia.

Milanović, M., Cvetkovska, M., and Knežević, P. (2015). Load-bearing capacity of fire exposed composite columns. Građevinar, 67(12.), 1187-1197.

Phan, L. T. (1996). Fire performance of high-strength concrete: A report of the state-of-the art. Gaithersburg. National Institute of Standards and Technology, Office of Applied Economics, Building and Fire Research Laboratory.

Piloto, P. A., Gavilán, A. B., Zipponi, M., Marini, A., Mesquita, L. M., and Plizzari, G. (2013). Experimental investigation of the fire resistance of partially encased beams. Journal of Constructional Steel Research, 80, 121-137.

Piquer, A., and Hernández-Figueirido, D. (2016). Protected steel columns vs partially encased columns: Fire resistance and economic considerations. Journal of Constructional Steel Research, 124, 47-56.

Ren, Q. X., Han, L. H., Hou, C., and Hua, Y. X. (2017). Experimental behaviour of tapered CFST columns under combined compression and bending. Journal of Constructional Steel Research, 128, 39-52.

Rodrigues, J. P. C., Correia, A. J., and Pires, T. A. (2015). Behaviour of composite columns made of totally encased steel sections in fire. Journal of Constructional Steel Research, 105, 97-106.

Rodrigues, J. P. C., and Laim, L. (2017). Fire response of restrained composite columns made with concrete filled hollow sections under different end-support conditions. Engineering Structures, 141, 83-96.

Romero, M. L., Moliner, V., Espinos, A., Ibañez, C., and Hospitaler, A. (2011). Fire behavior of axially loaded slender high strength concrete-filled tubular columns. Journal of Constructional Steel Research, 67(12), 1953-1965.

Saric-Coric, M., and Aïtcin, P. C. (2003). Bétons à haute performance à base de ciments composés contenant du laitier et de la fumée de silice. Canadian Journal of Civil Engineering, 30(2), 414-428.

Schaumann, P., Kodur, V., and Bahr, O. (2009). Fire behaviour of hollow structural section steel columns filled with high strength concrete. Journal of Constructional Steel Research, 65(8-9), 1794-1802.

Schleich, J. B., and Chantrain, P. (1998). Simplified version of Eurocode 4 for usual buildings. EUR(Luxembourg).

Shah, A. H., and Sharma, U. K. (2017). Fire resistance and spalling performance of confined concrete columns. Construction and Building Materials, 156, 161-174.

Su, S., Li, X., Wang, T., and Zhu, Y. (2016). A comparative study of environmental performance between CFST and RC columns under combinations of compression and bending. Journal of Cleaner Production, 137, 10-20.

Ukanwa, K. U., Sharma, U., Hicks, S. J., Abu, A., Lim, J. B., and Clifton, G. C. (2017). Behaviour of continuous concrete filled steel tubular columns loaded concentrically in fire. Journal of constructional steel research, 136, 101-109.

Wang, W., Kodur, V., Yang, X., and Li, G. (2014). Experimental study on local buckling of axially compressed steel stub columns at elevated temperatures. Thin-Walled Structures, 82, 33-45.

Wang, Y. C. (2002). Steel and composite structures: behaviour and design for fire safety. CRC Press.

Won, D. H., Han, T. H., Kim, S., and Kang, Y. J. (2016). Fire resistance of double-skinned composite tubular columns including concrete confinement. Materials and Structures, 49(4), 1269-1284.

Yang, D., and Hancock, G. J. (2004). Compression tests of high strength steel channel columns with interaction between local and distortional buckling. Journal of Structural Engineering, 130(12), 1954-1963.

Zhou, X., Wang, W., Song, K., and Chen, Y. F. (2019). Fire resistance studies on circular tubed steel reinforced concrete stub columns subjected to axial compression. Journal of Constructional Steel Research, 159, 231-244.